INTERFERENCE TEST ANALYSIS WITH TWO FRACTURED HORIZONTAL WELLS

by

Andreas Marsahala Lumban Gaol

A thesis submitted to the Faculty and the Board of Trustees of the Colorado School of Mines in partial fulfilment of the requirements for the degree of Master of Science (Petroleum Engineering).

Golden, Colorado

Date _____

Signed: _____
Andreas Marsahala Lumban Gaol

Signed: _____
Dr. Erdal Ozkan
Thesis Advisor

Golden, Colorado

Date _____

Signed: _____
Dr. Erdal Ozkan
Professor and Interim Head
Department of Petroleum Engineering

ABSTRACT

Fracturing horizontal wells is a common technique to produce hydrocarbons from low-permeability reservoirs (milli- to micro-Darcy). Recently, interest in and study of pressure response and performance (analytical and numerical) of fractured horizontal wells have increased significantly. However, despite numerous studies that show the advantages of fractured horizontal wells, understanding of their performance characteristics in low-permeability reservoirs is still limited. One of the most important questions in field applications is the optimum spacing of fractured horizontal wells. The issue of well spacing is closely related to reservoir connectivity and it is customary to run interference tests involving two wells (active and observation wells) to obtain information about the connectivity and characteristics of the reservoir between the two wells.

This thesis presents a semi-analytical solution to simulate interference tests that involve two fractured horizontal wells in low-permeability reservoirs. Three mathematical models are used to generate the semi-analytical solution: (1) the finite-conductivity fracture model developed by Cinco-Ley and Meng (1988), (2) the pressure distribution model for an infinite and closed rectangular reservoir developed by Ozkan (1988), and (3) the fractured horizontal well model developed by Raghavan et al. (1997). These three models are combined into a general equation using the superposition theorem and evaluated by a semi-analytical approach. This model is used to generate pressure transient responses (p_{wD} and $dp_{wD}/dlnt_D$ versus t_D) of a pair of fractured horizontal wells and the results are evaluated to understand their interference characteristics in naturally fractured, low-permeability reservoirs. Sensitivities of results to the number of hydraulic fractures, well separation (spacing), and matrix permeability are documented to highlight the general characteristics of interference tests in low-permeability reservoirs. Flow regimes in both

active and observation wells are also discussed.

The results of this study show that the existence of a fractured horizontal observation well does not influence the responses of the active well for practical well spacing used in the field. The responses of the active well are merely influenced by its own properties, configuration, and reservoir properties. In contrast, the pressure transient responses of the observation well are greatly affected by the configuration of both wells, distance between wells, and reservoir properties. This thesis also provides applications of the semi-analytical model for other cases of practical interest such as interference tests in a closed rectangular reservoir, with open horizontal sections, and when a stand-alone fracture crosses both wells.

TABLE OF CONTENTS

LIST OF FIGURES

LIST OF TABLES

ACKNOWLEDGEMENT

I am using this opportunity to express my gratitude to everyone who has contributed to the accomplishment of my thesis at Colorado School of Mines.

First and foremost, I would like to thank my Advisor, Dr. Erdal Ozkan, for his continuous support and guidance of my MS study and research. Without his direction, I would not have been able to finish my thesis on time. His passion and knowledge of well testing and fluid flow in porous media have also influenced me to learn more about these areas.

I am also thankful for my committee members, Dr. Xiaolong Yin and Dr. Hulya Sarak, who have given many technical suggestions to improve the quality of my thesis.

I would like to thank my friends from PERMIAS Golden who have helped me throughout my time in Golden. I also recognize the extensive support of my employer and sponsor, ConocoPhillips Indonesia.

Finally, I am so thankful to have a family (Papa, Mama, Bang Sanggam, Kak Tiska, and Atis) who never stops supporting and praying for me in every circumstance I am facing and during my research period.

"Thou hast thrust sore at me that I might fall: but The LORD help me.

The LORD is my strength and song, and is become my salvation."

(Psalm 118: 13-14)

CHAPTER 1

INTRODUCTION

This thesis presents the results of a Master of Science (MS) study conducted under the auspices of the Unconventional Reservoir Engineering Project (UREP) in the Petroleum Engineering Department of the Colorado School of Mines. The MS research reported in this thesis has led to a semi-analytical technique to simulate an interference test with two fractured horizontal wells in a tight, homogeneous or naturally fractured reservoir. Flow of a single-phase, small and constant compressibility, and constant viscosity fluid is considered. Background, problem statement, objectives, method and contribution of the study, and the organization of this thesis are presented below.

1.1. Background

Over the past several years, the development of unconventional resources has been growing drastically in popularity in the US. This popularity is driven by the abundant hydrocarbon volumes in-place that lie in unconventional resources, such as tight sand and shale formations. The US Energy Information Administration (EIA) 2013 summary report for shale oil and shale gas resources shows that estimated technically recoverable resources in the US are 58 Bbbls shale oil and 665 Tcf shale gas. This abundance makes it very attractive to develop these resources to meet the energy demands in the US. Nonetheless, producing hydrocarbons from such complex reservoirs with low-permeability has been very challenging, especially for reservoir engineers who are responsible for reservoir modeling and development.

A common way to produce from low-permeability (milli- to micro-Darcy) reservoirs is to use horizontal wells with multiple hydraulic fractures (Figure 1.1). The production in this type of reservoir is a result of flow in the reservoir matrix, in the reservoir natural fractures, and in

hydraulic fractures. The purpose of hydraulic fractures in low-permeability reservoirs is to serve as a high-conductivity path that connects the wellbore to the reservoir and allows hydrocarbons to move to the wellbore from the reservoir. The main advantage of fractured horizontal wells in low-permeability reservoirs over other techniques (e.g., un-fractured vertical and horizontal wells or fractured vertical wells) is that this method increases the contact area exposure significantly and improves project economics. Although the fractured horizontal well technique has been widely used in the last decade, current understanding of the physical mechanisms of the fluid flow is still limited. Another practical question, which still awaits a satisfactory answer, is the drainage area and optimum spacing of fractured horizontal wells. Nevertheless, there are many ways to improve the understanding of the performances of fractured horizontal wells in low-permeability reservoirs, one of which is the interference test.

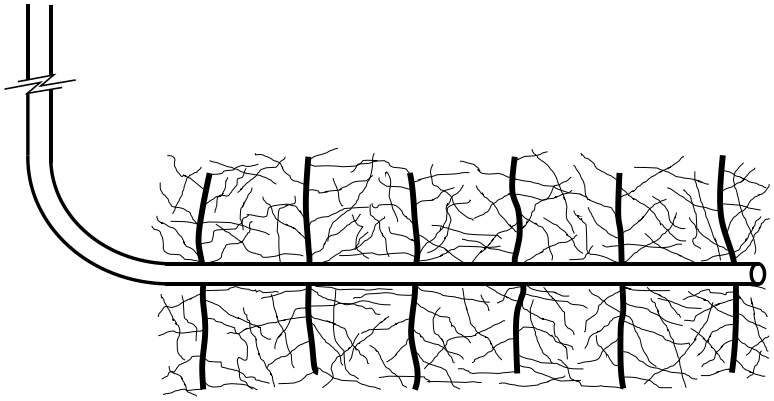

Figure 1.1. Schematic of fractured horizontal wells (Torcuk et al. 2013).

An interference test involves an active point and an observation point separated by a distance (Figure 1.2) and is run to obtain information about reservoir connectivity. Theoretically, the active and observation points may be in the same well or in two separate wells. In this thesis, interference tests with two wells (an active and an observation well) are considered. Such a test requires the creation and measurement of a noticeable pressure drop at a shut-in observation well resulting from production or injection at an active well. This test may provide information about

reservoir properties such as reservoir permeability, reservoir connectivity, dual-porosity variables (storativity and flow capacity ratio), and hydraulic fracture properties (fracture half-length and conductivity). It also has the advantage of generally investigating a more widely influenced region of the reservoir than a single-fractured-horizontal-well test.

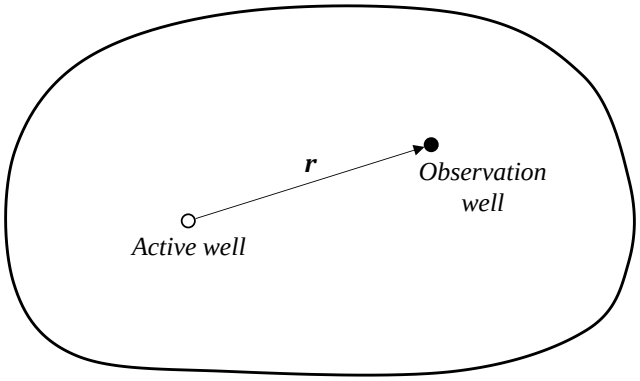

Figure 1.2. Active and observation points in an interference test.

The interference characteristics of fractured horizontal wells in low-permeability reservoirs may be different from other types of interference tests such as conventional horizontal-well or vertical-well interference tests. In low-permeability reservoirs, the pressure pulse created at the active well requires a longer time to arrive in the observation well. Furthermore, in tight unconventional reservoirs, the response can be significantly more complicated due to high reservoir heterogeneity. Interference between fractures also complicates the pressure transient response. Moreover, the response can be non-unique if there is a long stand-alone fracture that intersects both the active and observation wells or if the horizontal well sections are perforated. These challenges need to be accounted for in the analysis of the interference test and should be studied in detail. To do so is the objective of this study.

1.2. Problem Statement

Even though interest in pressure-transient analysis and flow mechanisms in low-permeability reservoirs has been growing significantly, to our knowledge, no study about

interference effects between two fractured horizontal wells has been conducted. The last extensive analysis of interference tests with conventional horizontal wells was done by Al-Khamis et al. (2001 and 2005), but their studies do not cover multiple-fracture systems or flow complications owing to low-permeability matrix and natural fractures. Therefore, there are two main reasons for this study.

The first reason is that in planning for a successful development of any field, one of the key parameters that needs to be investigated is the remaining infield potential (Khan and Callard 2010). However, ultra-low reservoir permeability of unconventional reservoirs presents one of the main difficulties in assessing the remaining reservoir potential by using more conventional tools such as production decline analysis. In such reservoirs, the productive lives of the wells are dominated by infinite-acting rather than boundary-dominated flow regimes. If the well is still under an infinite-acting flow regime, then the remaining potential can be estimated by studying the interference between wells in the same flow network. It must be emphasized, however, that, unlike most conventional systems, well interference characteristics (or lack thereof) in tight naturally fractured reservoirs are not straightforward identifiers of reservoir connectedness or flow (drainage) boundaries between the wells. Although the two wells may be hydraulically connected through fracture(s), their pressure pulses may not overlap in the matrix system, which constitutes the storage capacity of the reservoir between the two wells. Therefore, the optimum well spacing question in these plays should not be simply reduced to a discussion of well interference. Well spacing based on interference in the fracture system may contribute to project economics by yielding higher short-term production, while spacing based on matrix drainage may contribute to higher ultimate recovery. Although optimizing these two considerations seems to be the natural answer, the decisive factor for such optimization is the oil and gas price, which ties the question

of well spacing to the ever more difficult question of price predictability. Nevertheless, reducing the uncertainties in the technical input should unequivocally lead to better optimization.

It is not a new idea that the analysis of interference tests can give valuable information for optimum well spacing and reservoir connectivity in low-permeability reservoirs without having to drill many wells. In their recent investigation of the interference effect of 179 wells in the Woodford Shale, Ajani and Kelkar (2012) showed that an infill well can have a negative impact on the production of an offset well. For example, one of the fractured horizontal wells (O-6) was significantly impacted by an infill well (I-16) at 798 ft distance (Figure 1.3). However, well O-6 was not impacted by another infill well (I-14) at 8,633 ft distance. The negative impact caused by well I-16 could have been avoided by implementing an interference test between the two wells.

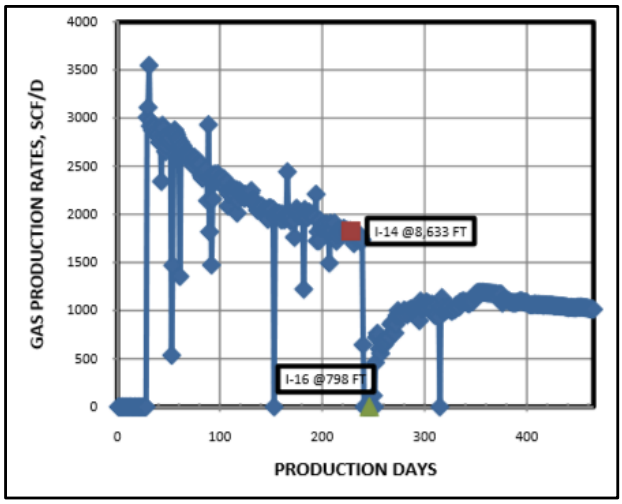

Figure 1.3. Gas production profile of offset producer O-6 in the Woodford Shale (Ajani and Kelkar 2012).

Another area where interference tests may be useful is in the understanding of the effect of a stand-alone fracture that intersects both active and observation wells, especially in the case of injection. Furthermore, the pressure response can be altered if the horizontal sections are opened (such as in the case of open-hole fracturing) to increase well productivity. This can be investigated by doing an interference test.

For these reasons, semi-analytical modeling of interference between wells in low-permeability reservoirs is considered in this work. One of the main outcomes of this research is a robust algorithm to analyze the interference tests in low-permeability reservoirs. This semi-analytical model also includes the connection between finite-conductivity fractures at active and observation wells, which allows us to study the altered flux distribution due to well interference.

1.3. Objectives

The main goal of this thesis is to investigate the characteristics of pressure transient responses of two interfering fractured horizontal wells in the same reservoir. This main objective can be elaborated into five objectives:

(1) Develop semi-analytical models to investigate the fundamental characteristics of interference effects of two fractured horizontal wells.

(2) Provide the solution of a mathematical model with efficient computational code and minimum computational time.

(3) Document data and computational results that can be used to calibrate other (analytical and numerical) models.

(4) Provide general guidelines for the use of the interference-test model in low-permeability reservoirs.

(5) Document the interference characteristics for fractured horizontal wells.

1.4. Method of the Study

To accomplish the research objectives, a series of tasks will be performed. All computational codes of the semi-analytical model are written in MATLAB® software.

The first task is to develop an analytical model for a horizontal well with multiple fractures in a low-permeability reservoir. The mathematical expression for reservoir pressure distribution is

similar to that provided by Ozkan (1988), and the flow within the finite-conductivity fractures in a dual-porosity reservoir is modeled using the same lines as Cinco-Ley and Meng (1988). This analytical model will incorporate the effect of boundaries. The first model has no boundaries (infinite reservoir) and the second model has a closed rectangular boundary (Figure 1.4). For the second model, the general mathematical solution must be recast into a computationally convenient form (Ozkan and Raghavan 1991b) to obtain a robust algorithm. The wellbore of a horizontal well is assumed to be an infinite-conductivity medium, an assumption that requires the pressure to be identical at each point where the wellbore intersects the fractures. This horizontal section can be opened to increase well productivity. The final solution for the multiple finite-conductivity fractures is obtained by implementing a matrix formulation (Chen and Raghavan 1997).

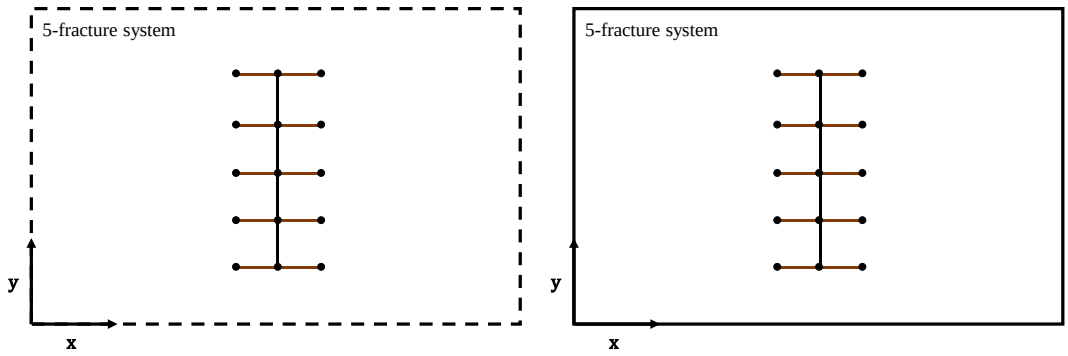

Figure 1.4. Schematics of a fractured horizontal well in an infinite reservoir (left) and in a closed rectangular system (right).

The second task is to generate a solution for an interference test in low-permeability reservoirs. The solution is obtained by adding an observation well into the same flow network with the active well. Two boundary types are considered for the low-permeability reservoir: infinite reservoir and closed rectangular reservoir (Figure 1.5). The solution of the two-well system is generated by using the superposition theorem $\left(\Delta p = \Delta p_1 + \Delta p_2\right)$ or $\left(\sum_{i=1}^{n_w} \Delta p_i\right)$, where the number of wells, n_w, includes all the wells in the system. By using the superposition theorem in the same

coordinate system, the computational code will be able to calculate the interference effect between the active and observation wells.

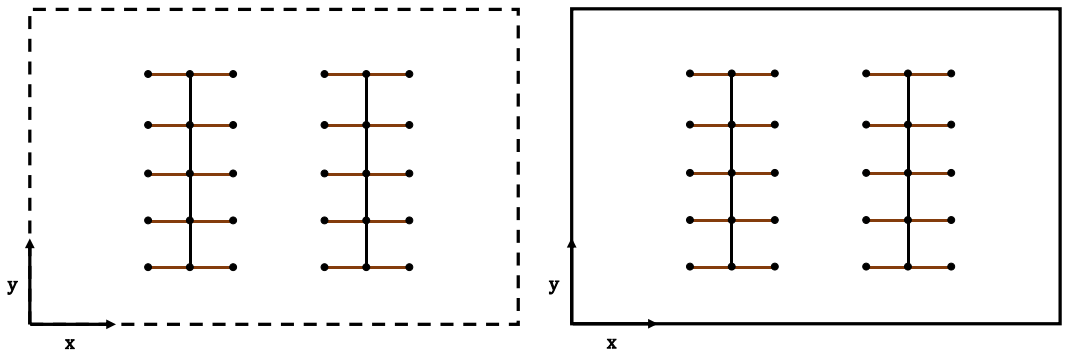

Figure 1.5. Schematics of two fractured horizontal wells in an infinite reservoir (left) and in a closed rectangular system (right).

The third task is to thoroughly analyze the dimensionless pressure and pressure derivative responses of the two-well system. After obtaining the relevant results, the algorithm will be used to do sensitivity analysis. In this step, the key parameters are investigated to see their effects on the interference in low-permeability reservoirs. This task is followed by building the pressure and pressure derivative type curves for interference tests in low-permeability reservoirs and examining how the model can meet the thesis objectives.

1.5. Contribution of the Study

The primary product of this thesis is a semi-analytical technique to simulate the single-phase fluid flow for an interference test with two fractured horizontal wells. This is also the primary contribution of this thesis, since a rigorous analytical or semi-analytical model for interference tests with two fractured horizontal wells in low-permeability reservoirs has not been reported in the literature.

Thorough analyses of the pressure transients and general guidelines for the interference tests with two fractured horizontal wells in low-permeability reservoirs are presented. The approach used in this thesis can also be extended to the study of interference of multiple fractured

horizontal wells producing from a common, low-permeability reservoir. The mathematical formulation of the semi-analytical technique is therefore used to properly analyze the characteristics of interference and the key parameters that affect flow characteristics and hydraulic connectivity. To demonstrate the versatility of the semi-analytical technique, dimensionless and pressure derivative type curves for interference tests in low-permeability reservoirs are also generated. The semi-analytical technique presented in this thesis can generate other type curves that are not included or analyzed in this thesis. Discussion of each type curve, including the sensitivity results, establishes the second primary product of this thesis.

1.6. Organization of this Thesis

This thesis is divided into five chapters. This chapter, Chapter 1, introduces the background, offers a problem statement that elaborates the importance of this thesis and its application, sets forth the objectives, describes the method for how the study is conducted, and explains the main contributions of the thesis.

Chapter 2 presents the literature review pertinent to this thesis.

Chapter 3 is one of the most important chapters in this thesis. It consists of the mathematical background and derivations to explain how the final analytic solutions are obtained. This is followed by the method to obtain the solution using the semi-analytical technique. This chapter also includes the verification of the solution technique with the results provided in the literature. The guideline to use the semi-analytical technique is also presented.

Chapter 4 presents the analysis and general observations of the results obtained by the semi-analytical technique presented in Chapter 3. This chapter includes the sensitivity analysis of number of fractures, well separation between two wells, and matrix permeability, followed by the results of three specific cases of interest: closed rectangular boundaries, open horizontal well, and

the existence of a stand-alone fracture crossing both active and observation wells.

Chapter 5 summarizes all the important issues into conclusions and provides some recommendations for future work on interference tests with two fractured horizontal wells.

CHAPTER 2

LITERATURE REVIEW

This chapter contains a summary of the past work, which is relevant to interference tests with fractured horizontal wells in naturally fractured tight unconventional reservoirs.

2.1. Naturally Fractured Reservoir (Dual-Porosity)

For naturally fractured reservoirs, two dual-porosity models, by Warren and Root (1963) and Kazemi (1969), are widely used in the petroleum industry. These models are the idealized versions of naturally fractured reservoir systems that comprise matrices and fissures. Warren and Root introduced the model in which the matrices and fractures are uniformly distributed and overlapping (Figure 2.1). The fluid transfer from the matrix to the fracture network is in a pseudosteady state and follows Darcy's Law. There is no direct communication between matrix elements and between matrix system and wellbore; flow is only between matrix and fractures and between fractures and wellbore.

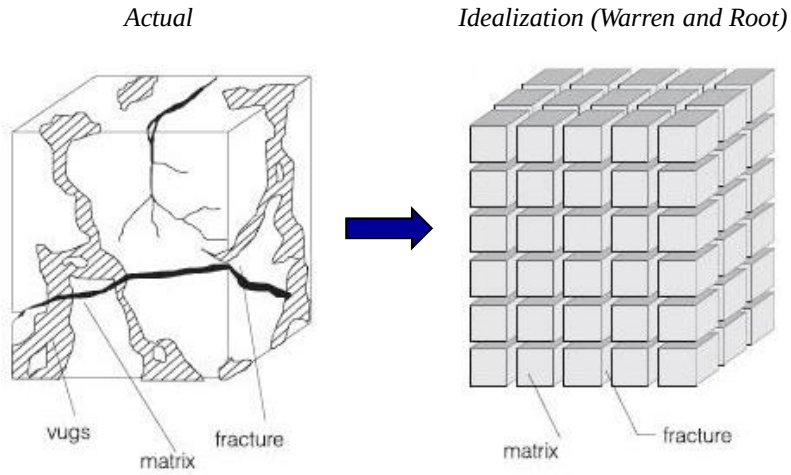

Figure 2.1. Warren and Root (1963) dual-porosity idealization; cubed dual-porosity model representation.

Kazemi (1969) introduced a different idealization for naturally fractured reservoirs. This model consists of horizontal matrices and fractures extending throughout the reservoir (Figure

2.2). It considers the flow within the matrix and transient fluid transfer from the matrix to the fracture. Flow in the matrix system is one dimensional (1-D) and in a normal direction to the fracture system. This is essentially a layered reservoir model in which matrix and fracture have distinct properties. Similar to the Warren and Root (1963) model, communication only exists between matrix and fractures and between fractures and wellbore.

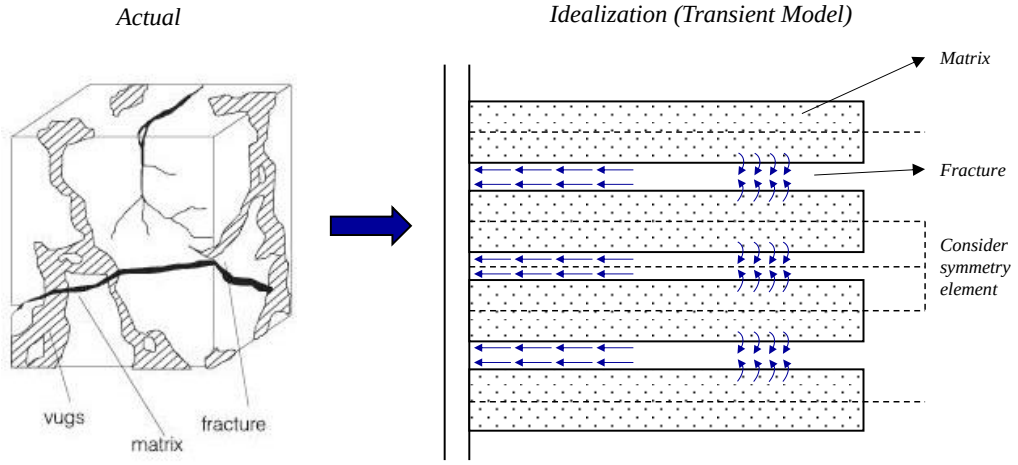

Figure 2.2. Kazemi (1969) dual-porosity idealization; layered dual-porosity model representation.

2.2. Fluid Flow toward a Well with Finite-Conductivity Fracture

Cinco L. et al. (1978) introduced the general solution of the transient behavior of a well with a finite-conductivity vertical fracture in a homogeneous reservoir. They modeled the fluid flow in a finite-conductivity vertical fracture intercepted by a vertical well (Figure 2.3) using Green's and source functions (Gringarten and Ramey 1973). Two flow regions were considered in their mathematical model: the reservoir and the fracture. The analytical solutions for both flow regions were then coupled through flux and pressure continuity along the fracture surface. The final integral equation was then discretized in both time and space.

The results of their mathematical solutions do not change significantly when both fracture half-length and time are discretized into more than 20 segments and 10 time intervals, respectively.

The calculated pressure shows that for dimensionless fracture conductivity, with C_{FD} equal to or greater than 300, the solution is essentially identical to the infinite-conductivity solution given by Gringarten et al. (1974). Another significant finding in their study is that the plots of dimensionless wellbore pressure drop (p_{wD}) versus logarithm of dimensionless time (t_D), for larger times, have a straight line of slope equal to 1.151, which is the basis of semi-logarithmic analysis.

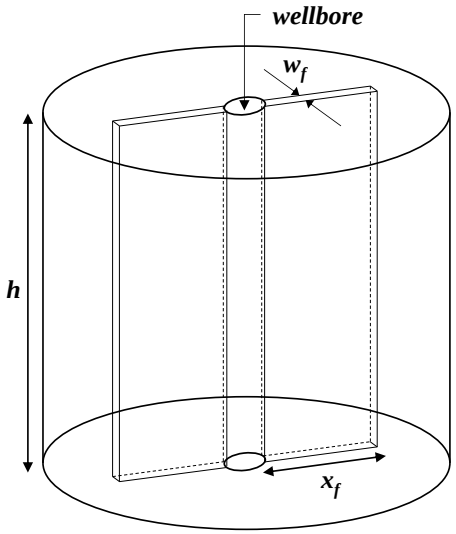

Figure 2.3. Finite-conductivity vertical fracture schematic in an infinite reservoir (Cinco L. et al. 1978).

Cinco-Ley and Samaniego (1981) presented a technique for analyzing the pressure transient data for a well intercepted by a finite-conductivity fracture. Based on their investigations, transient flow behavior of a vertically fractured well may exhibit four flow periods: fracture linear flow, bilinear flow, formation linear flow, and pseudoradial flow (Figure 2.4). In the fracture linear flow period, fluids entering the wellbore are merely the fluids in the fracture caused by fluid expansion. They introduced the bilinear flow period in which two linear flows occur simultaneously (fracture linear flow and formation linear flow). Half-slope and one-fourth-slope straight lines characterize fracture linear and bilinear flow periods, respectively, on a log-log plot of p_{wD} vs. t_D.

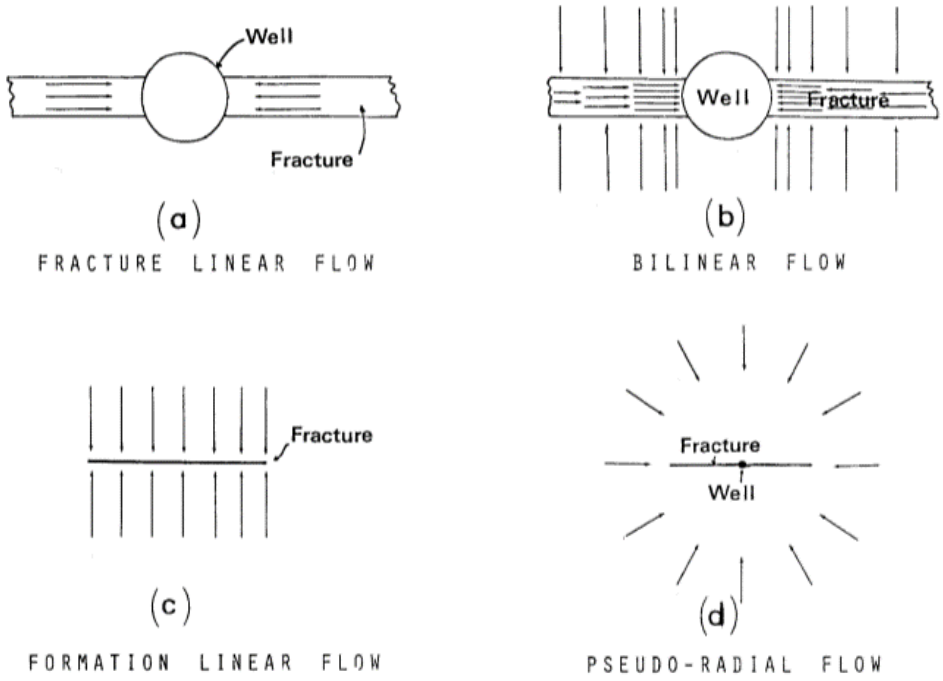

Figure 2.4. Four flow periods for a vertically fractured well (Cinco-Ley and Samaniego 1981).

Cinco-Ley and Meng (1988) modeled fluid flow toward a vertical well intercepted by a finite-conductivity fracture in a dual-porosity reservoir (Figure 2.5). They presented a simplified fully analytical model and a general semi-analytical model in Laplace space. Their semi-analytical approach is faster than the solution given by Cinco L. et al. (1978) because the superposition in time is simplified in the Laplace space (thus, the need for discretization in time is eliminated). Their formulation is also more flexible to be run in either prescribed rate or prescribed wellbore pressure. Cinco-Ley and Meng introduced two additional flow periods that result from a dual-porosity reservoir: trilinear flow period and formation bilinear flow period. Trilinear flow happens in the bilinear flow periods when the flow is strongly supported by the matrix linear flow in the reservoir. Hence, three linear flows take place simultaneously. Characteristically, this flow period is indicated by a straight line with a slope of 1/8 in a log-log graph of p_{wD} versus t_D. The formation bilinear flow period takes place during the pseudolinear flow when the flow is strongly supported by the matrix linear flow in the reservoir. Typically, this flow period is indicated by a straight line

with a slope of 1/4 in a log-log graph of p_{wD} versus t_D.

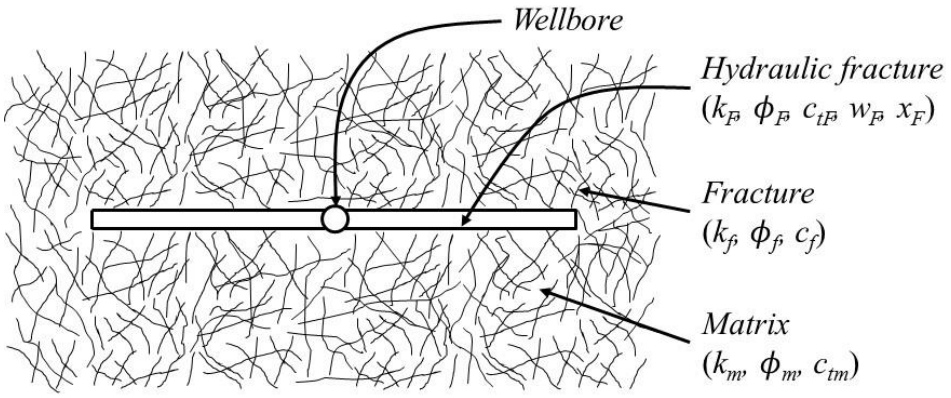

Figure 2.5. Illustration of a vertically fractured well in a dual-porosity reservoir (Cinco-Ley and Meng 1988).

2.3. Fractured Horizontal Well

Raghavan et al. (1997) developed a mathematical model to determine the characteristic responses of fractured horizontal wells in an infinite reservoir. Their model applies the superposition theorem that combines all fractures into one system (i.e., horizontal well) and assumes that those fractures are created in an infinite-conductivity horizontal wellbore. Each fracture is assumed to have distinct properties (conductivity, fracture half-length, and skin) but is produced at a mutual wellbore pressure. Their formulation includes finite-conductivity fractures and may be either transverse or longitudinal. The total flow rate of the system is described as the summation of the flow from each perforated section and each fracture. Their finite-conductivity fracture solutions follow the same lines as Cinco-Ley and Meng (1988). Raghavan et al.'s results show that it is possible to obtain an overall conductivity for the system from the prediction of long-time performance of a fractured horizontal well by using the formulation they developed.

Different from Raghavan et al. (1997), Chen and Raghavan (1997) examined the productivity of a fractured horizontal well in a closed rectangular reservoir. They considered various flow regimes that may be exhibited by multiple fractures that intersect a horizontal well.

Figure 2.6 illustrates four possible flow regimes in a two-fracture system (parallel and normal fractures). The concept and workflow of their study are similar to what was presented by Raghavan et al. (1997). The pressure distribution solution at any point in a rectangular drainage area is given by Ozkan and Raghavan (1988). Chen and Raghavan concluded that the length of the fractures should depend on fracture spacing and reservoir permeability level (long fractures for low-permeability reservoirs and short and wide fractures for high-permeability reservoirs).

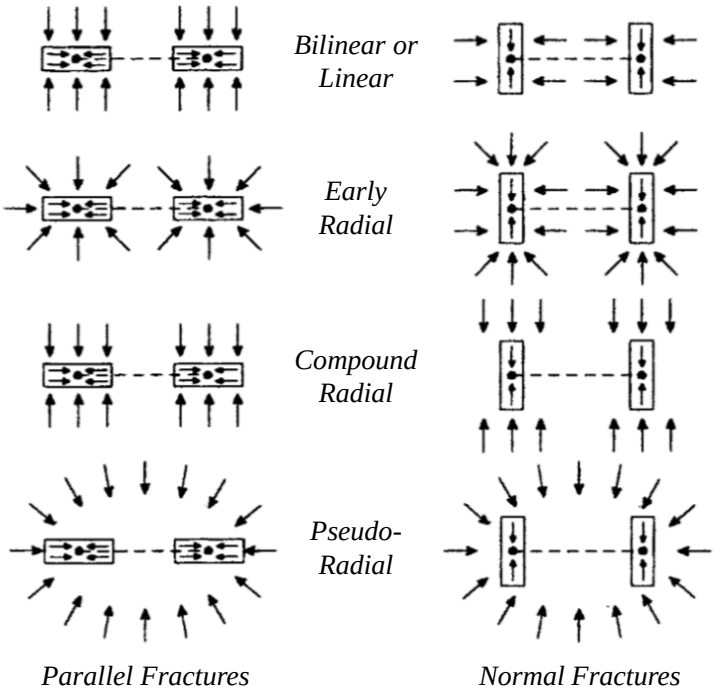

Figure 2.6. Type of possible flow regimes in a fractured horizontal well (Chen and Raghavan 1997).

Brown et al. (2011) presented a practical analytical trilinear-flow solution to simulate the pressure-transient and production behaviors of fractured horizontal wells in unconventional reservoirs (Figure 2.7). This is a practical alternative to more rigorous but computationally intensive and time-consuming solutions (e.g., Raghavan et al. 1997). Their model comprises three regions: outer reservoir (homogeneous), inner reservoir (dual-porosity), and hydraulic fractures. They also used their formulation to show the derivation of asymptotic solutions and provide insight

about possible flow periods and the conditions of these flow periods in unconventional reservoirs. Their trilinear-flow model was derived analytically by following the same lines as Cinco-Ley and Meng (1988), who presented the finite-conductivity fracture solution in a dual-porosity reservoir. Brown et al. considered both pesudosteady state and transient dual-porosity models. Their solutions include the early time, intermediate time, and late time flow behaviors. Each flow regime shows distinct characteristics on a log-log graph of p_{wD} versus t_D. There are multiple possibilities for the diagnostic slope relationship commonly identified through pressure and derivative responses of shale wells, such as 1/2 or 1/4.

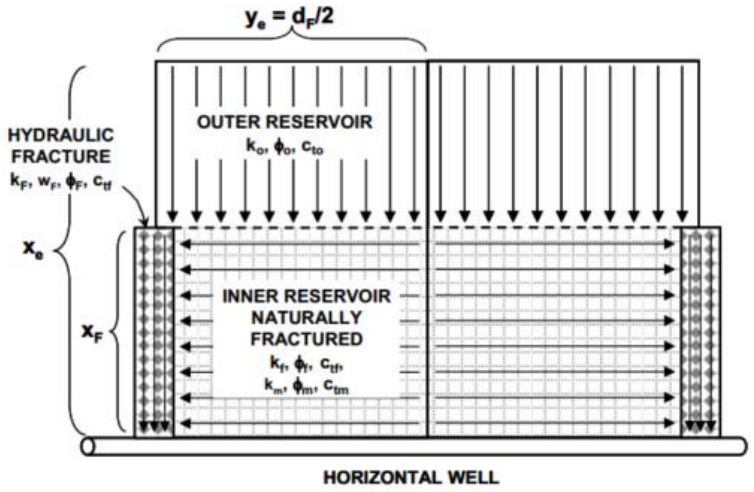

Figure 2.7. Schematic of trilinear flow (Brown et al. 2011).

Greenwood (2015) presented approximate solutions for naturally-fractured unconventional reservoirs by superimposing independent solutions corresponding to flow in various reservoir sections. One of the solutions is practical for composite unconventional reservoirs consisting of three regions similar to the regions in the trilinear flow study (Brown et al. 2011). Another composite model considered by Greenwood has an additional transition zone between the stimulated reservoir volume (SRV) and the outer (virgin) reservoir (see Figure 2.8). Greenwood concluded that the near-well pressure transients, flow regimes, and well productivity rely on the

conditions of the fluxes at the SRV boundary.

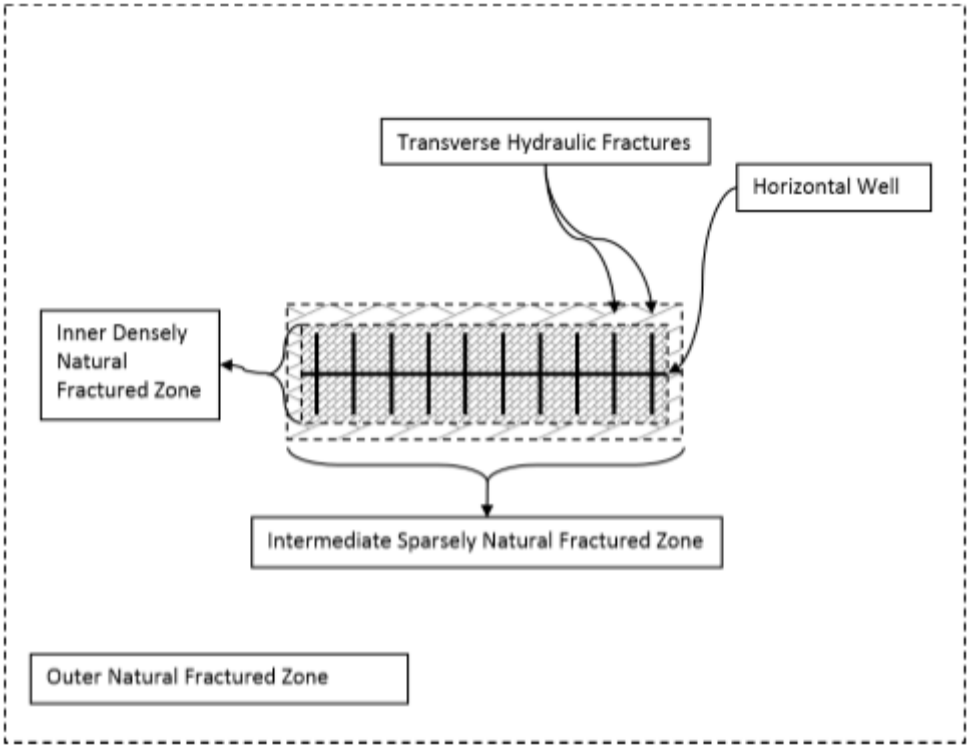

Figure 2.8. Composite reservoir system with transitional zone between SRV and outer reservoir (Greenwood 2015).

2.4. Interference Tests with Fractured Vertical Wells

Meehan et al. (1989) presented techniques for the design and analysis of interference tests when both the active and observation well are intercepted by hydraulic fractures. Their solution is generated for the combined interference problem of finite-conductivity fractures intercepting both active and observation wells (Figure 2.9). Their mathematical model is derived by following similar lines as Cinco-Ley and Meng (1988). For mathematical modeling of the interference test, the concept of superposition is used to include the pressure distribution within the fracture of the active and observation wells. Their solution is modified for different fracture lengths and conductivities. These two parameters are shown to alter the duration and magnitude of fracture interference. Their results proved that, at late times, the effect (contribution) of either a large

natural fracture or a hydraulically fractured well could be approximated by a negative skin at the active well. Their solution also quantifies the effects of azimuth and well spacing. They showed that the pressure response at an active well is not sensitive to the pressure of the observation well for $r_D \geq 2$.

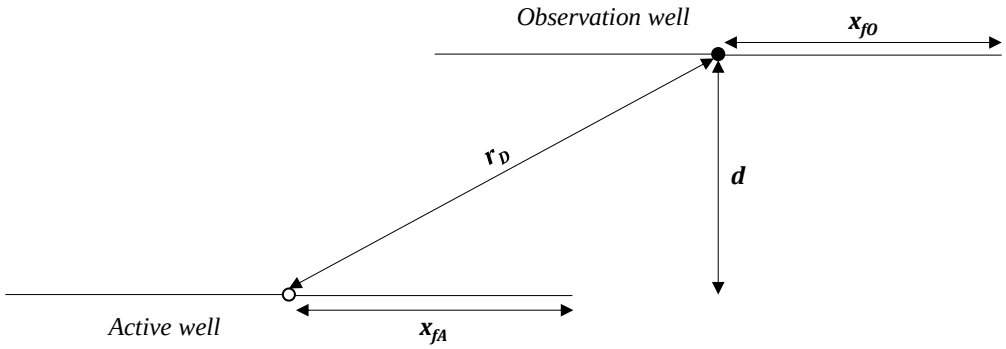

Figure 2.9. Interference test with two vertically-fractured wells (Meehan et al. 1989).

2.5. Interference Tests with Horizontal Wells

Al-Khamis et al. (2001) modeled a semi-analytical solution for interference tests with horizontal wells. Their model considered two horizontal wells (active and observation wells) in the same coordinate system (Figure 2.10) and incorporated the effect of wellbore hydraulics. Later, Al-Khamis et al. (2005) used this model to analyze the effects of horizontal and vertical separation between the wells, skin factors, permeability anisotropy, azimuth angles, and wellbore-hydraulics on the interference test. Their analysis indicated that the theory of interference tests between two vertical wells is not always valid for interference testing between two horizontal wells. Similarly, the horizontal observation well responses do not follow the exponential integral solution. They also showed that if the distance between the two wells is large enough, then the geometry of both wells may be ignored and the exponential integral solution may be used to analyze horizontal-well interference test responses. They provide a useful formula to calculate the effective radial distance between the wells to apply the exponential integral approximation correctly.

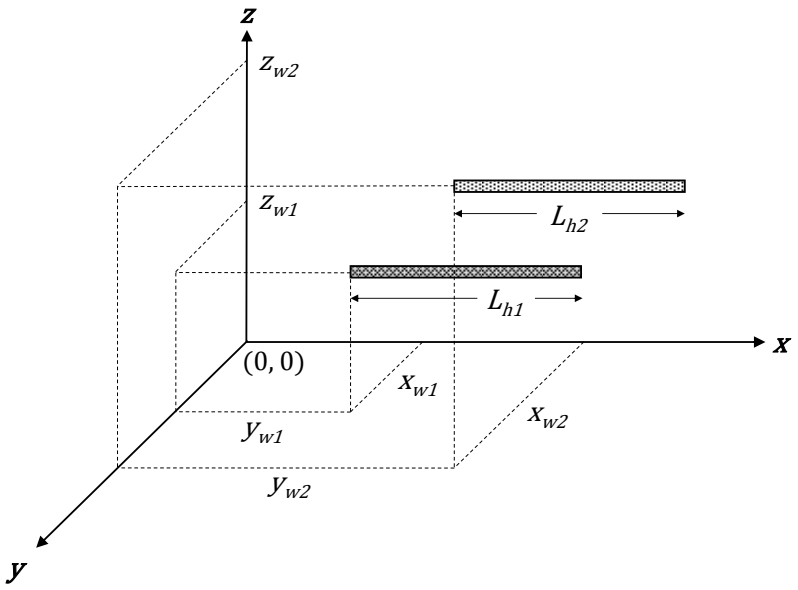

Figure 2.10. Horizontal well configuration for the first model, 3-D view (Al-Khamis et al. 2001).

2.6. Interference Analysis in Shale Reservoirs

Ajani and Kelkar (2012) reviewed the fracture and production data of 179 wells in the Woodford Shale of the Arkoma Basin to quantify the impact of interference between wells on their performances. First, to quantify the impact after addition of an infill well, they defined an ellipse around it. The impact was identified by the change in the offset wells' gas production trend after putting an infill well into production. Secondly, the decline rates for all impacted wells were calculated by using the method of least squares before when they were impacted. The production decline is therefore calculated by using Arps' exponential decline. The difference between the predicted and the actual rates represents the impact. Ajani and Kelkar showed two major factors that cause interference effects: how long the well has been in production and the distance of an offset well from the production well.

To obtain the optimum well spacing, Ajani and Kelkar (2012) plotted sixty days of initial production (IP) per lateral length and showed the relationship between normalized IP versus effective distance. Their observations showed that the normalized IP is strongly correlated to the

equivalent distance. Interference between wells causes the IP of the well to decline as the distances between wells decrease. However, their analysis to find the optimum well spacing still needs to be coupled with economic considerations since it requires more than two wells to be drilled.

Yaich et al. (2014) discussed the existence of well interference and its impact using real production and pressure data from the Marcellus Shale. They studied the interference effect of fractured horizontal wells to optimize the well spacing and ultimately the economics of field development. They considered three scenarios of communication between fractured horizontal wells (Figure 2.11): communication through fractures intercepting both wells, communication because of the overlap of the SRV's of the wells, and communication because of both natural fractures intercepting the wells and overlapping SRVs. Their approach led to a well spacing suggestion that would optimally produce the Marcellus Shale.

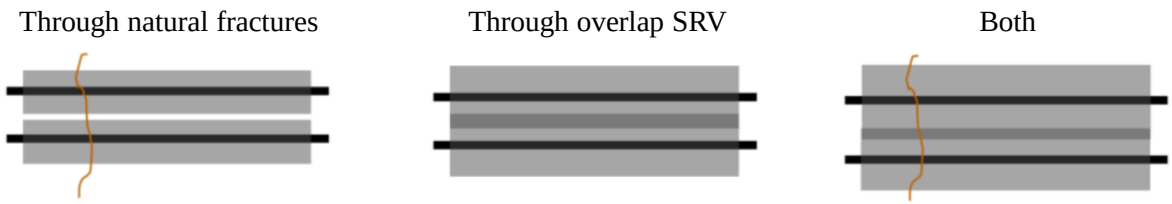

Figure 2.11. Interference mediums in shale reservoirs (Yaich et al. 2014).

CHAPTER 3

MATHEMATICAL MODEL

To develop the semi-analytical solution for this study, the reservoir is assumed to be an anisotropic but homogeneous reservoir of thickness *h*. The flow is single phase and isothermal. The fluid is assumed to have a constant compressibility, *c*, and constant viscosity, μ. The reservoir pressure is initially uniform and equal to p_i. For the analysis of gas wells, the calculation follows the approach of Al-Hussainy et al. (1966) and incorporates their liquid-flow analogy through the pseudo-pressure transformation, given by

$$m(p) = 2\int_{p_b}^{p} \frac{p'}{\mu z} dp' \tag{3.1}$$

In the following mathematical derivation, the fluid flow takes place in a dual-porosity reservoir consisting of matrix and natural fractures (see Figure 2.1 and Figure 2.2). The flow from reservoir to the wellbore, however, is only through the hydraulic fractures (it can also be through the wellbore if it is opened or perforated). The mathematical model considers a finite-conductivity fracture in a dual-porosity reservoir which follows the same lines as Cinco-Ley and Meng (1988), a semi-analytical solution for a fractured horizontal well which follows the same lines as Chen and Raghavan (1997), and an interference test physical model which applies the superposition theorem and follows the same lines as Meehan et al. (1989) and Al-Khamis (2003). The final semi-analytical solution can be readily modified to obtain other solutions that include open horizontal wells following the general guidelines of the use of the semi-analytical solution.

Figure 3.1 shows a sketch of the system considered in this study. Two fractured horizontal wells are parallel and aligned with the permeability in the *y*-direction, whereas the fractures are parallel and aligned with the permeability in the *x*-direction. The convention in this study is that

Well A is the active well and Well O is the observation well. The lengths of the active and observation wells are L_{hA} and L_{hO}, respectively, which are assumed to be equal for the purposes of this study, and the fractures are equally spaced along the horizontal wells. The coordinates of the center of the first hydraulic fracture (i.e., closest to the heel of the horizontal well) are denoted by x_{wi}, y_{wi}, z_{wi} for $i = A$ or O. For the case of a closed rectangular reservoir, the dimensions of the reservoir are x_e and y_e in the x and y directions. The fracture half-length is denoted by x_F and the distance between the two outermost fractures (center to center) is denoted by D_i for $i = A$ or O. The fracture half-length is uniform for each well but can be distinct between the active and observation wells. All the solutions are in the Laplace space, which allows us to easily implement the variable rate production condition and dual-porosity formulation (Ozkan and Raghavan 1991a, 1991b). These solutions will be inverted back numerically to the time domain by using Stehfest's (1970) algorithm.

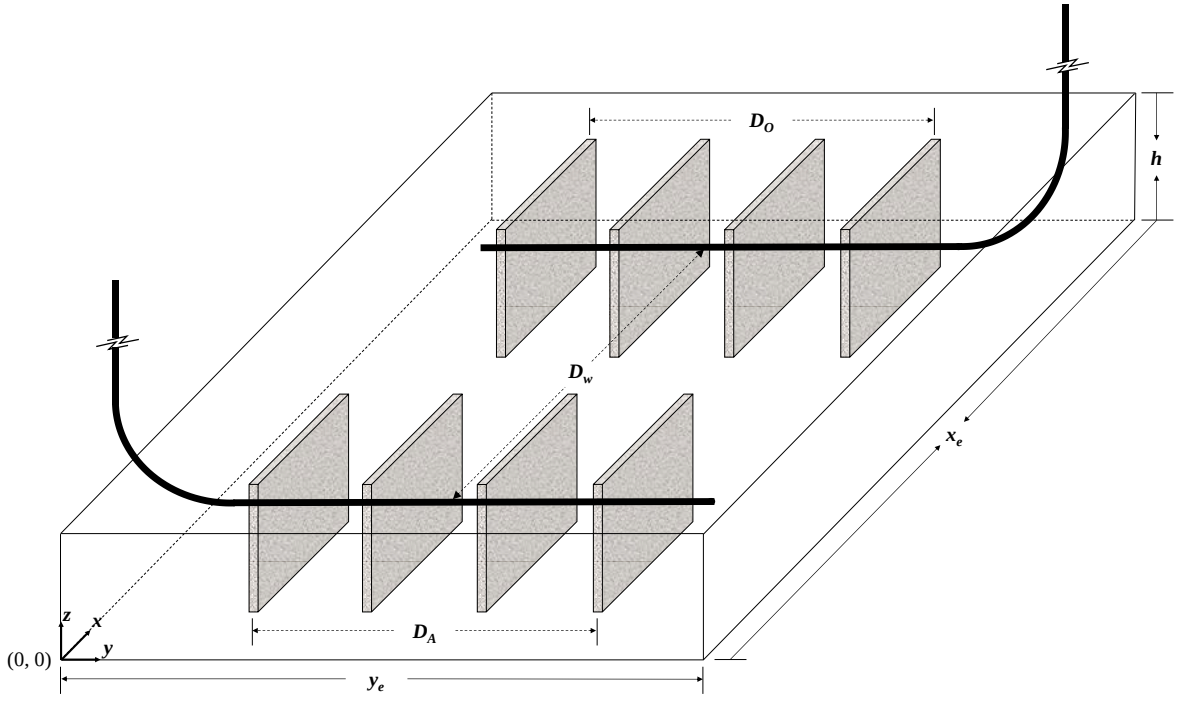

Figure 3.1. Schematic of two fractured horizontal wells in the same coordinate system.

The solution is extended to the case with a conductive natural fracture crossing both the active and observation wells. This crossing fracture is treated as an asymmetric finite-conductivity fracture in the model. The horizontal wellbore will also be opened to consider another type of well completion. The pertinent solutions for this particular option are given by Ozkan (1988).

3.1. Dimensionless Variables

For convenience and generality, all equations are expressed in dimensionless variables. These dimensionless variables are used for both the active and observation wells. Dimensionless pressures (for the case of constant production rate), dimensionless rate (for the case of constant wellbore pressure), and dimensionless time are defined, respectively, by

$$p_D\left(x_D, y_D, t_D\right) = \frac{kh}{\alpha q B \mu}\left[p_i - p\left(x, y, t\right)\right] \tag{3.2}$$

$$q_D\left(t_D\right) = \frac{\alpha B \mu}{kh\Delta p} q\left(t\right) \tag{3.3}$$

and

$$t_D = \frac{\beta k t}{\phi \mu c L^2} \tag{3.4}$$

where α and β are the constants defined, respectively, by

$$\alpha = \begin{cases} 1/2\pi & \textit{for consistent unit} \\ 141.2 & \textit{for field unit} \end{cases} \tag{3.5}$$

$$\beta = \begin{cases} 1 & \textit{for consistent unit} \\ 6.329\times10^{-3} & \textit{for field unit with t in days} \end{cases} \tag{3.6}$$

Dimensionless fracture conductivity is defined by

$$C_{FD} = \frac{k_F w_F}{kL} \tag{3.7}$$

The reference length, L, is recommended to be the longest dimension of the well-fracture system.

For a fractured horizontal well, the reference length is $D/2$, where D is the distance between the two outermost fractures. The reservoir permeability k is the average of the permeabilities in x, y, and z directions $\left(k = \sqrt{k_x k_y k_z}\right)$. The dimensionless distances in x, y, and z directions are defined by

$$x_D = \frac{x}{L}\sqrt{\frac{k}{k_x}}, \quad y_D = \frac{y}{L}\sqrt{\frac{k}{k_y}}, \quad z_D = \frac{z_w + r_w}{h} \tag{3.8}$$

The dimensionless variables of the well position (heel of the horizontal well) and the dimensions of the reservoir are defined by the following expressions, respectively:

$$x_{wD} = \frac{x_w}{L}\sqrt{\frac{k}{k_x}}, \quad y_{wD} = \frac{y_w}{L}\sqrt{\frac{k}{k_y}}, \quad z_{wD} = \frac{z_w}{h} \tag{3.9}$$

and

$$x_{eD} = \frac{x_e}{L}\sqrt{\frac{k}{k_x}}, \quad y_{eD} = \frac{y_e}{L}\sqrt{\frac{k}{k_y}}, \quad z_{eD} = \frac{z_e}{L}\sqrt{\frac{k}{k_z}} \tag{3.10}$$

The expressions for the dimensionless horizontal well length, fracture half-length, and wellbore radius are as follows, respectively:

$$L_{hD} = \frac{L_h}{2L}\sqrt{\frac{k}{k_z}}, \quad x_{FD} = \frac{x_F}{L}\sqrt{\frac{k}{k_x}}, \quad r_{wD} = \frac{r_w}{h} \tag{3.11}$$

The other dimensionless variables used in this thesis (dimensionless distance between the two outermost fractures and distance between two wells) are defined, respectively, by

$$D_D = \frac{D}{L}\sqrt{\frac{k}{k_y}} \tag{3.12}$$

and

$$D_{wD} = \frac{D_w}{L}\sqrt{\frac{k}{k_x}} \tag{3.13}$$

3.2. Finite-Conductivity Fracture

To model a finite-conductivity fracture, a single vertical fracture with finite width is considered. The fracture is assumed to be a homogeneous porous medium of uniform properties with height h, width w_F, and half-length x_F (Figure 3.2). It intersects the wellbore, which allows the fluid to flow in a more conductive path in a dual-porosity system.

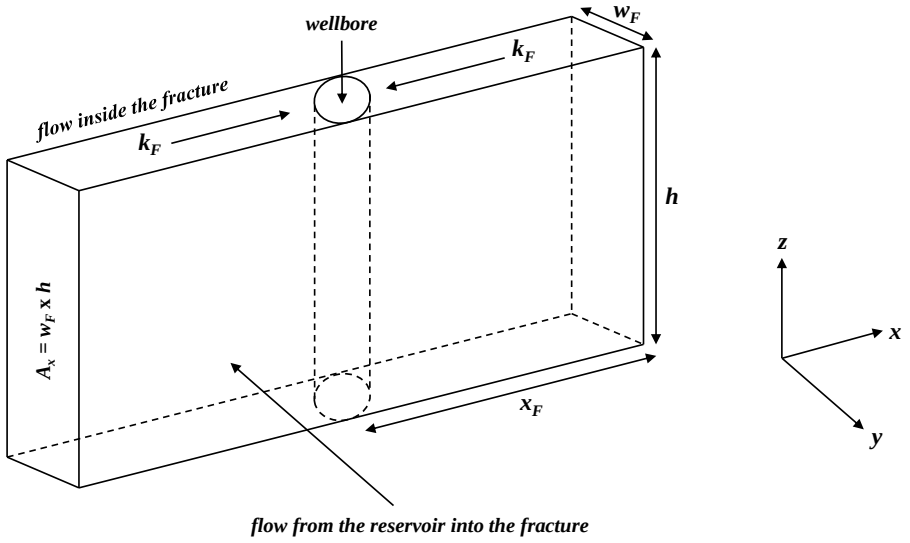

Figure 3.2. Schematic of a fully-penetrating and finite-conductivity fracture in a vertical well (Ozkan et al. 2009).

Since the fracture length is considerably longer than the fracture width ($x_F \gg w_F$), fluid flow through the fracture tips may be neglected. Thus, for all practical purposes, flow from the reservoir to the fracture is assumed to be perpendicular to the fracture surface (y direction). The details of the mathematical derivation of reservoir pressure and flow within the fracture are provided by Cinco-Ley and Meng (1988). Their solution for a vertically-fractured well is adopted in this study to provide the finite-conductivity fracture solution in a horizontal well. The following is the derivation to obtain the solution for the considered cases in this study. The reservoir pressure solution for a plane source representing the hydraulic fracture surface in an infinite reservoir is given by:

$$\bar{p}_{FD,inf}\left(x_D, y_D, s\right) = \frac{1}{2x_{FD}}\sqrt{\frac{k_z}{k}}\int_{-x_{FD}}^{+x_{FD}} \bar{q}_{FD}\left(\alpha, s\right) K_0\left[\sqrt{\left(x_D - x_{wD} - \alpha\right)^2 + \left(y_D - y_{wD}\right)^2}\sqrt{u}\right] d\alpha \tag{3.14}$$

In (3.14), $u = sf\left(s\right)$ is a parameter that incorporates the dual-porosity formulation, where *s* denotes the Laplace transform parameter and $f\left(s\right)$ is the transfer function between matrix and fracture, defined by

$$f\left(s\right) = \begin{cases} 1 & \textit{for homogeneous reservoir} \\ \dfrac{\omega s\left(1-\omega\right)+\lambda}{s\left(1-\omega\right)+\lambda} & \textit{for pseudosteady dual - porosity reservoir} \\ 1+\sqrt{\lambda'\omega'/3s}\tanh\left(\sqrt{3\omega' s/\lambda'}\right) & \textit{for transient dual - porosity reservoir} \end{cases} \tag{3.15}$$

The pressure solution in the fracture medium is given by

$$\bar{p}_{wD} - \bar{p}_{FD,inf} = \frac{\pi}{C_{FD}}\left[\frac{x_D}{s} - \int_{x_{wD}}^{x_D}\int_{x_{wD}}^{x_D'} \bar{q}_{FD}\left(x_D''\right) dx_D'' dx_D'\right] \tag{3.16}$$

Combining (3.14) and (3.16) yields

$$\begin{aligned} \bar{p}_{wD} - \frac{1}{2x_{FD}}\sqrt{\frac{k_z}{k}}\int_{-x_{FD}}^{+x_{FD}} \bar{q}_{FD}\left(\alpha, s\right) K_0\left[\sqrt{\left(x_D - x_{wD} - \alpha\right)^2 + \left(y_D - y_{wD}\right)^2}\sqrt{u}\right] d\alpha \\ + \frac{\pi}{C_{FD}}\int_{x_{wD}}^{x_D}\int_{x_{wD}}^{x_D'} \bar{q}_{FD}\left(x_D''\right) dx_D'' dx_D' = \frac{\pi x_D}{C_{FD} s} \end{aligned} \tag{3.17}$$

The integration limit in (3.17) may be changed from $\left[-x_{FD}, +x_{FD}\right]$ to $\left[0, x_{FD}\right]$ but is only applicable to a single-well system with symmetric hydraulic fractures. For interference problems, in which there are at least two wells involved, this symmetrical approach cannot be used (Meehan et al. 1989).

(3.17) is the solution for a finite-conductivity fracture in an infinite reservoir. Numerical evaluation of (3.17) requires discretization of the hydraulic fractures. Figure 3.3 shows the

discretization of the length of a fracture into *m* segments (the number of segments of fracture half-length at both sides must be equal).

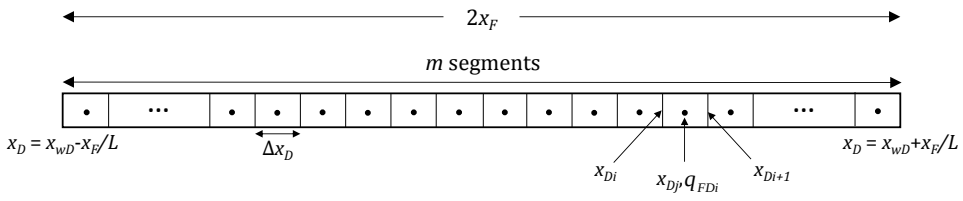

Figure 3.3. Discretization of total fracture length ($2x_F$) into m segments.

The term q_{FDi} (or in Laplace space, $\bar{q}_{FDi}$) is the flux at the center of the fracture element extending between x_{Di} and x_{Di+1}. After discretization, (3.14) can be expressed as follows

$$\frac{1}{2x_{FD}}\sqrt{\frac{k_z}{k}}\int_{-x_{FD}}^{+x_{FD}}\bar{q}_{FD}(\alpha,s)K_0\left[\sqrt{(x_D-x_{wD}-\alpha)^2+(y_D-y_{wD})^2}\sqrt{u}\right]d\alpha = \frac{1}{2x_{FD}}\sqrt{\frac{k_z}{k}}\sum_{i=1}^{m}\bar{q}_{FDi}(s)\int_{x_{Di}}^{x_{Di+1}}K_0\left[\sqrt{(x_{Dj}-x_{wD}-\alpha)^2+(y_D-y_{wD})^2}\sqrt{u}\right]d\alpha \tag{3.18}$$

where x_{Di} and x_{Di+1} are the beginning and the end of the *i*-th segment. The integral part of (3.16) can also be approximated as follows:

$$\int_{x_{wD}}^{x_{Dj}}\int_{x_{wD}}^{x_D'}\bar{q}_{FD}(x_D'')dx_D''dx_D' = \sum_{i=1}^{j-1}\bar{q}_{FDi}(s)\left[\frac{(\Delta x_D)^2}{2}+\Delta x_D(x_{Dj}-i\Delta x_D)\right]+\frac{(\Delta x_D)^2}{8}\bar{q}_{FDj}(s) \tag{3.19}$$

Equations (3.18) and (3.19) assume segments of equal length and consider x_{Dj} as the midpoint of the *j*-th segment. Combining (3.17) with (3.18) and (3.19) yields

$$\bar{p}_{wD}-\frac{1}{2x_{FD}}\sqrt{\frac{k_z}{k}}\sum_{i=1}^{m}\bar{q}_{FDi}(s)\int_{x_{Di}}^{x_{Di+1}}K_0\left[\sqrt{(x_{Dj}-x_{wD}-\alpha)^2+(y_D-y_{wD})^2}\sqrt{u}\right]d\alpha + \frac{\pi}{C_{FD}}\sum_{i=1}^{j-1}\bar{q}_{FDi}(s)\left[\frac{(\Delta x_D)^2}{2}+\Delta x_D(x_{Dj}-i\Delta x_D)\right]+\frac{(\Delta x_D)^2}{8}\bar{q}_{FDj}(s)=\frac{\pi x_{Dj}}{C_{FD}s} \tag{3.20}$$

If (3.20) is written for every fracture segment, it constitutes *m* equations for $(m+1)$ unknowns,

$\bar{q}_{FDi}$ and $\bar{p}_{wD}$. An additional equation is obtained by considering that the sum of the fluxes is equal to the total flow rate and given, in dimensionless form, as follows:

$$\sum_{i=1}^{m} \bar{q}_{FDi} = \frac{m}{s} \tag{3.21}$$

The unknowns are found by solving the system of equations

$$\left[a_{i,j}\right]\begin{bmatrix} \bar{q}_{FDi}(s) \\ \bar{p}_{wD}(s) \end{bmatrix} = \left[b_j\right] \tag{3.22}$$

or

$$\begin{bmatrix} a_{1,1} & a_{1,2} & . & . & . & a_{1,m} & 1 \\ a_{2,1} & a_{2,2} & . & . & . & a_{2,m} & 1 \\ a_{3,1} & a_{3,2} & . & . & . & a_{3,m} & 1 \\ . & . & . & . & . & . & . \\ . & . & . & . & . & . & . \\ a_{m,1} & a_{m,2} & . & . & . & a_{m,m} & 1 \\ 1 & 1 & . & . & . & 1 & 0 \end{bmatrix} \times \begin{bmatrix} \bar{q}_{FD1}(s) \\ \bar{q}_{FD2}(s) \\ \bar{q}_{FD3}(s) \\ . \\ . \\ \bar{q}_{FD(m)}(s) \\ \bar{p}_{wD}(s) \end{bmatrix} = \begin{bmatrix} \pi x_{D1}/C_{FD}s \\ \pi x_{D2}/C_{FD}s \\ \pi x_{D3}/C_{FD}s \\ . \\ . \\ \pi x_{Dm}/C_{FD}s \\ m/s \end{bmatrix} \tag{3.23}$$

The principal advantage of this algorithm is that the system eliminates the necessity of time discretization since it is in Laplace space. After some time, however, the flux distribution stabilizes and becomes independent of time. It must be noted that (3.23) represents the well response for constant rate production. If it is desired to consider constant wellbore pressure production, the solution for $\bar{q}_D$ can be obtained by using $\bar{p}_{wD}$ from (3.23) in the following convolution relationship noted by van Everdingen and Hurst (1949), given by

$$\bar{p}_{wD}\bar{q}_D = \frac{1}{s^2} \tag{3.24}$$

For a fracture in a closed rectangular reservoir, the reservoir pressure distribution solution is more complex. The solution for this particular case may be obtained by integrating the point-source solution derived by Ozkan (1988). The appropriate solution (Chen and Raghavan 1997) is as follows:

$$\overline{p}_D\left(x_D, y_D\right) = \frac{\pi}{x_{eD}} \int_{-x_{FD}}^{+x_{FD}} \overline{q}_{FD}\left(\alpha, s\right) \left\{ \frac{\left[\cosh\left(\sqrt{u}\, y_{eD1}\right) + \cosh\left(\sqrt{u}\, y_{eD2}\right)\right]}{\in} \right.$$
$$+ \frac{2x_{eD}}{\pi x_{FD}} \sum_{k=1}^{\infty} \frac{1}{k} \sin\left(k\pi \frac{x_{wD1}}{x_{eD}}\right) \cos\left(k\pi \frac{x_{wD2}}{x_{eD}}\right) \cos\left(k\pi \frac{x_D}{x_{eD}}\right) \tag{3.25}$$
$$\left. \frac{\left[\cosh\left(\in_k y_{eD1}\right) + \cosh\left(\in_k y_{eD2}\right)\right]}{\widetilde{\in_k}} \right\} d\alpha$$

where

$$y_{eD1} = y_{eD} - \left(y_D + y_{wD}\right) \tag{3.26}$$

$$y_{eD2} = y_{eD} - \left|y_D - y_{wD}\right| \tag{3.27}$$

$$x_{wD1} = \frac{\left(x_{wD} + \alpha_2\right) - \left(x_{wD} + \alpha_1\right)}{2} \tag{3.28}$$

$$x_{wD2} = \frac{\left(x_{wD} + \alpha_2\right) + \left(x_{wD} + \alpha_1\right)}{2} \tag{3.29}$$

$$\in_k = \sqrt{u + k^2\pi^2 / x_{eD}^2} \tag{3.30}$$

$$\in = \sqrt{u} \sinh\left(\sqrt{u}\, y_{eD}\right) \tag{3.31}$$

$$\in_k = \in_k \sinh\left(\in_k y_{eD}\right) \tag{3.32}$$

Since (3.25) may pose difficulties in calculation for small values of *s* (large times) and for large values of *s* (small times), it needs to be recast as follows (Chen and Raghavan 1997):

$$\overline{p}_D\left(x_D, y_D\right) = \overline{p}_{D,inf} + \overline{p}_{Db1} + \overline{p}_{Db2} + \overline{p}_{Db3} \tag{3.33}$$

Expressions of the terms on the right side of (3.33) are

$$\bar{p}_{D,inf} = \frac{1}{2x_{FD}} \int_{\alpha_1}^{\alpha_2} \bar{q}_{FD}(\alpha, s) K_0 \left[\sqrt{\left(x_D - x_{wD} - \alpha\right)^2 + \left(y_D - y_{wD}\right)^2}\, \sqrt{u} \right] d\alpha \tag{3.34}$$

$$\begin{aligned} \bar{p}_{Db1} = \frac{\pi}{2x_{eD}\sqrt{u}} \int_{\alpha_1}^{\alpha_2} \bar{q}_{FD}(\alpha, s) \Big\{ & \exp\left(-\sqrt{u}\,|y_D + y_{wD}|\right) + \exp\left(-\sqrt{u}\,|y_D - y_{wD}|\right) \\ & + \exp\left[-\sqrt{u}\left(2y_{eD} - |y_D + y_{wD}|\right)\right] + \exp\left[-\sqrt{u}\left(2y_{eD} - |y_D - y_{wD}|\right)\right] \Big\} \\ & \left[1 + \sum_{m=1}^{\infty} \exp\left(-2m\sqrt{u}\, y_{eD}\right)\right] d\alpha \end{aligned} \tag{3.35}$$

$$\begin{aligned} \bar{p}_{Db2} = \frac{\pi}{x_{eD} x_{FD}} \int_{x_{wD} - \alpha_1}^{x_{wD} + \alpha_2} \bar{q}_{FD}(\alpha, s) \sum_{k=1}^{\infty} \frac{\sin\left(k\pi \dfrac{x_{wD1}}{x_{eD}}\right) \cos\left(k\pi \dfrac{x_{wD2}}{x_{eD}}\right) \cos\left(k\pi \dfrac{x_D}{x_{eD}}\right)}{\in_k} \\ \Big\{ \exp\left(-\in_k |y_D + y_{wD}|\right) + \Big\{ \exp\left[-\in_k \left(-2y_{eD} |y_D + y_{wD}|\right)\right] \\ + \exp\left[-\in_k \left(-2y_{eD} |y_D - y_{wD}|\right)\right] \Big\} \left[1 + \sum_{m=1}^{\infty} \exp\left(-2m \in_k y_{eD}\right)\right] \\ + \exp\left(-\in_k |y_D - y_{wD}|\right) \sum_{m=1}^{\infty} \exp\left(-2m \in_k y_{eD}\right) \Big\} d\alpha \end{aligned} \tag{3.36}$$

$$\begin{aligned} \bar{p}_{Db3} = & \frac{1}{2x_{FD}} \int_{\alpha_1}^{\alpha_2} \bar{q}_{FD}(\alpha, s) K_0 \left[\sqrt{\left(x_D + x_{wD} - \alpha\right)^2 + \left(y_D - y_{wD}\right)^2}\, \sqrt{u} \right] d\alpha \\ & + \frac{1}{2x_{FD}} \sum_{k=1}^{\infty} \int_{\alpha_1}^{\alpha_2} \bar{q}_{FD}(\alpha, s) \left[K_0\left(\sqrt{\in_{k1} u}\right) + K_0\left(\sqrt{\in_{k2} u}\right) + K_0\left(\sqrt{\in_{k3} u}\right) + K_0\left(\sqrt{\in_{k4} u}\right) \right] d\alpha \\ & - \pi \exp\left(-\sqrt{u}\,|y_D - y_{wD}|\right) \Big/ \left(x_{eD}\sqrt{u}\right) \end{aligned} \tag{3.37}$$

where

$$\in_{k1} = \left(x_D + x_{wD} + 2kx_{eD} - \alpha\right)^2 + \left(y_D - y_{wD}\right)^2 \tag{3.38}$$

$$\in_{k2} = \left(x_D + x_{wD} - 2kx_{eD} - \alpha\right)^2 + \left(y_D - y_{wD}\right)^2 \tag{3.39}$$

$$\in_{k3} = \left(x_D - x_{wD} + 2kx_{eD} - \alpha\right)^2 + \left(y_D - y_{wD}\right)^2 \tag{3.40}$$

$$\in_{k4} = \left(x_D - x_{wD} - 2kx_{eD} - \alpha\right)^2 + \left(y_D - y_{wD}\right)^2 \tag{3.41}$$

The reformulation of (3.25) noted in (3.34) to (3.37) is an important step in obtaining a robust algorithm for the case of a closed rectangular reservoir; without this reformulation, the solutions will not converge rapidly and accurately during the transient period and late time (Ozkan 1988). For a multiple-fracture system in an infinite reservoir, the only equation used is (3.34), in which the first hydraulic fracture is centered at the origin and is considered the center of the system.

3.3. Multiple-Fracture System

The algorithm to obtain the pressure distribution for a multiple fracture system is similar to that discussed by Raghavan et al. (1997). The basic building block is the algorithm for a single vertical fracture in a rectangular drainage region. In this study, a horizontal well is assumed to have n_F fractures. For an infinite reservoir, the wellbore pressure solution is given as follows:

$$\begin{aligned}\bar{p}_{wD} - \sum_{k=1}^{n_F}\Bigg\{ &\frac{1}{2x_{FD}}\sqrt{\frac{k_z}{k}}\sum_{i=1}^{m}\bar{q}_{FDi,k}(s)\int_{x_{Di,k}}^{x_{Di+1,k}} K_0\left[\sqrt{\left(x_{Dj,k} - x_{wD} - \alpha\right)^2 + \left(y_{D,k} - y_{wD}\right)^2}\sqrt{u}\right] d\alpha \\ &+ \frac{\pi}{C_{FD}}\sum_{i=1}^{j-1}\bar{q}_{FDi,k}(s)\left[\frac{\left(\Delta x_D\right)^2}{2} + \Delta x_D\left(x_{Dj,k} - i\Delta x_D\right)\right] + \frac{\left(\Delta x_D\right)^2}{8}\bar{q}_{FDj,k}(s)\Bigg\} = \frac{\pi x_{Dj,k}}{C_{FD}s}\end{aligned} \tag{3.42}$$

The algorithm to solve (3.42) is described as follows. Let q_{Dk} be the production rate from fracture *k*, then

$$\sum_{k=1}^{n_F} q_{Dk} = 1 \tag{3.43}$$

This study assumes an infinite-conductivity wellbore, which requires identical wellbore pressures at each point where the wellbore intersects the fracture. Thus,

$$p_{wD}\left(t_D\right) = p_{wDk} \tag{3.44}$$

where $k = 1, 2, ..., n$. The wellbore pressure drop may be obtained by convolution and is given by

$$p_{wD}(t_D) = \sum_{k=1}^{n_F} \int_0^{t_D} q_{Dk}(\tau)\, p'_{wDkl}(t_D - \tau)\, d\tau \tag{3.45}$$

Here, the subscript *kl* represents the effect of the fracture at location *k* on the pressure at location *l*. The expression of p_{wDkl} is given in (3.14) and (3.33) for an infinite and a closed rectangular reservoir, respectively. In terms of the Laplace transformation, (3.43) to (3.45) may be written, respectively, as

$$\sum_{k=1}^{n_F} \bar{q}_{Dj} = \frac{1}{s} \tag{3.46}$$

$$\bar{p}_{wD} = \bar{p}_{wDk} \tag{3.47}$$

$$\bar{p}_{wD} = \sum_{k=1}^{n_F} s\bar{q}_{Dk}\, \bar{p}_{wDkl} \tag{3.48}$$

The three equations, (3.46) through (3.48), above are applied to each fracture location and form the matrix equation below.

$$\begin{bmatrix} s\bar{p}_{wD1,1} & s\bar{p}_{wD1,2} & \cdots & s\bar{p}_{wD1,n_F} & -1 \\ s\bar{p}_{wD2,1} & s\bar{p}_{wD2,2} & \cdots & s\bar{p}_{wD2,n_F} & -1 \\ \cdots & \cdots & s\bar{p}_{wDp,q} & \cdots & -1 \\ s\bar{p}_{wDn_F,1} & s\bar{p}_{wDn_F,2} & \cdots & s\bar{p}_{wDn_F,n_F} & -1 \\ s & s & s & s & 0 \end{bmatrix} \begin{bmatrix} \bar{q}_{D1} \\ \bar{q}_{D2} \\ \cdots \\ \bar{q}_{Dn_F} \\ \bar{p}_{wD} \end{bmatrix} = \begin{bmatrix} 0 \\ 0 \\ \cdots \\ 0 \\ 1 \end{bmatrix} \tag{3.49}$$

By solving the matrix equation in (3.49), the wellbore pressure at each time step can be obtained. The basis of this algorithm is similar to the single-fracture algorithm. All fractures are combined into the matrix-vector form, $Ax = B$, by using the superposition theorem.

3.4. Horizontal Line Source Well (Open Horizontal Section)

One option to increase well productivity is to open the surface of the horizontal well to production (perforated or open-hole completion). The solution for this case may be obtained by

integrating the point-source solution derived by Ozkan (1988). For an infinite reservoir, the appropriate solution is as follows:

$$\begin{aligned}\overline{p}_{hD,inf}\left(x_D,y_D,z_D,s\right)=&\frac{1}{2sL_{hD}}\int_{-L_{hD}/2}^{+L_{hD}/2}K_0\left[\sqrt{\left(x_D-x_{wD}-\alpha\right)^2+\left(y_D-y_{wD}\right)^2}\sqrt{u}\right]d\alpha\\&+\frac{1}{sL_{hD}}\sum_{n=1}^{\infty}\cos n\pi z_D\cos n\pi z_{wD}\\&\int_{-L_{hD}/2}^{+L_{hD}/2}K_0\left[\varepsilon_n\sqrt{\left(x_D-x_{wD}-\alpha\right)^2+\left(y_D-y_{wD}\right)^2}\right]d\alpha\end{aligned}\tag{3.50}$$

where

$$\varepsilon_n=\sqrt{u+n^2\pi^2/h_D}\tag{3.51}$$

As in the case of a closed rectangular reservoir, (3.50) is arduous for calculation but it may be recast in the following form for computational convenience:

$$\overline{p}_{hD}\left(x_D,y_D,z_D,s\right)=\overline{p}_{FD}\left(x_D,y_D,s\right)+\overline{F}\left(x_D,y_D,z_D,s\right)\tag{3.52}$$

where $\overline{p}_{FD}$ is the fracture solution, given by

$$\overline{p}_{FD,inf}=\frac{1}{2sL_{hD}}\int_{-L_{hD}/2}^{+L_{hD}/2}K_0\left[\sqrt{\left(x_D-x_{wD}-\alpha\right)^2+\left(y_D-y_{wD}\right)^2}\sqrt{u}\right]d\alpha\tag{3.53}$$

and $\overline{F}$ is defined by

$$\begin{aligned}\overline{F}\left(x_D,y_D,z_D,s\right)=&\frac{1}{s}\left(\frac{2L}{L_h}\sqrt{\frac{k_z}{k}}\right)\sum_{n=1}^{\infty}\cos n\pi z_D\cos n\pi z_{wD}\\&\int_{-L_{hD}/2}^{+L_{hD}/2}K_0\left[\varepsilon_n\sqrt{\left(x_D-x_{wD}-\alpha\right)^2+\left(y_D-y_{wD}\right)^2}\right]d\alpha\end{aligned}\tag{3.54}$$

The computational aspects of (3.53) and (3.54) are addressed in Appendix A.

3.5. Semi-Analytical Solution for Interference Test

To obtain the semi-analytical solution for an interference test with two fractured horizontal wells, the mathematical solution for a fractured horizontal well, (3.49), must be modified to accommodate another well involved in the system. As mentioned earlier, to obtain the dimensionless pressure at a point (x_D, y_D) that results from two fractured horizontal wells, the superposition theorem is used as follows:

$$\bar{p}_D(x_D, y_D, s) = \bar{p}_{D1}(x_D, y_D, s) + \bar{p}_{D2}(x_D, y_D, s) \tag{3.55}$$

In (3.55), superposition takes care of the calculation of intra-well (between fractures in each well) and inter-well (between fractures in both wells) interference in the reservoir. From (3.55), for a multiple-fracture system in an infinite reservoir the dimensionless pressure drop in Laplace space at the active well is

$$\begin{aligned}\bar{p}_{wDA} &- \sum_{k=1}^{n_{FA}}\left\{\frac{1}{2x_{FDA}}\sum_{i=1}^{m_A}\bar{q}_{FDi,kA}(s)\int_{x_{Di,kA}}^{x_{Di+1,kA}} K_0\left[\sqrt{\left(x_{Dj,kA}-x_{wDA}-\alpha\right)^2+\left(y_{D,kA}-y_{wDA}\right)^2}\sqrt{u}\right]d\alpha\right. \\ &+\frac{\pi}{C_{FDA}}\sum_{i=1}^{j-1}\bar{q}_{FDi,kA}(s)\left[\frac{\left(\Delta x_{DA}\right)^2}{2}+\Delta x_{DA}\left(x_{Dj,kA}-i\Delta x_{DA}\right)\right]+\left.\frac{\left(\Delta x_{DA}\right)^2}{8}\bar{q}_{FDj,kA}(s)\right\}=\frac{\pi x_{Dj,kA}}{C_{FDA}s} \\ &+\sum_{k=1}^{n_{FO}}\left\{\frac{1}{2x_{FDO}}\sum_{i=1}^{m_O}\bar{q}_{FDi,kO}(s)\int_{x_{Di,kO}}^{x_{Di+1,kO}} K_0\left[\sqrt{\left(x_{Dj,kO}-x_{wDO}-\alpha\right)^2+\left(y_{D,kO}-y_{wDO}\right)^2}\sqrt{u}\right]d\alpha\right\}\end{aligned} \tag{3.56}$$

Similarly, for the observation well,

$$\begin{aligned}\bar{p}_{wDO} &- \sum_{k=1}^{n_{FO}}\left\{\frac{1}{2x_{FDO}}\sum_{i=1}^{m_O}\bar{q}_{FDi,kO}(s)\int_{x_{Di,kO}}^{x_{Di+1,kO}} K_0\left[\sqrt{\left(x_{Dj,kO}-x_{wDO}-\alpha\right)^2+\left(y_{D,kO}-y_{wDO}\right)^2}\sqrt{u}\right]d\alpha\right. \\ &+\frac{\pi}{C_{FDO}}\sum_{i=1}^{j-1}\bar{q}_{FDi,kO}(s)\left[\frac{\left(\Delta x_{DO}\right)^2}{2}+\Delta x_{DO}\left(x_{Dj,kO}-i\Delta x_{DO}\right)\right]+\left.\frac{\left(\Delta x_{DO}\right)^2}{8}\bar{q}_{FDj,kO}(s)\right\}= \\ &\sum_{k=1}^{n_{FA}}\left\{\frac{1}{2x_{FDA}}\sum_{i=1}^{m_A}\bar{q}_{FDi,kA}(s)\int_{x_{Di,kA}}^{x_{Di+1,kA}} K_0\left[\sqrt{\left(x_{Dj,kA}-x_{wDA}-\alpha\right)^2+\left(y_{D,kA}-y_{wDA}\right)^2}\sqrt{s}\right]d\alpha\right\}\end{aligned} \tag{3.57}$$

If the fractures in both wells are discretized into a different number of segments, $m_A \neq m_O$, and the number of fractures, n_F, is also different for both wells, then (3.56) and (3.57) constitute $\left(m_A * n_{FA} + m_O * n_{FO}\right)$ equations for $\left[\left(m_A * n_{FA} + m_O * n_{FO}\right) + 2\right]$ unknowns. Two additional equations are the total flux equation of the active and observation wells, respectively, defined by

$$\sum_{k=1}^{n_{FA}} \sum_{i=1}^{m_A} \bar{q}_{FDi,kA} = \frac{m_A}{s} \tag{3.58}$$

and

$$\sum_{k=1}^{n_{FO}} \sum_{i=1}^{m_O} \bar{q}_{FDi,kO} = 0 \tag{3.59}$$

In (3.59), the sum of the dimensionless fluxes of the observation well is zero. The unknowns are found by solving the system of equations

$$Ax = B \tag{3.60}$$

Components of the coefficient matrix, A, are given by

$$A = \begin{bmatrix}
a_{1,1} & a_{1,2} & . & . & a_{1,m_A*n_{FA}} & b_{1,1} & b_{1,2} & . & . & b_{1,m_O*n_{FO}} & 1 & 0 \\
a_{2,1} & a_{2,2} & . & . & a_{2,m_A*n_{FA}} & b_{2,1} & b_{2,2} & . & . & b_{2,m_O*n_{FO}} & 1 & 0 \\
. & . & . & . & . & . & . & . & . & . & . & . \\
. & . & . & . & . & . & . & . & . & . & . & . \\
a_{m_A*n_{FA},1} & a_{m_A*n_{FA},2} & . & . & a_{m_A*n_{FA},m_A*n_{FA}} & b_{m_O*n_{FO},1} & b_{m_O*n_{FO},2} & . & . & b_{m_O*n_{FO},m_O*n_{FO}} & 1 & 0 \\
c_{1,1} & c_{1,2} & . & . & c_{1,m_A*n_{FA}} & d_{1,1} & d_{1,2} & . & . & d_{1,m_O*n_{FO}} & 0 & 1 \\
c_{2,1} & c_{2,2} & . & . & c_{2,m_A*n_{FA}} & d_{2,1} & d_{2,2} & . & . & d_{2,m_O*n_{FO}} & 0 & 1 \\
. & . & . & . & . & . & . & . & . & . & . & . \\
. & . & . & . & . & . & . & . & . & . & . & . \\
c_{m_A*n_{FA},1} & c_{m_A*n_{FA},2} & . & . & c_{m_A*n_{FA},m_A*n_{FA}} & d_{m_O*n_{FO},1} & d_{m_O*n_{FO},2} & . & . & d_{m_O*n_{FO},m_O*n_{FO}} & 0 & 1 \\
1 & 1 & . & . & 1 & 0 & 0 & . & . & 0 & 0 & 0 \\
0 & 0 & . & . & 0 & 1 & 1 & . & . & 1 & 0 & 0
\end{bmatrix} \tag{3.61}$$

The solution vector, x, has the following components:

$$x = \left[\bar{q}_{FDA1,1}(s) \quad \bar{q}_{FDA2,1}(s) \quad . \quad . \quad . \quad \bar{q}_{FDO1,1}(s) \quad \bar{q}_{FDAO2,1}(s) \quad . \quad . \quad . \quad \bar{p}_{wDA}(s) \quad \bar{p}_{wDO}(s) \right] \quad (3.62)$$

The components of the right-hand-side vector, *B*, are given by

$$B = \left[\frac{\pi x_{DjA1}}{C_{FDA} s} \quad \frac{\pi x_{DjA2}}{C_{FDA} s} \quad . \quad . \quad \frac{\pi x_{DjAn_{FA}}}{C_{FDA} s} \quad 0 \quad 0 \quad . \quad . \quad 0 \quad \frac{m_A}{s} \quad 0 \right] \quad (3.63)$$

In the coefficient matrix *A*, the definition of each term is similar to what was defined by Meehan et al. (1989) for an interference test with fractured vertical wells. The terms $a_{i,j}$ and $d_{i,j}$ are the pressure drops of the multiple fractures at the active and observation wells, respectively, whereas $b_{i,j}$ and $c_{i,j}$ are the terms that contribute to the effects of the multiple-fracture fluxes of the active well on the wellbore pressure of the observation well and vice versa. Different from common numerical modeling, the coefficient matrix in this study will not be sparse because each element has a "value". Thus each element calculation becomes extremely important and needs to be performed as accurately as possible. Otherwise, the matrix inversion can be singular or badly scaled, which leads to an inaccurate result.

To make the mathematical model applicable to the case of a closed rectangular reservoir, the dimensionless fracture pressure terms in (3.56) and (3.57) need to be modified to the definition given by (3.33). The matrix equation, (3.61) to (3.63), can be modified to obtain the solution for the case in which the horizontal well sections between fractures are open or if a stand-alone fracture crosses both wells. The basic technique can also be extended to the cases not presented in this thesis. Figure 3.4 shows the general guideline of how to use the semi-analytical solution for an interference test with two fractured horizontal wells. An important point to note is that the parameter, *L* (an even integer), controlling the number of terms used in the Stehfest algorithm significantly affects the accuracy of the Laplace inversion process. For the interference test case, it is recommended to use *L* within the range of 6 to 12.

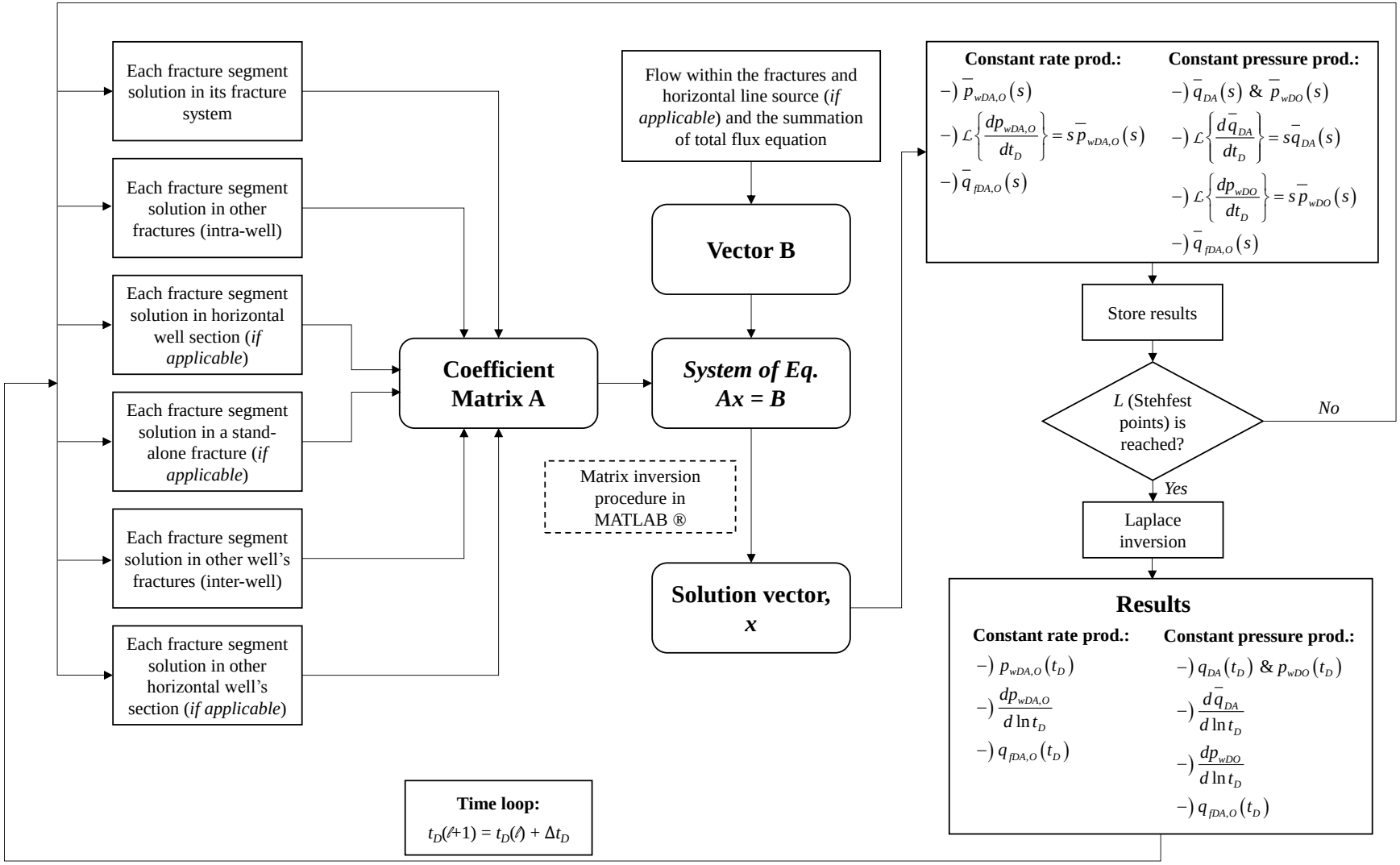

Figure 3.4. Flow chart of general guideline to use semi-analytical solution of interference test with two fractured horizontal wells.

3.6. Model Verification

Since the final solutions are obtained numerically (by discretizing the fractures into segments), the results from the semi-analytical model in this thesis need to be verified. There are some data in the literature that can be used for model verification. However, as mentioned earlier, there is no solution available in the literature for an interference test with two fractured horizontal wells, therefore, only some models are verified in this section.

3.6.1. Model Verification #1: Infinite-Conductivity and Uniform Flux

The first models used for verification are the infinite-conductivity and uniform flux models described by Gringarten et al. (1974). Even though the calculation procedure is relatively simple, it is important to verify the mathematical model since it involves the integral of the modified Bessel function of the second kind of order zero, $\int_{-a}^{+a} K_0\left[f\left(x-a\right)\right]$. Ozkan (1988) provides an evaluation of this integral and recasts it into a form that is convenient for computational purposes. Figure 3.5 shows identical results with Gringarten et al. when using Ozkan's evaluation of the integral.

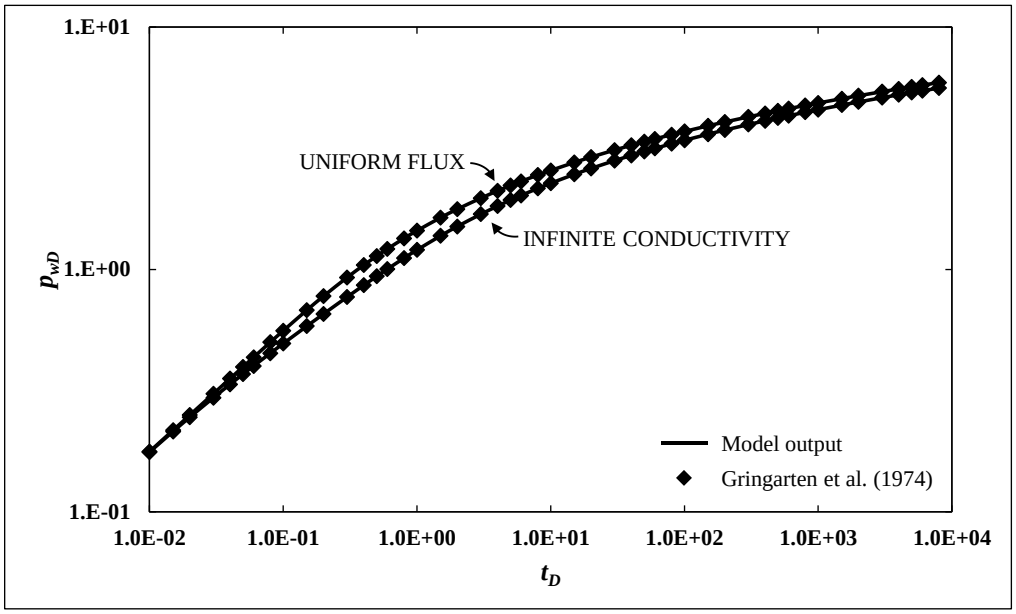

Figure 3.5. Infinite-conductivity and uniform flux model verification compared to Gringarten et al. (1974).

3.6.2. Model Verification #2: Uniform Flux Vertical Fracture in a Closed Rectangular Reservoir

The second model used for verification is Ozkan's (1988) single-segment model in a closed rectangular reservoir. This solution is useful for a case in which there is a vertical fracture crossing a well in a closed rectangular reservoir. This verification is also crucial to verifying the infinite sums, $\sum_{i=1}^{\infty} f(i)$, in (3.36) and (3.37). The computational considerations for these infinite sums and late time calculation are discussed by Greenwood (2015). Figure 3.6 shows the results of the model in this thesis compared to Ozkan's results. The results are nearly identical, and the associated error for this model is approximately 0.1%.

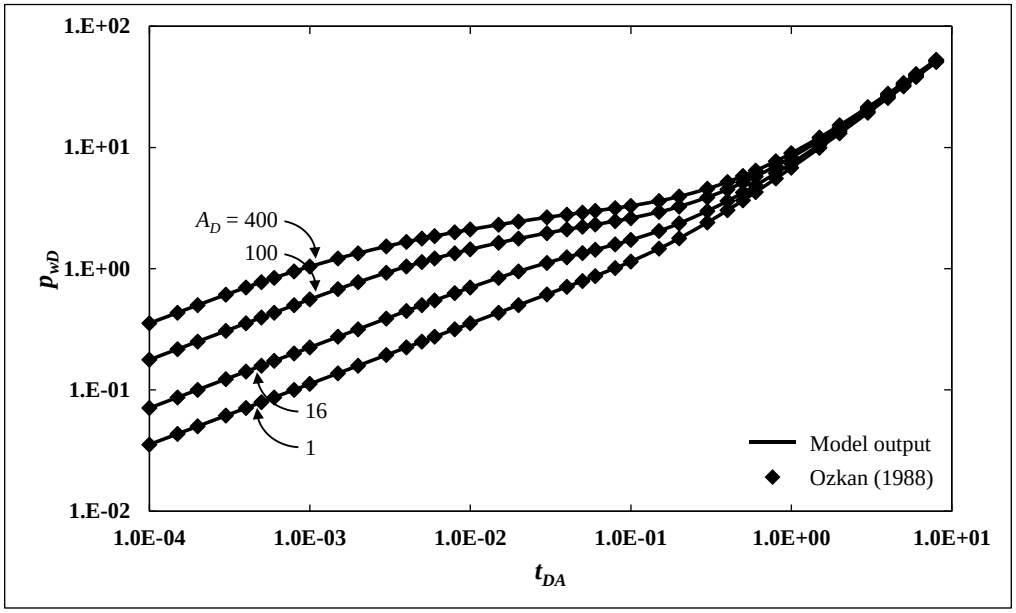

Figure 3.6. Uniform flux vertical fracture in a closed rectangular model verification compared to Ozkan (1988).

In Figure 3.6, the *x*-axis is represented by t_{DA}, instead of t_D, which is defined as

$$t_{DA} = \frac{t_D}{\left(A/x_F^2\right)} \tag{3.64}$$

3.6.3. Model Verification #3: Single Finite-Conductivity Fracture

The third model used for verification is Cinco L. et al.'s (1978) single finite-conductivity fracture in an infinite reservoir. This is crucial to the semi-analytical model in this study since the process of building the computational code mainly starts from this model. Figure 3.7 shows the results in this thesis compared to those of Cinco L. et al.'s solutions. This model, however, is strongly dependent on the fracture segments; lower C_{FD} requires a higher number of fracture segments. The results are in good agreement, and the associated error for this model is approximately 0.6%.

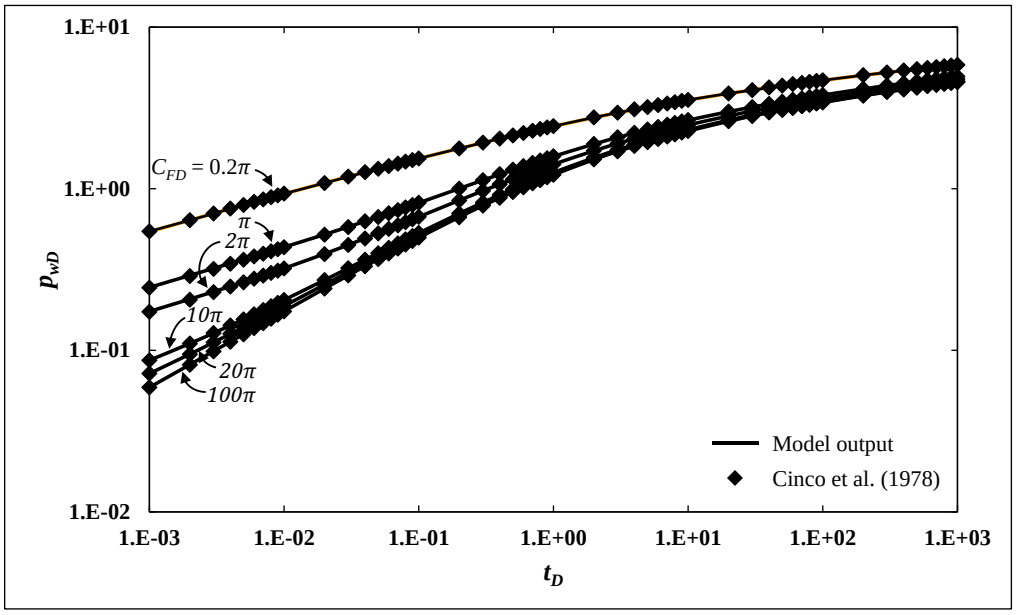

Figure 3.7. Single finite-conductivity fracture in an infinite reservoir model verification compared to Cinco L. et al. (1978).

3.6.4. Model Verification #4: Fractured Horizontal Well in a Closed Rectangular Reservoir

The fourth model used for verification is Chen and Raghavan's (1997) fractured horizontal well solution for finite fracture conductivities and a closed rectangular reservoir. In this case, the horizontal well is positioned at the center of the reservoir and the fractures are equally spaced and parallel to the *x*-axis (Figure 3.8). The data used in the model are shown in Table 3.1 and the results

are shown in Figure 3.9 for pressure transient and Figure 3.10 for rates of fractures. The results in Figure 3.9 are in good agreement, and the associated error for this model is approximately 1%.

The next parameter to be verified is the fracture rates (average of fracture fluxes of each fracture). The verification of fluxes is important since the assumption of symmetrical fractures is not practical in interference analysis. The model output for fracture rates shows a good agreement with Chen and Raghavan (1997), and the associated error for this model is approximately 1%. Figure 3.10 only shows fractures 1 to 3 because fractures 4 and 5 are identical with fractures 2 and 1, respectively.

Table 3.1. Input parameters in model verification #4

Data	
Dimensionless reservoir size in x-direction, x_{eD}	100
Dimensionless reservoir size in y-direction, y_{eD}	80
Number of fractures, n_F	5
Dimensionless distance between two outermost fractures, D_D	20
Combined dimensionless fracture conductivity, C_{FD}	100

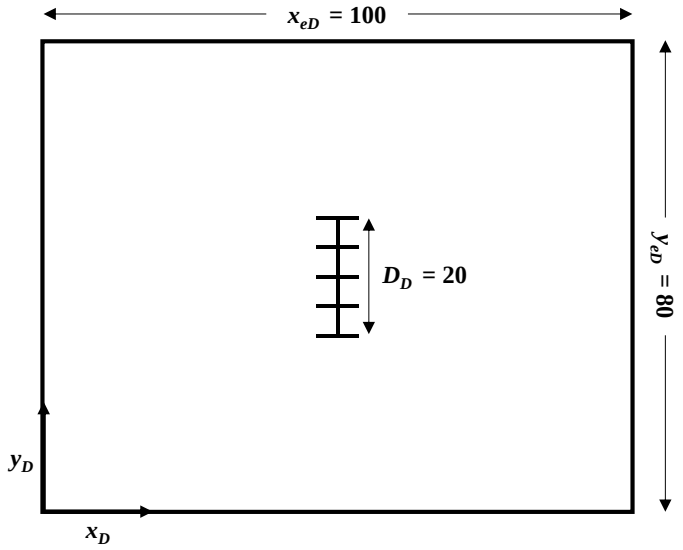

Figure 3.8. Schematic of the well and the reservoir for model verification #4.

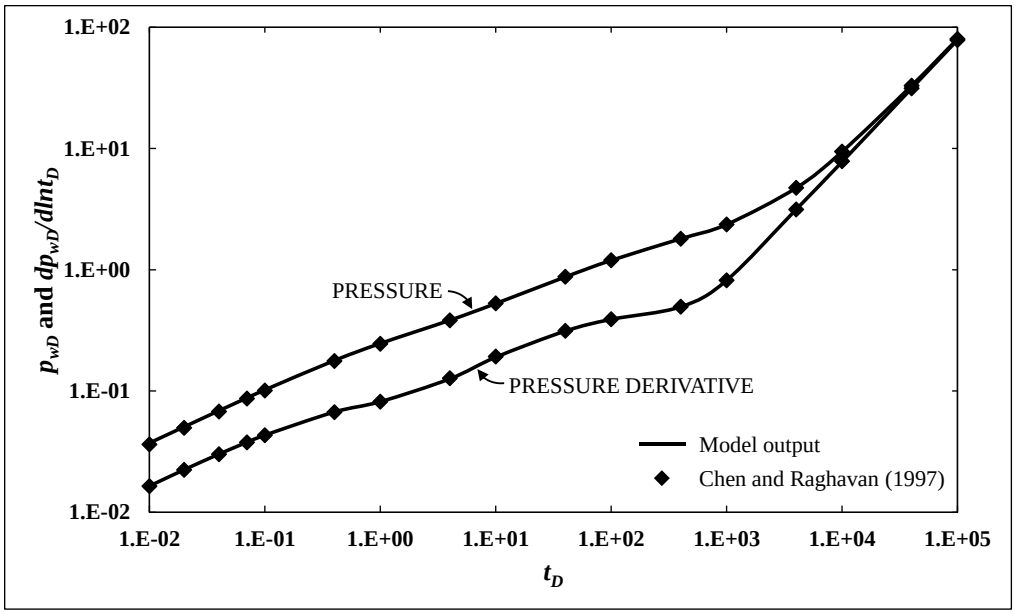

Figure 3.9. Model verification (pressure) compared to Chen and Raghavan (1997).

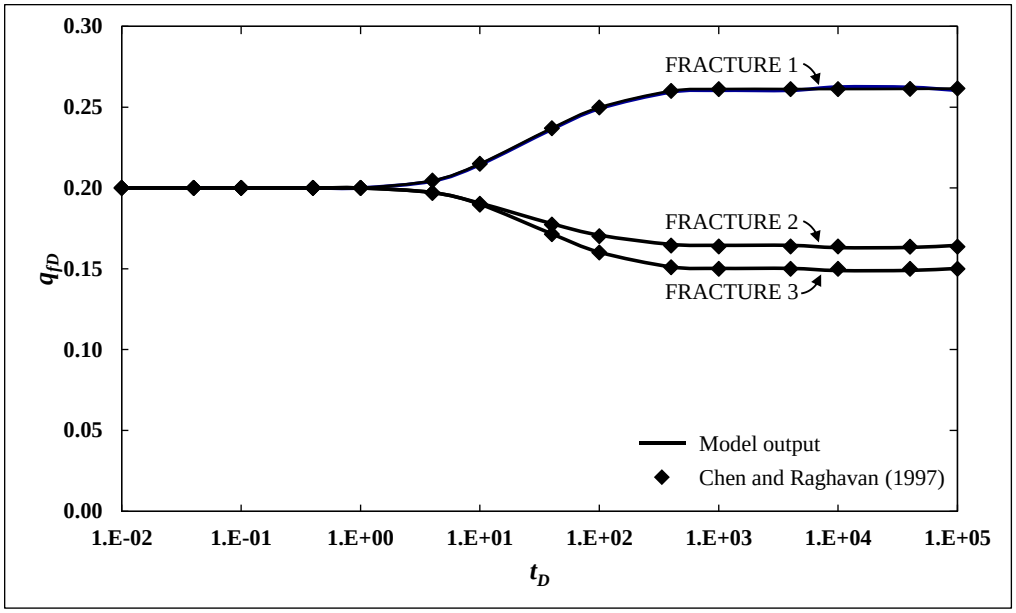

Figure 3.10. Model verification (fractures rate) compared to Chen and Raghavan (1997).

CHAPTER 4

RESULTS AND DISCUSSION

This chapter presents detailed investigations of the results of interference tests with two fractured horizontal wells generated by the semi-analytical model developed in the previous chapter. To understand the general characteristic of the interference test in a low-permeability reservoir, pressure transient responses (pressure and pressure derivative) are generated. The discussion begins with the sensitivity analyses, followed by a series of results from the application of the semi-analytical model to different cases. All of these cases are examined to delineate the pressure-transient characteristics of both the active and observation wells. The cases covered in this thesis are as follows:

- Sensitivities of:
  - Number of hydraulic fractures (n_{FA} and n_{FO})
  - Separation on *x*-direction $\left(\Delta x_{wD}\right)$ or transversal separation
  - Separation on *y*-direction $\left(\Delta y_{wD}\right)$ or longitudinal separation
  - Matrix permeability (k_m)
- Applications:
  - Interference test in a closed rectangular reservoir
  - Open horizontal well sections
  - A stand-alone fracture crossing both active and observation wells

Table 4.1 and Table 4.2 show the basic properties used for all cases in this chapter. The dual-porosity idealization used in this study to model naturally fractured media is the transient model by Kazemi (1969). This idealization is selected because it is more appropriate in a low-permeability reservoir (Brown et al. 2011). Although specific data sets are used, the results are not

limited to the cases discussed in this thesis.

Table 4.1. Reservoir and well data used for semi-analytical solutions

Reservoir and Well Data	
Formation thickness, h (ft)	100
Active horizontal well length, L_{hA} (ft)	4,000
Active horizontal well position (z-direction), z_{wA} (ft)	50
Observation horizontal well length, L_{hO} (ft)	4,000
Observation horizontal well position (z-direction), z_{wO} (ft)	50
Wellbore radius, r_{wA} and r_{wO} (ft)	0.1
Distance between two outermost fractures, D_A and D_O (ft)	4,000

Table 4.2. The properties of hydraulic fractures, matrix, and natural fractures

Hydraulic Fracture, Matrix Properties, and Natural Fractures Data	
Hydraulic fracture permeability, k_F (mD)	1E+05
Hydraulic fracture porosity, ϕ_F	0.2
Hydraulic fracture compressibility, c_{tF} (psi^{-1})	1E-04
Well hydraulic fracture half-length, x_F (ft)	250
Hydraulic fracture width, w_F (ft)	0.1
Matrix permeability, k_m (mD)	1E-05
Matrix porosity, ϕ_m	0.05
Matrix compressibility, c_{tm} (psi^{-1})	1E-06
Matrix block thickness, h_m (ft)	10
Number of matrix blocks, n_m	10
Fracture permeability, k_f (mD)	1,000
Fracture porosity, ϕ_f	0.4
Fracture compressibility, c_{tf} (psi^{-1})	1E-05
Fracture thickness, h_f (ft)	0.001
Number of fractures, n_f	10

The storativity and flow-capacity ratios for the transient dual-porosity model, derived by Serra et al. (1983), are defined, respectively, by

$$\omega = \frac{(\phi c_t)_m h_m}{(\phi c_t)_f h_f} \tag{4.1}$$

$$\lambda = 12\left(\frac{L^2}{h_m^2}\right)\left(\frac{k_m h_m}{k_f h_f}\right) \tag{4.2}$$

Total compressibility (c_t) is the summation of the compressibility of the fluid in the matrix (m), in the fracture (f), or in the hydraulic fractures (F) and the rock compressibility. It is defined by

$$c_t = c_{fluid} S_{fluid} + c_r \tag{4.3}$$

The dimensionless fracture conductivity in this thesis is calculated by using fracture bulk permeability, defined by

$$k_{fb} = k_f \left[h_f / \left(h_f + h_m \right) \right] \tag{4.4}$$

4.1. Sensitivity Analysis 1: Number of Hydraulic Fractures (n_{FA} and n_{FO})

This section examines the pressure transient responses of twin fractured horizontal wells in an infinite reservoir. The typical schematic of these twin wells in an infinite reservoir is shown in Figure 1.5. The dimensionless distance between the wells (D_{wD}) is 0.375 and C_{FD} for both wells is 50. In this case, the active fractured horizontal well produces at a constant rate and the observation well is shut in at the heel (flow in and out of the observation horizontal well and its fractures, however, is permitted). Of interest here is the number of finite-conductivity fractures crossing the horizontal wells, n_F. Figure 4.1 shows the pressure transient responses of the active well, and Figure 4.2 and Figure 4.3 show the pressure transient responses of the observation well. The data for Figure 4.1 to Figure 4.3 are tabulated in Appendix B for those who desire to compare their results with this study. This set of data is useful as a benchmark for numerical model results. Figure 4.4 shows the pressure transient responses of the observation well in which the distance between wells is closer than the base case (D_{wD} = 0.275) in Figure 4.3.

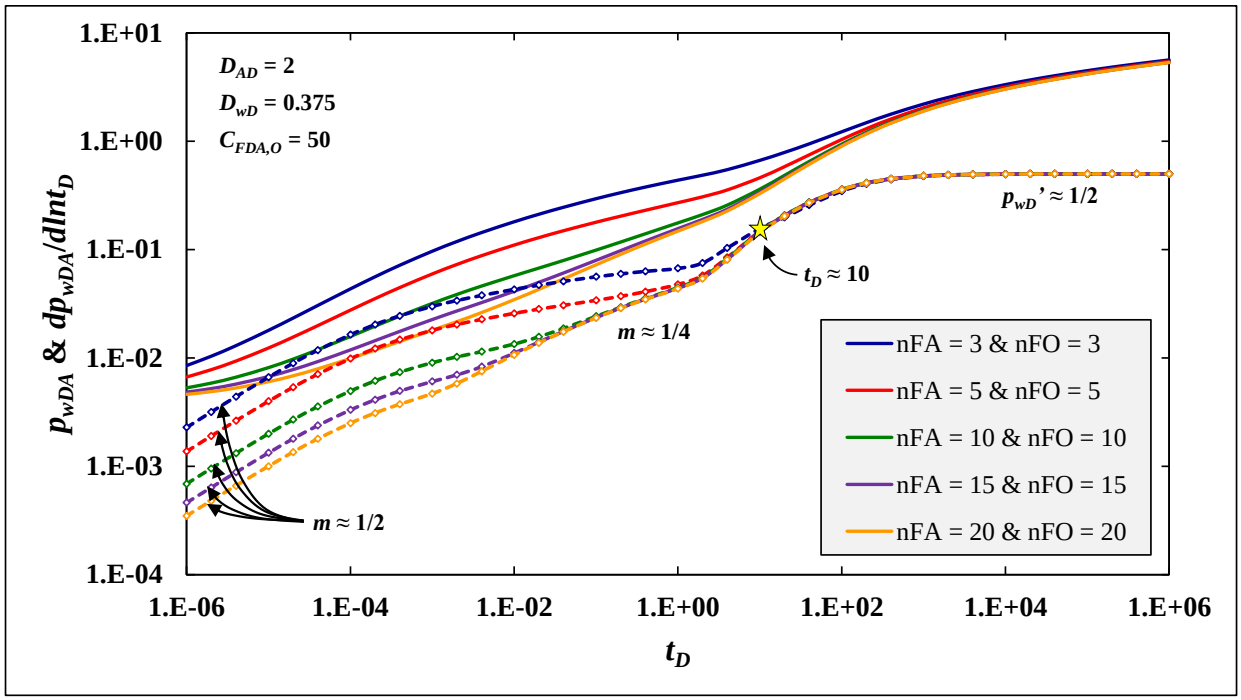

Figure 4.1. Active well responses as a function of the number of hydraulic fractures.

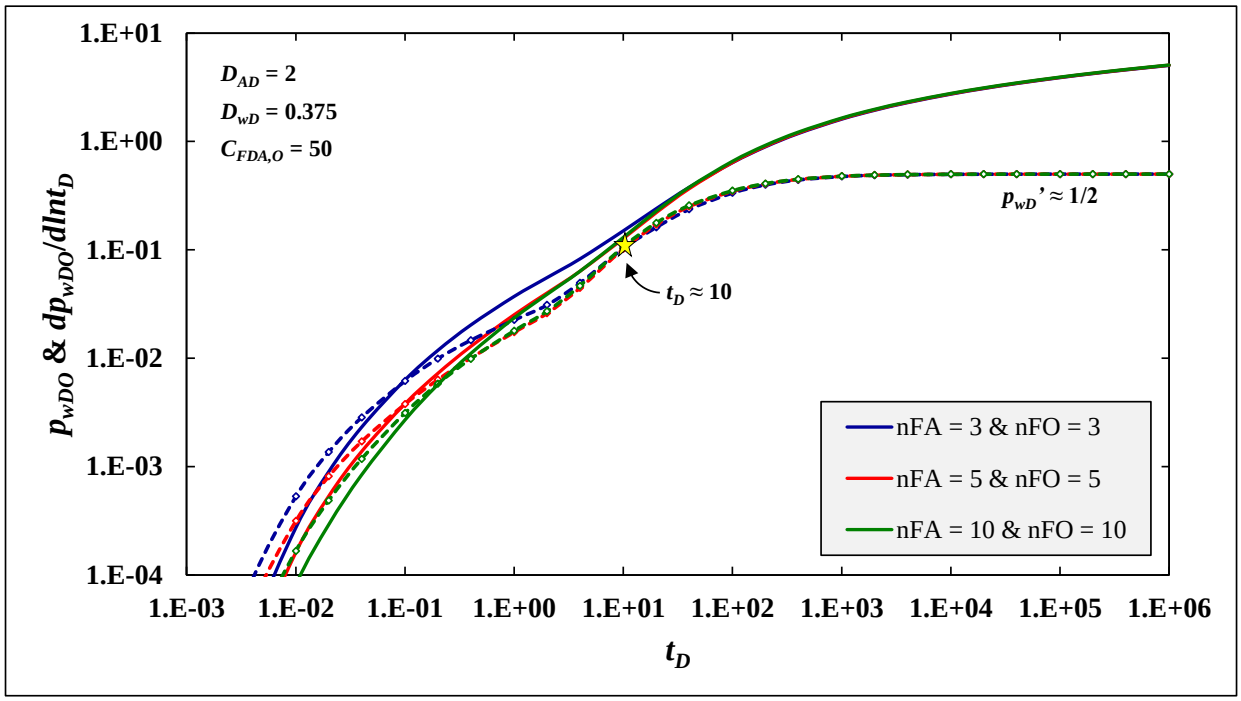

Figure 4.2. Observation well responses as a function of the number of hydraulic fractures (n_{FA} and $n_{FO} \leq 10$).

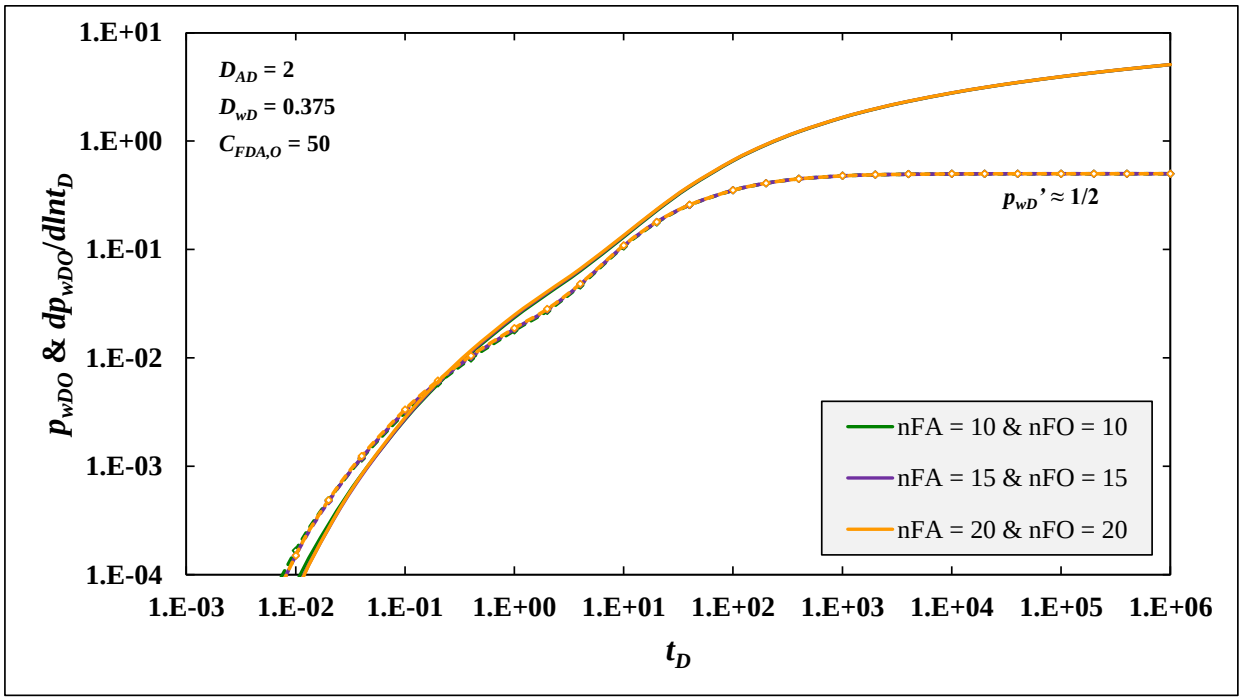

Figure 4.3. Observation well responses as a function of the number of hydraulic fractures (n_{FA} and $n_{FO} \geq 10$) for D_{wD} = 0.375.

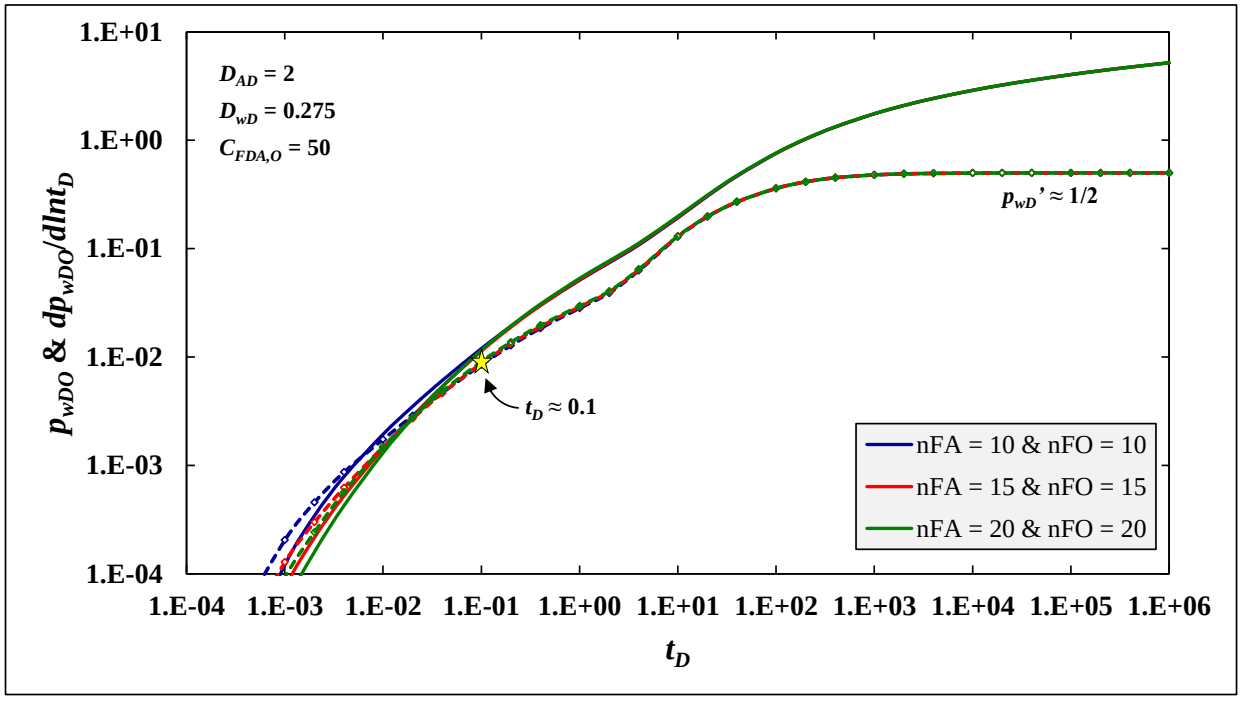

Figure 4.4. Observation well responses as a function of the number of hydraulic fractures (n_{FA} and $n_{FO} \geq 10$) for D_{wD} = 0.275.

As expected, the pressure drop of the active well in Figure 4.1 is lower as n_{FA} increases. This result is consistent with what was presented by Raghavan et al. (1997) in which normalized-effective-radius of fracture and normalized-effective-radius of the system become smaller and the pressure drop differences become lower and less significant as n_{FA} increases. Some flow regime characteristics can be observed from the pressure derivative responses in Figure 4.1. The linear flow ($m \approx 1/2$) occurs in early times ($t_D \leq 10^{-4}$), when the flow is dominated by the flow within the hydraulic fractures. It is followed by the bilinear flow characterized by a 1/4-slope trend. This flow regime period becomes less evident or shorter as n_{FA} decreases. The final flow regime that can be observed is the pseudoradial flow in late times. Before this flow regime, all curves merge for $t_D > 10$ (denoted by a yellow star). The observation also shows that the active well pressure responses do not display any interference disturbance because of the existence of the observation well. In fact, at n_{FA} and $n_{FA} \geq 10$, the effect of the observation well on the active well pressure response becomes more insignificant.

Figure 4.2 displays the pressure responses of the observation well. For $n_{FO} \leq 10$ (3, 5, and 10), the interference responses become more pronounced. The pressure responses merge for $t_D > 10$ (denoted by a yellow star) at the same time in the active well. Before this time, there is a change of slope in the pressure derivative response, which is the characteristic of a transient dual-porosity reservoir in the observation well region. For $n_{FA} \geq 10$ (10, 15, and 20), shown in Figure 4.3, pressure and pressure derivative show similar responses. This can happen because the density of hydraulic fracture in the observation well is high enough to make a fractured horizontal well act like a long-and-conductive single fracture. However, this pressure response similarity is also a function of D_{wD}. Figure 4.4 shows different results for $D_{wD} = 0.275$ at early time ($t_D < 0.1$).

The next thing to be discussed is the flux distribution of the fractures at the active and observation wells. Understanding the flux distribution of each well on an interference test can aid the interpretation of production logs and provide valuable information about the flow convergence toward the hydraulic fractures (Al-Khamis 2003). Theoretically, the fracture flux is uniformly distributed along the finite-conductivity fracture if only one well is involved. In the interference test, the flux distribution becomes more complex due to the presence of an observation well. Figure 4.5 shows the flux distribution in the interference test when n_{FA} and n_{FO} are 3 for $t_D = 10^6$. The u-shaped flux of the active well and the negative-to-positive-shaped flux of the observation well are typical of interference tests with two fractured horizontal wells. Interesting to note here is the flux distribution at the observation well. At the far end of fractures 1 and 3 (large x_D), the fluid is "produced" but coming out at the other end (negative flux). Difference also happens at the active well. The flux at the far end (large x_D) is slightly higher than at the other end because it is supplied by the fractures of the observation well. This is similar to what happens if the interference test involves two horizontal wells that are laterally separated.

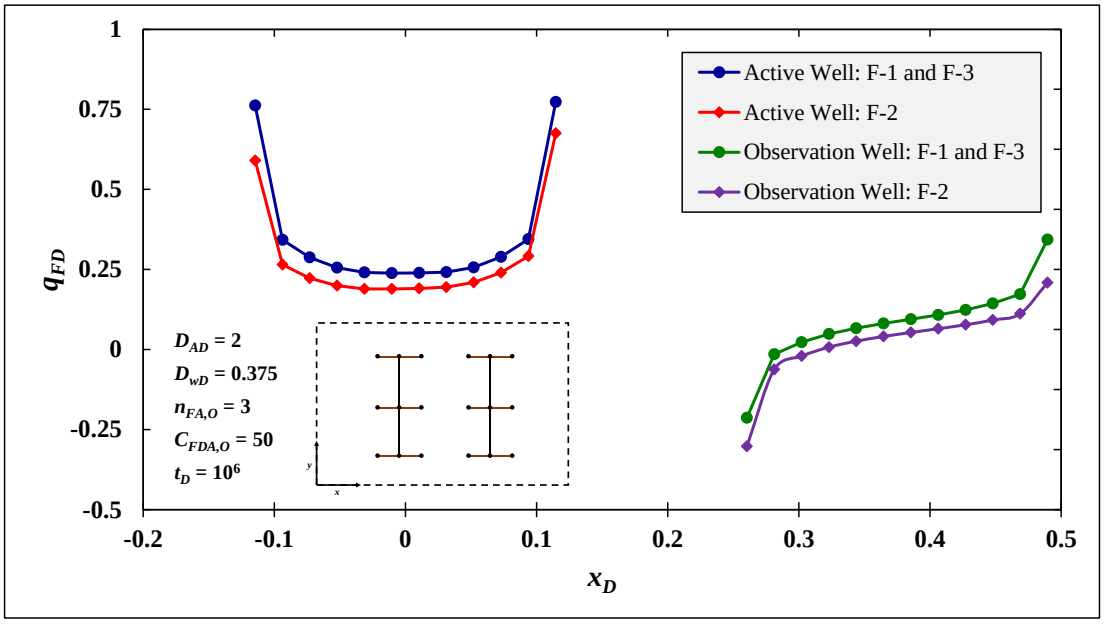

Figure 4.5. Flux distribution along the active and observation well for twin well configuration.

4.2. Sensitivity Analysis 2: Transversal Separation (Δx_{wD})

In this section, pressure responses for different transversal separations are investigated. Figure 4.6 displays the schematic of two fractured horizontal wells separated by a distance, Δx_{wD} (D_{wD} in previous chapters and sections). Here, the effects of transversal separation are investigated by keeping the wells' configuration and properties similar, and there is no longitudinal separation ($\Delta y_{wD} = 0$) between wells. The number of hydraulic fractures (n_{FA} and n_{FO}) is 5 and dimensionless fracture conductivity (C_{FDA} and C_{FDO}) is 50.

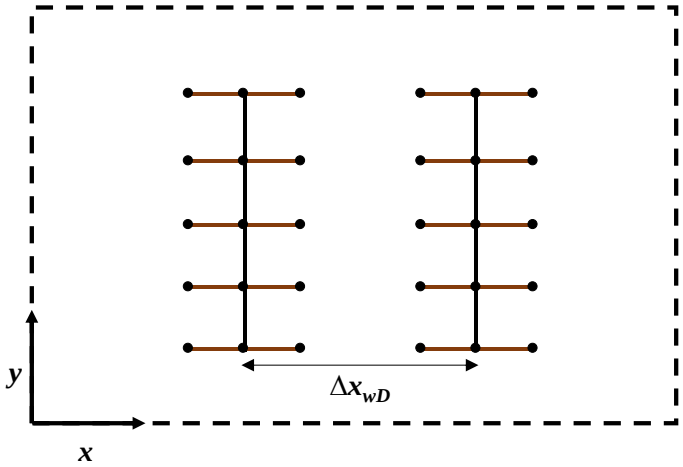

Figure 4.6. Schematic of two fractured horizontal wells separated by a transversal distance, Δx_{wD}.

In this section, the sensitivity shows that the pressure responses at the active well are not influenced by Δx_{wD}. This is similar to what is observed in the previous section in which pressure responses (p_{wD} and $dp_{wD}/dlnt_D$) of the active well are not significantly affected by the existence of the observation well, even though the distance between wells is closer. Similarity (between different cases) in responses may cause difficulties in the analysis. Therefore, the application of the active well type curve in this case cannot yield any information for the interference test; only the properties of the active well may be obtained. On the contrary, transversal separation greatly influences the pressure responses of the observation well (Figure 4.7). The pressure transient responses show more variety in this case than in the previous case (sensitivity of n_{FA} and n_{FO}). As

the transversal separation becomes larger, the test will require a sufficiently longer time to allow the influence of the active well to become noticeable in the observation well. When $\Delta x_{wD} = 1$, the pressure responses of the observation well show no dual-porosity characteristic in which there is a change of slope before the pseudoradial flow.

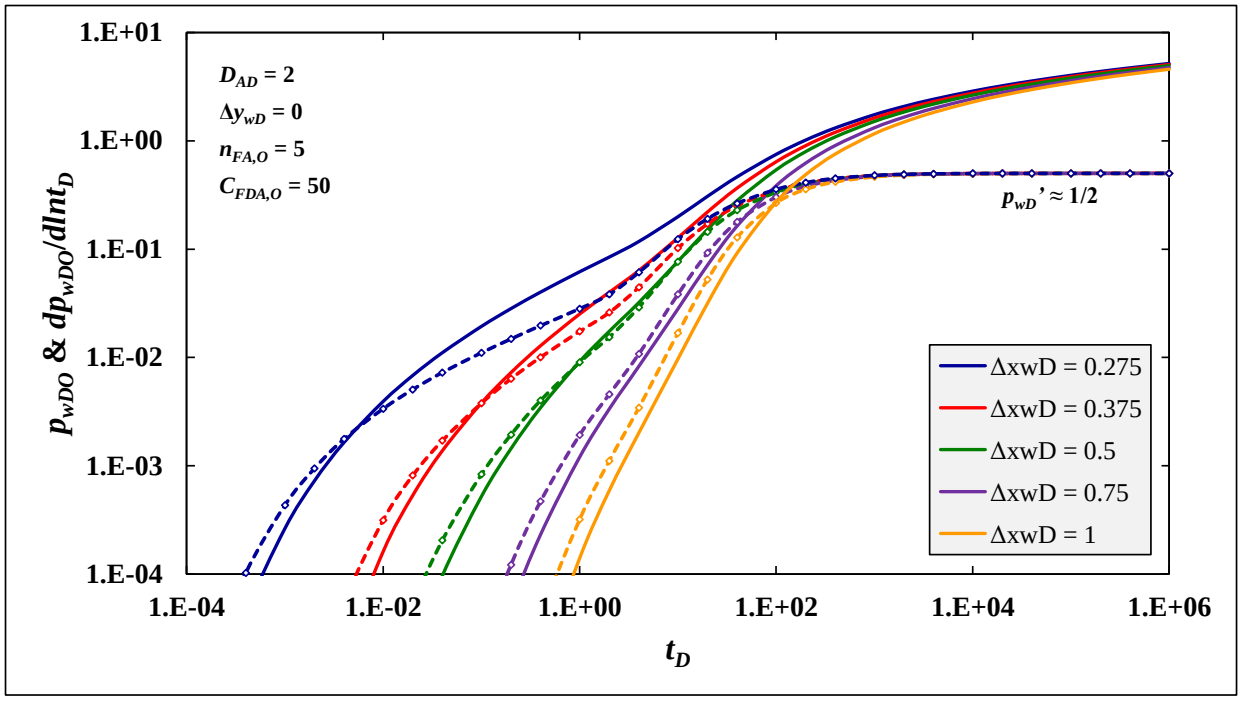

Figure 4.7. Observation well responses for different transversal separations, Δx_{wD}.

4.3. Sensitivity Analysis 3: Longitudinal Separation (Δy_{wD})

This section discusses the effect of longitudinal separation on the pressure responses in both active and observation wells. Figure 4.8 shows the schematic of two fractured horizontal wells with a zipper well configuration. A non-zipper well configuration is also considered to see the pressure response difference; the schematic is shown in Figure 1.5. Here, the effect of longitudinal separation is investigated by keeping the wells' configurations and properties similar and with constant transversal separation ($\Delta x_{wD} = 0.375$) between wells. Similar to the well configurations in the previous section, the number of hydraulic fractures (n_{FA} and n_{FO}) is 5 and dimensionless

fracture conductivity (C_{FDA} and C_{FDO}) is 50.

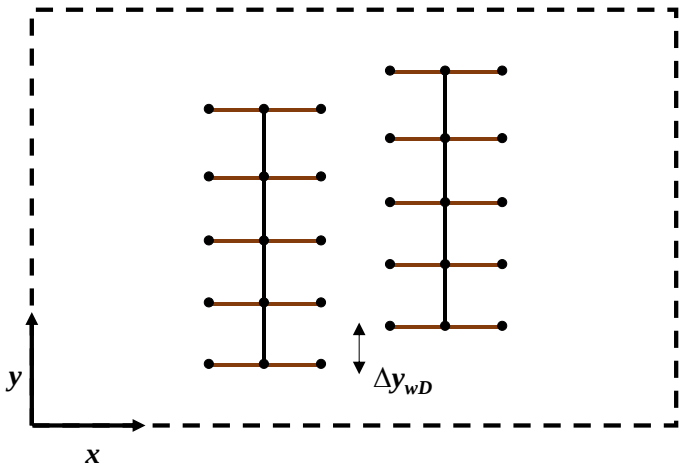

Figure 4.8. Schematic of two fractured horizontal wells separated by a longitudinal distance, Δy_{wD}.

Practically, the pressure responses of the active well show no substantial influence by the existence of the observation well. In a case in which the active well produces the hydrocarbon, these types of response may not change despite the number of fractures. However, the pressure response of both wells may show different characteristics in a case of injection, especially with the zipper well configuration. The observation well pressure responses to examine the sensitivity to longitudinal separation are shown in Figure 4.9. The general characteristic is similar for all the curves. However, there is a significant difference at early and intermediate times between the zipper (Δy_{wD} = 0.25 and 0.75) and non-zipper (Δy_{wD} = 0 and 1) well configurations. It can be observed that the zipper well configuration yields quicker interference between wells, which is faster than that shown in Figure 4.3 where n_{FA} and n_{FO} are 20. For this reason, the zipper well configuration is more suitable for the case of injection in low-permeability reservoirs than the non-zipper well configuration. The zipper well configuration can also decrease minimum fracture spacing if it is constrained by stress interference (Almulhim et al. 2014) or reservoir boundaries, but these issues are not discussed in this thesis.

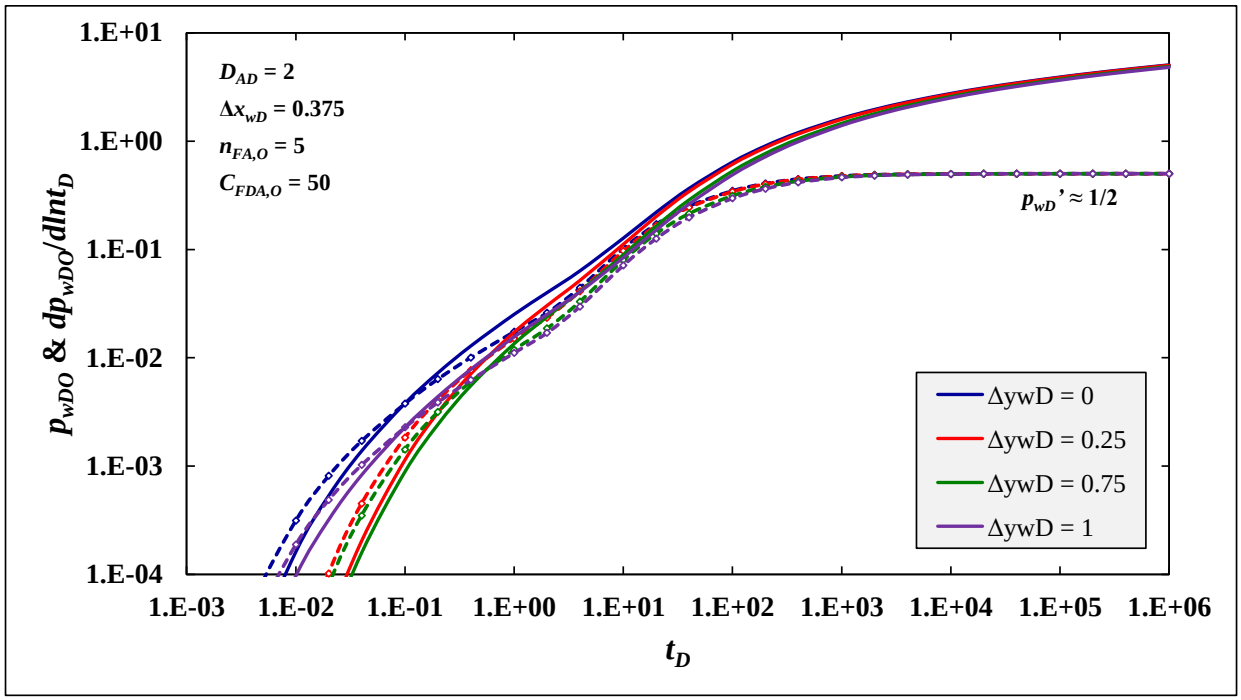

Figure 4.9. Observation well responses for different longitudinal separations, Δy_{wD}.

4.4. Sensitivity Analysis 4: Matrix Permeability (k_m)

This section examines the effect of matrix permeability (k_m) on the pressure transient responses of the interference test. The range of matrix permeability examined in this section is 10^{-7} to 10^{-3} mD. The reason for covering this permeability range is to accommodate the possible matrix permeability in conventional and unconventional reservoirs. In a dual-porosity reservoir, matrix permeability changes cause flow-capacity ratio (λ) changes. This variable controls the flow from the reservoir to the hydraulic fracture, therefore it is very crucial to study this effect on the interference test characteristic. In this section, the well configurations of both wells are identical. (n_{FA} and n_{FO}, = 5, C_{FDA} and C_{FDO} = 50). Figures 4.10 and 4.11 show the pressure transient responses of the active and the observation wells, respectively. For comparison, the pressure responses of a homogeneous reservoir with $k_m = 10^{-2}$ mD are also included.

In Figures 4.10 and 4.11, pressure drop is reduced as k_m increases in the dual-porosity reservoir cases. At the active well, pressure derivative responses indicate significant difference at different k_m. The flow regimes, shown by pressure derivative, vary for different k_m. The period of linear flow regime ($m \approx 1/2$) is shorter, but the period of bilinear flow regime ($m \approx 1/4$) is longer as k_m increases. This is driven by greater k_m which causes quicker fluid transfer from the matrix to the fracture. Another interesting feature in Figure 4.10 is the existence of early-radial flow regime, when $k_m = 10^{-7}$ mD, which happens when the hydraulic fractures do not communicate with each other but there is contribution from the fracture tips (Chen and Raghavan 1997). This flow regime is denoted by two yellow stars and the p_{wDA} value of this flow regime is 1/5 or proportional to the reciprocal of the number of fractures ($1/n_{FA}$).

Figure 4.11 shows the pressure transient responses of the observation well. The wide range of pressure responses show that the observation well pressure transient responses are greatly influenced by k_m. As k_m increases, the uniqueness of the pressure responses becomes unclear. When $k_m \leq 10^{-4}$ mD, the pressure responses show the typical shape of interference test with multiple fractures in a dual-porosity reservoir. However, when $k_m = 10^{-3}$ mD, the shapes of the pressure responses are similar to the responses when $\Delta x_{wD} = 1$ or in a homogeneous reservoir. This feature happens because the support from the matrix to the natural fractures can be realized sooner as k_m increases. This also shows that the time required to yield noticeable pressure to the observation well is also a function of k_m. Similar to the active well, it can be observed that when $k_m = 10^{-7}$ mD, early-radial flow regime happens (denoted by two yellow stars). The p_{wDO} value of this flow regime is 1/5 ($1/n_{FO}$). These observations emphasize the importance of having pressure-derivative responses for the pressure transient analysis.

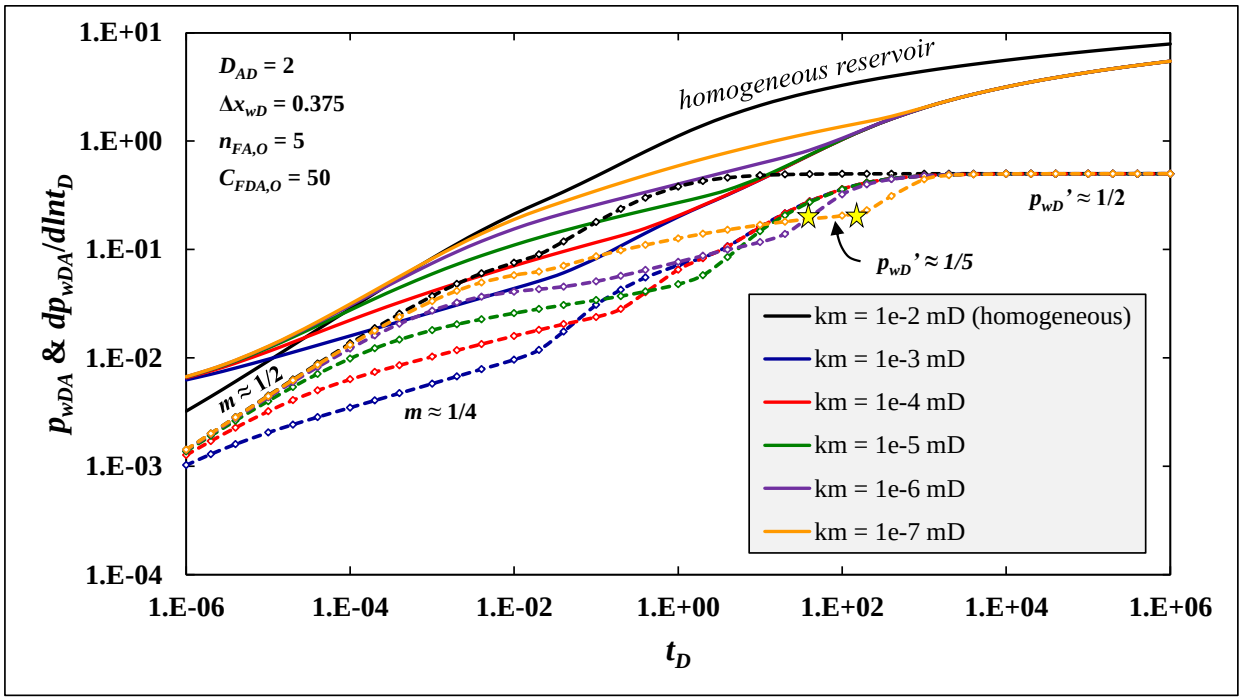

Figure 4.10. Active well responses for different matrix permeability, k_m.

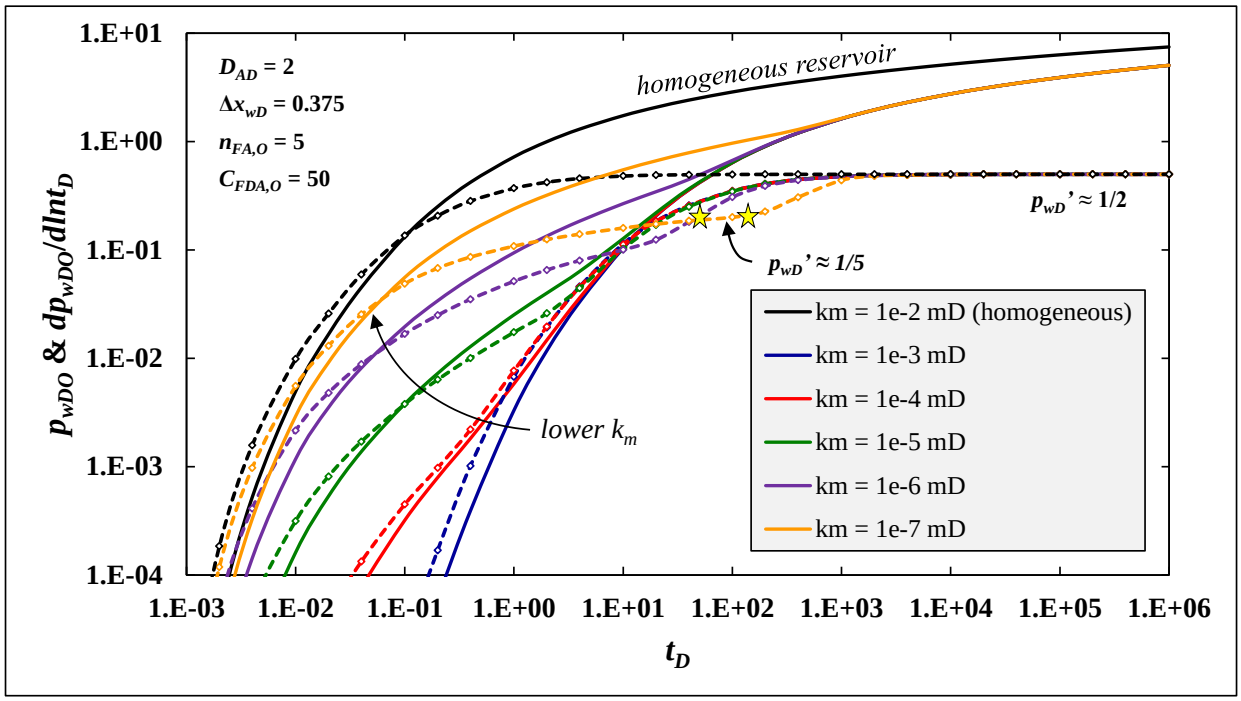

Figure 4.11. Observation well responses for different matrix permeability, k_m.

4.5. Application of Semi-Analytical Model in Interference Test 1: Closed Rectangular Reservoir

This section shows the interference test case in a closed rectangular reservoir as sketched in Figure 4.12. The active and observation well pressure responses of this case are displayed in Figure 4.13 and Figure 4.14, respectively. The objective of this case is to mimic one of the cases presented by Yaich et al. (2014) which considers overlapping SRVs without flow contribution from outside SRV. In this section, the well configurations of both wells are identical (n_{FA} and n_{FO}, = 5, C_{FDA} and C_{FDO} = 50).

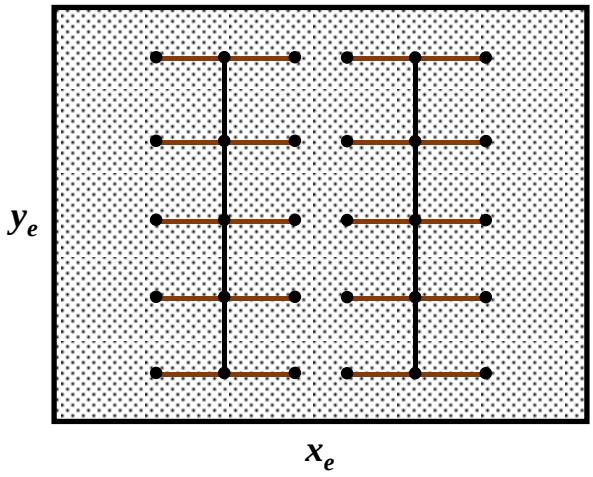

Figure 4.12. Schematic of two fractured horizontal wells in a closed rectangular reservoir.

Note that the active and observation well pressure responses in Figure 4.13 and Figure 4.14 show the characteristics of a closed rectangular reservoir at late times which are shown by a unit slope ($m \approx 1$). Before the boundary effect, the flow regimes are similar to the pressure responses in an infinite reservoir. However, there is an alteration when x_{eD} and y_{eD} are 0.525 and 2.5 (overlapping SRV), respectively. The p_{wD} and dp_{wD}/dt_D responses for this case are slightly higher than other curves in the active well and slightly lower than other curves in the observation well. This phenomenon happens because there is no flow across the fracture tips and is shown by $m \approx$ 1/4 in the pressure derivative plot of the active well. As discussed previously, the pressure response

of the active well is not too responsive to the existence of a nearby observation well with multiple conductive fractures. Thus, it can be concluded that the time required to reach the boundary is not related to the existence of the observation well. Detailed discussion about the effect of the boundary on a fractured horizontal well can be found in Greenwood (2015).

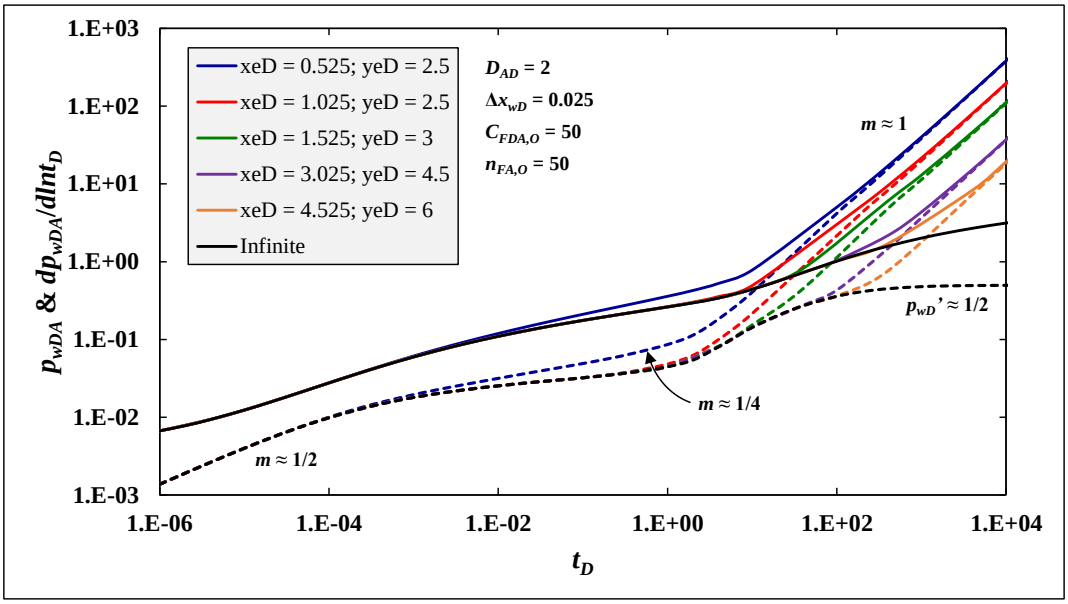

Figure 4.13. Active well responses for different reservoir size (x_{eD} and y_{eD}).

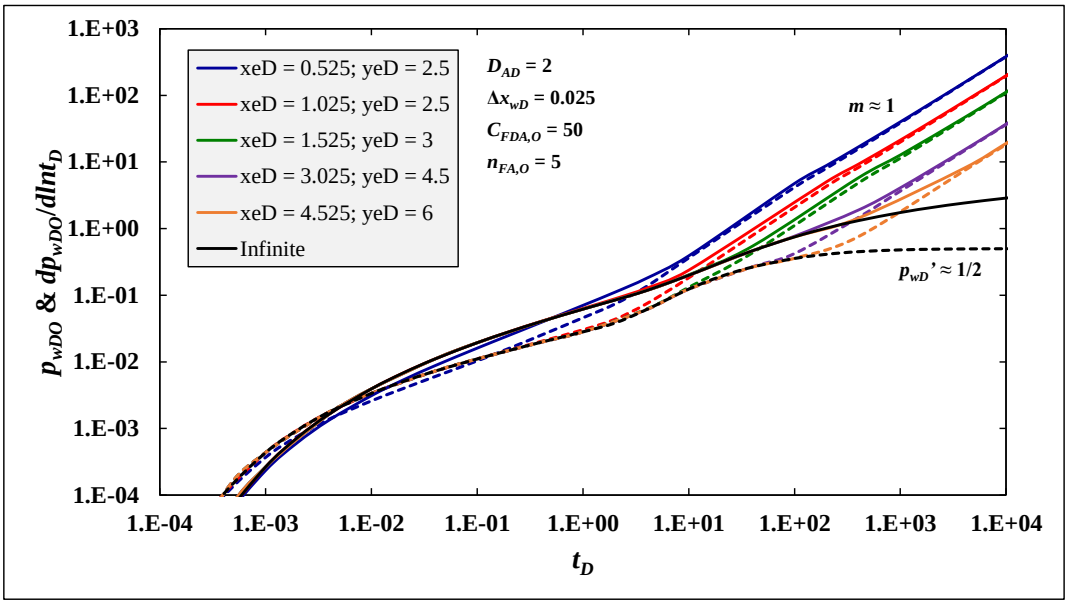

Figure 4.14. Observation well responses for different reservoir size (x_{eD} and y_{eD}).

4.6. Application of Semi-Analytical Model in Interference Test 2: Open Horizontal Well Sections

This section examines the effect of the open horizontal-well sections between hydraulic fractures to the pressure responses in an interference test with two fractured horizontal wells (Figure 4.15). Opening a horizontal section (perforated or open hole) of a fractured horizontal well may increase productivity. In this thesis, this case is investigated by opening a horizontal section in both wells. For simplicity, a horizontal well is assumed to be an infinite-conductivity line in which the pressure at each point is identical. In the semi-analytical model, the horizontal section can be incorporated in the matrix equation (3.61) by superposition and using (3.50) for the pressure solution.

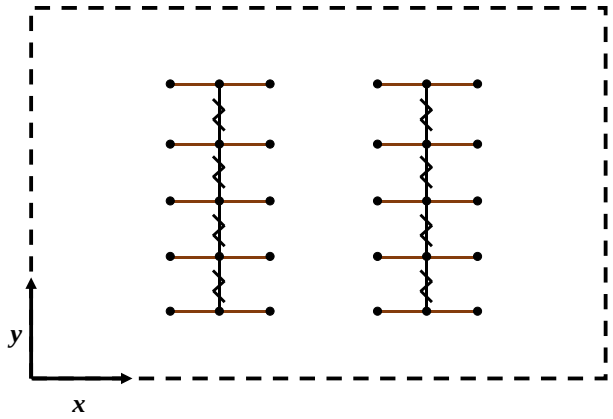

Figure 4.15. Schematic of two fractured horizontal wells with open horizontal well sections.

Figure 4.16 shows the pressure responses of the active and observation wells. For comparison, the base case (run in an infinite reservoir with no contribution from a horizontal section) is also shown. In the active well, the flow is dominated by the linear flow in fractures at early times. It is followed by bilinear flow ($m \approx 1/4$). This flow regime does not exist in the base case. Nevertheless, from a pressure drop perspective, it can be observed that the pressure drop at the active well is not too different, as shown by a semi-log plot of Δp_{wA} versus t (Figure 4.17). This figure is obtained by using following additional data: q = 1,000 rb/day, B = 1.5 STB/rb, and μ =

0.5 cp. This shows that the expected productivity can be realized without opening the horizontal section. The pressure drop throughout the reservoir is considerably small because the matrix permeability that indirectly contributes to the flow into the wellbore is low (k_m = 10^{-5} mD). In the observation well, the contribution of opened horizontal sections can be seen before $t_D \leq 10$.

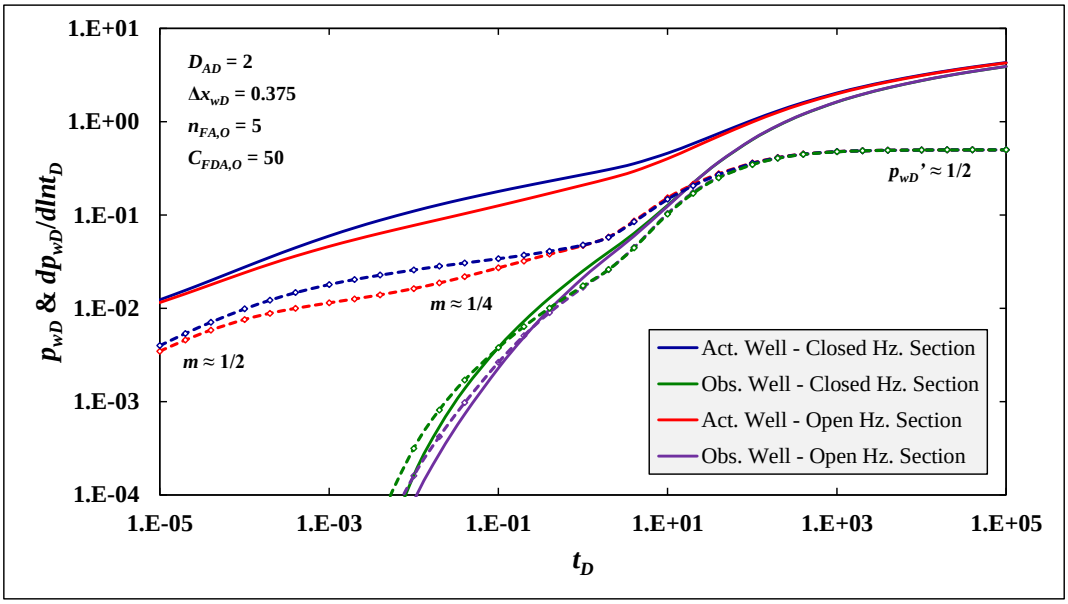

Figure 4.16. Pressure responses of closed and open horizontal sections.

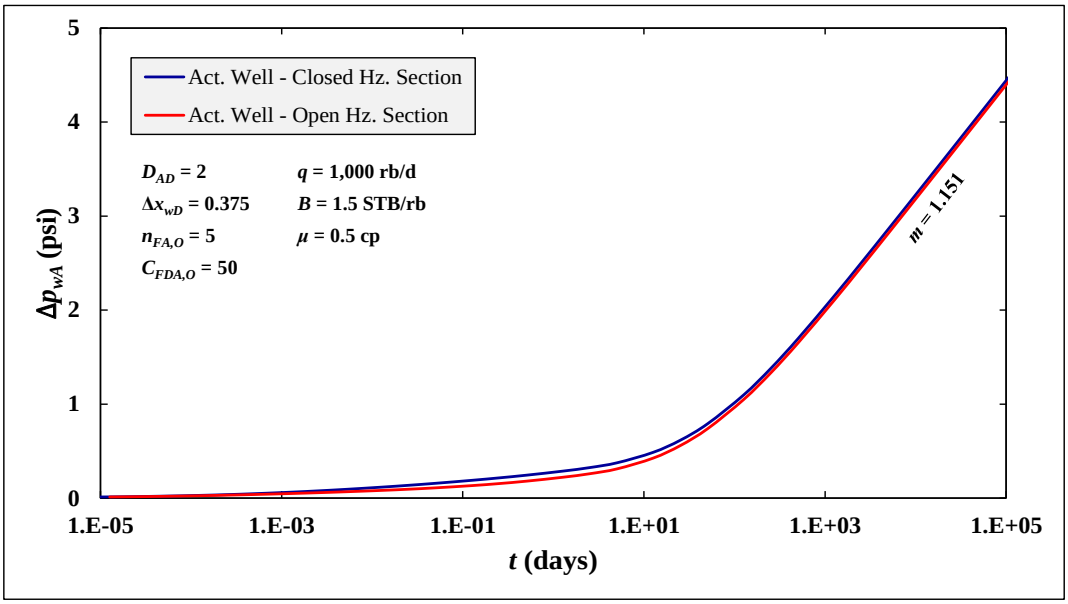

Figure 4.17. Active well pressure responses (semi-log plot).

4.7. Application of Semi-Analytical Model in Interference Test 3: A Stand-Alone Fracture

In this section, the effect of a stand-alone fracture as a pressure conduit crossing both active and observation wells is investigated. Figure 4.18 shows the schematic of this case. In low-permeability reservoirs, the connection between two wells can be caused by this single fracture (Yaich et al. 2014). Figure 4.19 and Figure 4.20 show the pressure and derivative responses of both wells in a dual-porosity and homogeneous reservoir, respectively. Figure 4.19 shows two interesting features. First, in the case with a stand-alone fracture, two linear flow regimes occur. The first linear flow is dominated by the flow within the hydraulic fractures. The flow within the stand-alone fracture also happens but is slower due to lower fracture conductivity ($C_{FDcross}$ = 0.5 C_{FD}). The second linear flow regime occurs after the first one when the flow within the stand-alone fracture stabilizes. It is then followed by a bilinear flow regime ($m \approx 1/4$) and finally by a pseudoradial flow. Second, in the pressure responses in the observation well, it can be observed that the interference responses between the two cases are slightly different. This informs us that the stand-alone fracture does not contribute significantly to the pressure response in the observation well. This happens because the stand-alone fracture conductivity is low enough to be similar to the natural fractures of the reservoir. However, the pressure responses are different in a homogeneous reservoir. There is a slight difference of the pressure responses both in the active and observation wells between the case with and without a stand-alone fracture.

Even though the response of the observation well is not too sensitive to the existence of a stand-alone fracture for production, the opposite may be true for the case of injection. The effect of a stand-alone fracture may be seen instantaneously in the injection case due to the conductive fracture. The effect of a stand-alone fracture on interference behavior during production/buildup and injection/fall-off is an interesting and relevant discussion, but it is not in the scope of this thesis

and is therefore suggested for a future study.

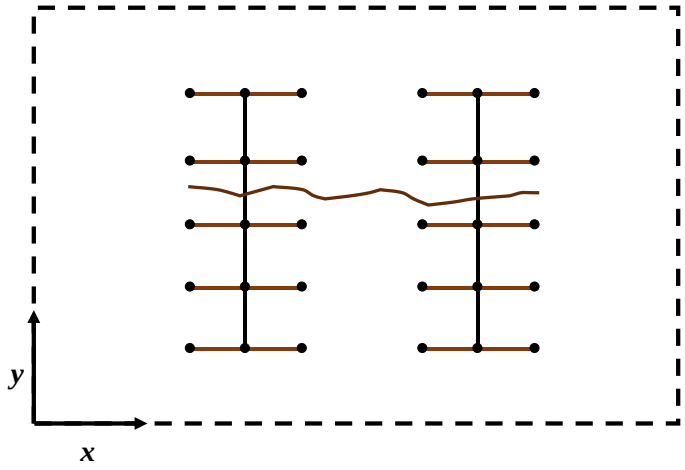

Figure 4.18. Schematic of two fractured horizontal wells with a stand-alone fracture.

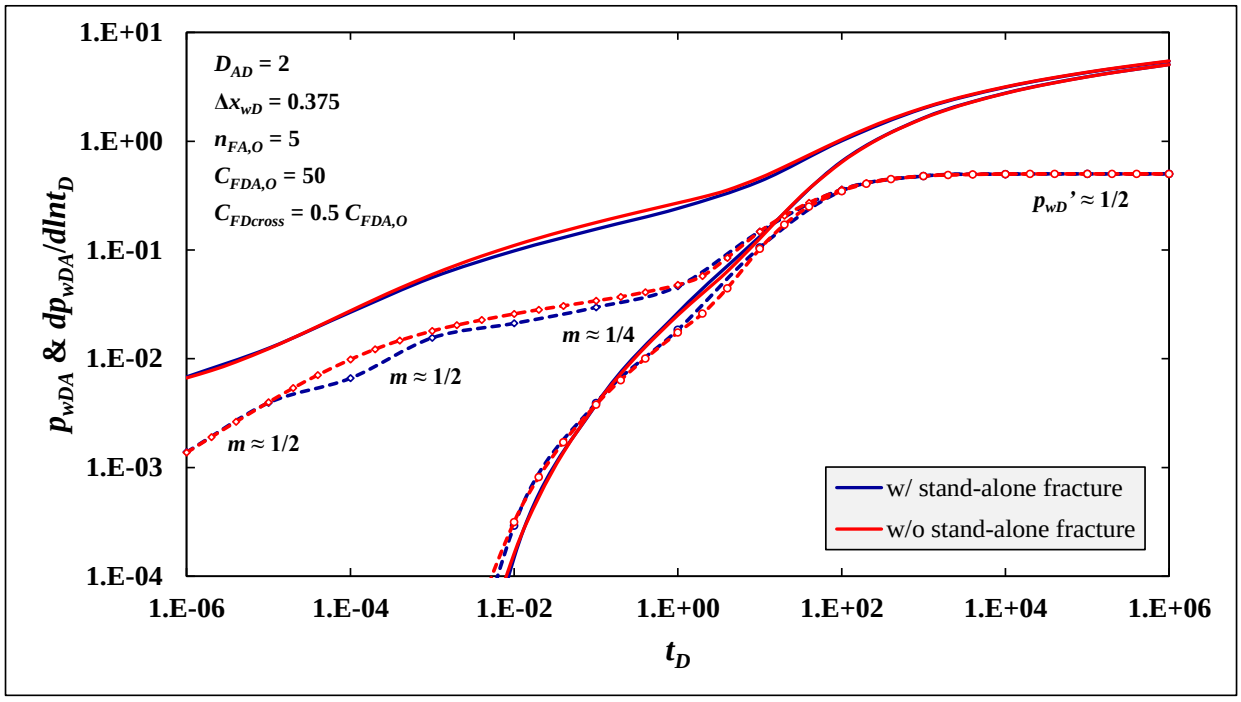

Figure 4.19. Pressure responses with and without stand-alone fracture in a dual-porosity reservoir (transient).

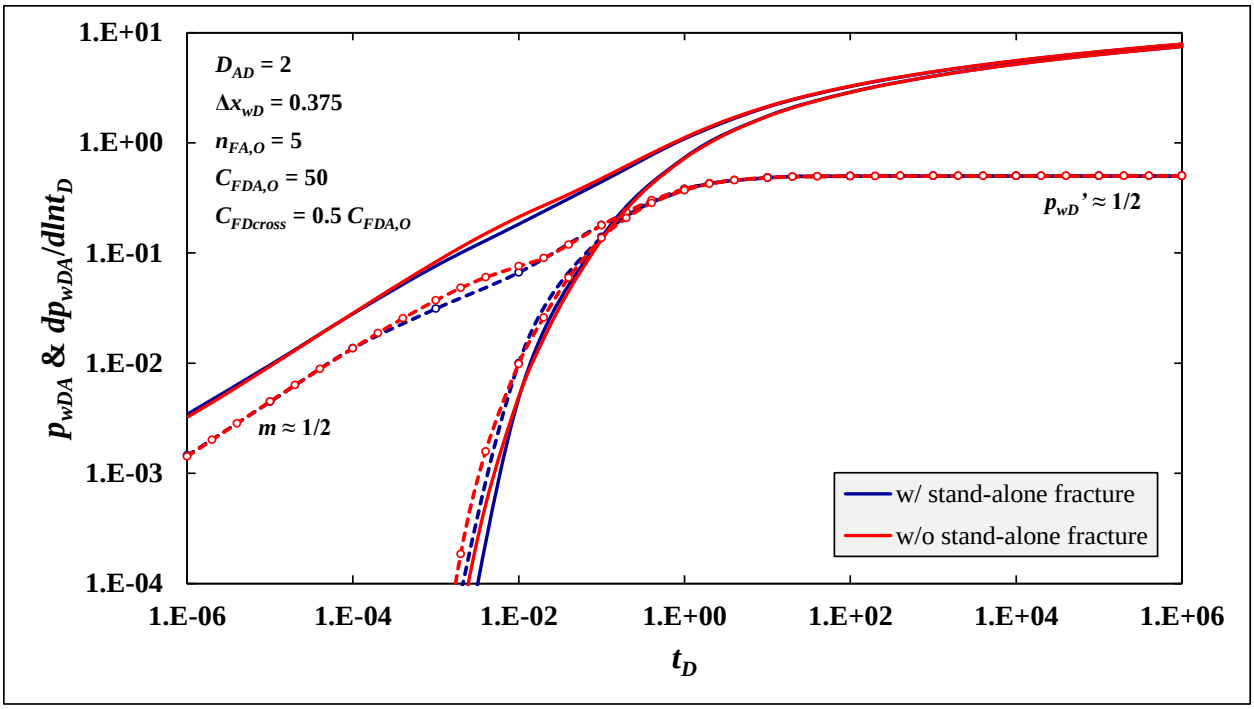

Figure 4.20. Pressure responses with and without stand-alone fracture in a homogeneous reservoir.

CHAPTER 5

CONCLUSIONS AND RECOMMENDATIONS

This chapter presents the major conclusions and contributions of this thesis and makes recommendations for future studies related to interference tests with two fractured horizontal wells.

5.1. Conclusions

The first main goal of this thesis was to present a solution that can be used to analyze the interference test with two fractured horizontal wells. This goal has been accomplished by developing a semi-analytical model. The mathematical model has been derived analytically and its solution has been obtained numerically. Thus, the solution is called a semi-analytical model. Recasting the solution in computationally efficient and accurate forms has resulted in a robust model, which is also versatile for application to other problems of interest. After obtaining the general semi-analytical solution, verifying the results with several data sets in the literature, and ensuring the stabilization of the code, this model has been used to study the effect of the number of hydraulic fractures, the effect of transversal and longitudinal separation between two wells, and the effect of the matrix permeability. Some applications of this semi-analytical technique have also been presented. The applications in this thesis include the interference test in a closed rectangular reservoir, with open horizontal sections, and involving a stand-alone fracture crossing both wells.

General guidelines have been established to use the semi-analytical model developed in this thesis and supported by application examples. In addition, numerical results have been tabulated for an example (the sensitivity case for the number of hydraulic fractures), which can be used by others to verify their analytical or numerical models.

The investigation of the pressure transient responses of all cases presented in this thesis gives deeper insight and more information about the general characteristics of interference tests with two fractured horizontal wells. The following are the primary conclusions of this thesis:

1. In low-permeability reservoirs, active well pressure response is unaffected by the presence of the observation well even though there are a large number of fractures (n_{FA} and n_{FO}), both wells have high dimensionless fracture conductivity (C_{FD}), and the distance between fractured horizontal wells is close. Nonetheless, the pressure responses of the active well can be different when the reservoir permeability is high.
2. It can be noticed that as n_{FA} increases, the pressure drop of the active well is lower and its difference becomes smaller as $n_{FA} \geq 10$. This follows the theory that was presented by Raghavan et al. (1997). However, the observation well responses become similar when $n_{FO} \geq 10$. This happens if the distance between wells is far enough and the observation well can be regarded as a long-and-conductive single fracture.
3. There are two typical flux distribution shapes for the interference test with two fractured horizontal wells: u-shape for the active well and negative-to-positive-shape for the observation well (see Figure 4.5).
4. Even though it has no effect on the active well, transversal separation (Δx_{wD}) plays an important role on the pressure transient responses of the observation well. As Δx_{wD} gets smaller, the pressure responses, especially in intermediate times, are dominated by the existence of multiple hydraulic fractures and a dual-porosity reservoir. However, if Δx_{wD} is large enough, the pressure response shows similarities to a horizontal well without multiple fractures.

5. In terms of longitudinal separation (Δy_{wD}), pressure responses are affected by zipper or non-zipper well configurations. In the observation well, a zipper well configuration has a lower pressure drop than a non-zipper well configuration and even lower than the case when n_{FO} is 20. This is caused by the zipper fracture design, which allows the fractures to communicate faster. Therefore, a zipper well configuration is more suitable for an injection case than a non-zipper well configuration.
6. Matrix permeability (k_m) greatly affects the pressure transient responses, even though the matrix has no direct communication with the hydraulic fractures or the well. In the active well, greater k_m reduces the pressure drop, shortens the linear flow regime period, and prolongs the bilinear flow regime period. The early-radial flow regime can exist if k_m is low enough; in this case, k_m should be 10^{-7} mD.
7. In the observation well, as k_m increases, the uniqueness of the pressure responses becomes unclear. When $k_m \leq 10^{-4}$ mD, the pressure responses show the typical shape of an interference test with multiple fractures in a dual-porosity reservoir. However, when $k_m = 10^{-3}$ mD, the shapes of pressure responses are akin to the responses when $\Delta x_{wD} = 1$ or in a homogeneous reservoir. The early-radial flow regime can also exist in the observation well. Similar to the active well, this flow regime occurs when $k_m = 10^{-7}$ mD.
8. In a closed rectangular reservoir, the time required to reach the boundary is not related to the existence of the observation well. The pressure transient responses of both wells follow the responses in the case of an infinite reservoir and follow the typical slope ($m = 1$) once the boundary is reached.
9. When there is no flow across the fracture tips because it is closed by the boundary, the pressure drop is higher than in other bounded reservoir cases. At this period, the flow

regime is also altered and shown by $m \approx 1/4$ or bilinear flow regime.

10. Opening horizontal sections to production causes changes to the pressure transient response of both wells. It also shows that pressure response measured at both active and observation wells are lower than the case without opening the horizontal sections. However, from a pressure drop perspective, opening horizontal sections does not create a significant difference at both wells. It can be concluded that in this case the expected well productivity can be achieved without having to open the active well horizontal section when n_{FA} is greater than 5.
11. In the presence of a stand-alone fracture, the pressure transient responses of the active well are also altered in a dual-porosity reservoir. There are two linear flow regimes ($m \approx 1/2$). The first linear flow regime is dominated by hydraulic fractures and the second is dominated by the stand-alone fracture that crosses both wells. The next flow regime is the bilinear flow regime ($m \approx 1/4$).
12. In a dual-porosity reservoir and production case, the response of the observation well is not affected significantly by the existence of a stand-alone fracture since its conductivity is similar to that of the natural fractures.

5.2. Recommendations

The solution developed in this thesis has great potential to apply to many problems of practical interest and to extend to a variety of other problems. However, considering the time limitations, only the development, verification, and fundamental evaluation of the model were in the scope of this thesis. The following are recommendations for future work related to this thesis:

1. Incorporate the composite reservoir system into both active and observation wells to accommodate the flow contribution from inside and outside the SRV. In this way, pressure

transient responses in ultra-low permeability reservoirs (i.e., shale formations) can be generated.

2. Study the effect of finite-conductivity horizontal wellbore, skin, and wellbore hydraulics on the pressure transient responses of an interference test with fractured horizontal wells.
3. Extend the interference case with geomechanical properties, such as stress interference, in determining the configuration of hydraulic fractures, x_F, and C_{FD}, in order to study real-world cases in more detail.

LIST OF SYMBOLS

A_x	Area of a surface in x-direction [ft^2]
B	Formation volume factor [rb/STB]
C_{FD}	Dimensionless fracture conductivity
c_{fluid}	Fluid compressibility [psi^{-1}]
c_r	Rock/formation compressibility [psi^{-1}]
c_t	Total compressibility [psi^{-1}]
D	Distance between two outermost hydraulic fractures at horizontal well [ft]
h	Reservoir height [ft]
h_f	Fracture height [ft]
h_m	Matrix height [ft]
K_0	Modified Bessel function of the second kind of order zero
k_f	Fracture permeability [mD]
k_F	Hydraulic fracture permeability [mD]
k_m	Matrix permeability [mD]
k_ξ	Permeability in $\xi = x, y, z$ [mD]
L	Reference length [ft]
L_h	Horizontal well-length [ft]
$m(p)$	Gas pseudopressure [psi^2/cp]
m_A	Number of segments of a hydraulic fracture at the active well
m_O	Number of segments of a hydraulic fracture at the observation well
n_f	Number of fractures in the reservoir
n_{FA}	Number of hydraulic fractures at the active well

n_{FO}	Number of hydraulic fractures at the observation well
n_m	Number of matrices in the reservoir
p	Pressure [psi]
p_b	Bubble-point pressure [psi]
p_D	Dimensionless pressure
p_i	Initial reservoir pressure [psi]
p_{Wd}	Dimensionless wellbore pressure
q	Production rate [rb/day]
q_D	Dimensionless production rate
q_{FD}	Dimensionless fracture rate
r_w	Wellbore radius [ft]
s	Laplace parameter
S_{fluid}	Fluid saturation
t	Time [days; hour]
t_D	Dimensionless time
w_F	Hydraulic fracture width [ft]
x_D	Dimensionless position in *x*-direction
x_e	Reservoir dimension in *x*-direction [ft]
x_F	Hydraulic fracture half-length [ft]
x_w	Well coordinate in *x*-direction [ft]
x_{Wd}	Dimensionless well position in *x*-direction
y_D	Dimensionless position in *y*-direction
y_e	Reservoir dimension in *y*-direction [ft]

y_w	Well coordinate in *y*-direction [ft]
y_{Wd}	Dimensionless well position in *y*-direction
z	Real gas compressibility factor
z_D	Dimensionless position in *z*-direction
z_e	Reservoir dimension in *z*-direction [ft]
z_w	Well coordinate in *z*-direction [ft]
z_{Wd}	Dimensionless well position in *z*-direction

GREEK

α	Constant at dimensionless pressure and production rate
β	Constant at dimensionless time
Δ	Difference operator
λ	Flow-capacity ratio
μ	Viscosity [cp]
π	Pi constant
ϕ	Porosity
ω	Storativity ratio

SUBSCRIPT

A	Active well
D	Dimensionless
e	Reservoir boundary
f	Fracture

F	Hydraulic fracture
inf	Infinite
m	matrix
O	Observation well
t	Total
w	Well
x, y, z	3D Cartesian-directions

REFERENCES CITED

Ajani, A.A. and Kelkar, M. 2012. Interference Study in Shale Plays. Presented at the SPE Hydraulic Fracturing Technology Conference, The Woodlands, Texas, 6-8 February. SPE-151045-MS. http://dx.doi.org/10.2118/151045-MS.

Al-Hussainy, R., Ramey, H.J., Jr., and Crawford, P.B. 1966. The Flow of Real Gases through Porous Media. *J Pet Technol* **18** (5): 624-636. SPE-1243-A-PA. http://dx.doi.org/10.2118/1243-A-PA.

Al-Khamis, M.N. 2003. *Analysis of Interference Tests with Horizontal Wells*. PhD dissertation, Colorado School of Mines, Golden, Colorado (March 2003).

Al-Khamis, M.N., Ozkan, E., and Raghavan, R.S. 2005. Analysis of Interference Tests with Horizontal Wells. *SPE Res Eval & Eng* **8** (4): 337-347. SPE-84292-PA. http://dx.doi.org/10.2118/84292-PA.

Al-Khamis, M., Ozkan, E., and Raghavan, R. 2001. Interference Testing with Horizontal Observation Wells. Presented at the SPE Annual Technical Conference and Exhibition, New Orleans, Louisiana, 30 September-3 October. SPE-71581-MS. http://dx.doi.org/10.2118/71581-MS.

Al-Kobaisi, M., Ozkan, E., and Kazemi, H. 2006. A Hybrid Numerical/Analytical Model of a Finite-Conductivity Vertical Fracture Intercepted by a Horizontal Well. *SPE Res Eval & Eng* **9** (4): 345-355. SPE-92040-PA. http://dx.doi.org/10.2118/92040-PA.

Almulhim, A., Tutuncu, A.N., Kazemi, H. et al. 2014. Flow Modeling in Multi-Stage Hydraulic Fracturing Patterns to Optimize Shale Reservoir Production. Presented at the SPE/AAPG/SEG Unconventional Resources Technology Conference, Denver, Colorado, 25-27 August. SPE-2014-1922172-MS. http://dx.doi.org/10.15530/urtec-2014-1922172.

Brown, M., Ozkan, E., Raghavan, R. et al. 2011. Practical Solutions for Pressure-Transient Responses of Fractured Horizontal Wells in Unconventional Shale Reservoirs. *SPE Res Eval & Eng* **14** (6):663-676. SPE-125043-PA. http://dx.doi.org/10.2118/125043-PA.

Chen, C. and Raghavan, R. 2013. On Some Characteristic Features of Fractured-Horizontal Wells and Conclusions Drawn Thereof. *SPE Res Eval & Eng* **16** (1): 19-28. SPE-163104-PA. http://dx.doi.org/10.2118/163104-PA.

Chen, C.-C and Raghavan, R. 1997. A Multiply-Fractured Horizontal Well in a Rectangular Drainage Region. *SPE J* **2** (4): 455-465. SPE-37072-PA. http://dx.doi.org/10.2118/37072-PA.

Cinco L., H., Samaniego V., F., and Dominguez A., N. 1978. Transient Pressure Behavior for a Well with a Finite-Conductivity Vertical Fracture. *SPE J* **18** (4): 253-264. SPE-6014-PA. http://dx.doi.org/10.2118/6014-PA.

Cinco-Ley, H. and Meng, H.Z. 1988. Pressure Transient Analysis of Wells with Finite Conductivity Vertical Fractures in Double Porosity Reservoir. Presented at the SPE Annual Technical Conference and Exhibition, Houston, Texas, 2-5 October. SPE-18172-MS. http://dx.doi.org/10.2118/18172-MS.

Cinco-Ley, H. and Samaniego-V., F. 1981. Transient Pressure Analysis for Fractured Wells. *J Pet Technol* **33** (9): 1,749-1,766. SPE-7490-PA. http://dx.doi.org/10.2118/7490-PA.

Greenwood, J.T. 2015. *An Analytical Investigation of Boundaries in Naturally Fractured Unconventional Reservoirs*. MS thesis, Colorado School of Mines, Golden, Colorado (2015).

Gringarten, A.C. and Ramey, H.J., Jr. 1973. The Use of Source and Green's Functions in Solving Unsteady-Flow Problems in Reservoirs. *SPE J* **13** (5): 285-296. SPE-3818-PA. http://dx.doi.org/10.2118/3818-PA.

Gringarten, A.C., Ramey, H.J., Jr., and Raghavan, R. 1974. Unsteady-State Pressure Distributions Created by a Well With a Single Infinite-Conductivity Vertical Fracture. *SPE J* **14** (4): 347-360. SPE-4051-PA. http://dx.doi.org/10.2118/4051-PA.

Kazemi, H. 1969. Pressure Transient Analysis of Naturally Fractured Reservoirs with Uniform Fracture Distribution. *SPE J* **9** (4): 451-462. SPE-2156-A. http://dx.doi.org/10.2118/2156-A.

Khan, M.U. and Callard, J.G. 2010. Reservoir Management in Unconventional Reservoirs. Presented at the SPE Hydrocarbon Economics and Evaluation Symposium, Dallas, Texas, 8-9 March. SPE-130146-MS. http://dx.doi.org/10.2118/130146-MS.

Medeiros, F., Jr. 2007. *Semi-Analytical Pressure Transient Model for Complex Well-Reservoir System*. PhD dissertation, Colorado School of Mines, Golden, Colorado (November 2007).

Meehan, D.N., Horne, R.N., and Ramey, H.J. 1989. Interference Testing of Finite Conductivity Hydraulically Fractured Wells. Presented at the SPE Annual Technical Conference and Exhibition, San Antonio, Texas, 8-11 October. SPE-19784-MS. http://dx.doi.org/10.2118/19784-MS.

Ozkan, E. 1988. *Performance of Horizontal Wells*. PhD dissertation, University of Tulsa, Tulsa, Oklahoma (1988).

Ozkan, E., Brown, M., Raghavan, R.S. et al. 2009. Comparison of Fractured Horizontal-Well Performance in Conventional and Unconventional Reservoirs. Presented at the SPE Western Regional Meeting, San Jose, California, 24-26 March. SPE-121290-MS. http://dx.doi.org/10.2118/121290-MS.

Ozkan, E. and Raghavan, R. 1991a. New Solutions for Well-Test-Analysis Problems: Part 1-Analytical Considerations. *SPE Form Eval* **6** (3): 359-368. SPE-18615-PA. http://dx.doi.org/10.2118/18615-PA.

Ozkan, E. and Raghavan, R. 1991b. New Solutions for Well-Test-Analysis Problems: Part 2-Computational Considerations and Applications. *SPE Form Eval* **6** (3): 369-378. SPE-18616-PA. http://dx.doi.org/10.2118/18616-PA.

Ozkan, E., Raghavan, R., and Joshi, S.D. 1989. Horizontal Well Pressure Analysis. *SPE Form Eval* **4** (4): 567-575. SPE-16378-PA. http://dx.doi.org/10.2118/16378-PA.

Raghavan, R. 1993. *Well Test Analysis*. Englewood Cliffs, New Jersey: PTR Prentice Hall.

Raghavan, R. and Ozkan, E. 1994. *A Method for Computing Unsteady Flows in Porous Media*. Harlow, Essex, England: Longman Scientific & Technical; New York: John Wiley & Sons.

Raghavan, R.S., Chen, C-C., and Agarwal, B. 1997. An Analysis of Horizontal Wells Intercepted by Multiple Fractures. *SPE J* **2** (3): 235-245. SPE-27652-PA. http://dx.doi.org/10.2118/27652-PA.

Serra, K., Reynolds, A.C., and Raghavan, R. 1983. New Pressure Transient Analysis Methods for Naturally Fractured Reservoirs. *J Pet Tech* **35** (12): 2271-2283. SPE-10780-PA. http://dx.doi.org/10.2118/10780-PA.

Stehfest, H. 1970. Algorithm 368: Numerical Inversion of Laplace Transforms. *Communication of the ACM* **13** (1): 47-49. http://dx.doi.org/10.1145/361953.361969.

Torcuk, M.A., Kurtoglu, B., Alharthy, N. et al. 2013. Analytical Solutions for Multiple Matrix in Fractured Reservoirs: Application to Conventional and Unconventional Reservoirs. *SPE J* **18** (5): 969 – 981. SPE-164528-PA. http://dx.doi.org/10.2118/164528-PA.

U.S. Energy Information Administration (EIA). 2013. Technically Recoverable Shale Oil and Shale Gas Resources: An Assessment of 137 Shale Formations in 41 Countries Outside the United States. *EIA*, 10 June 2013, http://www.eia.gov/analysis/studies/worldshalegas/ (accessed 15 July 2015).

van Everdingen, A.F. and Hurst, W. 1949. The Application of the Laplace Transformation to Flow Problems in Reservoirs. *J Pet Tech* **1** (12): 305-324. SPE-949305-G. http://dx.doi.org/10.2118/949305-G.

Warren, J.E. and Root, P.J. 1963. The Behavior of Naturally Fractured Reservoirs. *SPE J* **3** (3): 245-255. SPE-426-PA. http://dx.doi.org/10.2118/426-PA.

Yaich, E., Diaz De Souza, O.C., Foster, R.A. et al. 2014. A Methodology to Quantify the Impact of Well Interference and Optimize Well Spacing in the Marcellus Shale. Presented at the

SPE/CSUR Unconventional Resources Conference, Calgary, Alberta, 30 September-2 October. SPE-171578-MS. http://dx.doi.org/10.2118/171578-M

APPENDIX A

PRESSURE SOLUTION FOR HORIZONTAL LINE SOURCE

This appendix presents the mathematical derivation of the pressure solution in section 3.4, which addresses a horizontal line source well in an infinite reservoir. It is derived from the source function developed by Ozkan (1988). The solution for pressure distribution is given by

$$\begin{aligned}\overline{p}_{hD,inf}\left(x_D,y_D,z_D,s\right)=&\frac{1}{2s}\left(\frac{2L}{L_h}\sqrt{\frac{k_z}{k}}\right)\int_{-L_{hD}/2}^{+L_{hD}/2}K_0\left[\sqrt{\left(x_D-x_{wD}-\alpha\sqrt{k/k_x}\right)^2+\left(y_D-y_{wD}\right)^2}\sqrt{u}\right]d\alpha\\&+\frac{1}{s}\left(\frac{2L}{L_h}\sqrt{\frac{k_z}{k}}\right)\sum_{n=1}^{\infty}\cos n\pi z_D\cos n\pi z_{wD}\\&\int_{-L_{hD}/2}^{+L_{hD}/2}K_0\left[\varepsilon_n\sqrt{\left(x_D-x_{wD}-\alpha\sqrt{k/k_x}\right)^2+\left(y_D-y_{wD}\right)^2}\right]d\alpha\end{aligned}\tag{A.1}$$

or

$$\overline{p}_{hD,inf}=\overline{p}_{FD,inf}+\overline{F}\tag{A.2}$$

where

$$\overline{p}_{FD,inf}=\frac{1}{2s}\left(\frac{2L}{L_h}\sqrt{\frac{k_z}{k}}\right)\int_{-L_{hD}/2}^{+L_{hD}/2}K_0\left[\sqrt{\left(x_D-x_{wD}-\alpha\sqrt{k/k_x}\right)^2+\left(y_D-y_{wD}\right)^2}\sqrt{u}\right]d\alpha\tag{A.3}$$

and

$$\begin{aligned}\overline{F}=\frac{1}{s}\left(\frac{2L}{L_h}\sqrt{\frac{k_z}{k}}\right)\sum_{n=1}^{\infty}\Bigg\{&\cos n\pi z_D\cos n\pi z_{wD}\\&\int_{-L_{hD}/2}^{+L_{hD}/2}K_0\left[\varepsilon_n\sqrt{\left(x_D-x_{wD}-\alpha\sqrt{k/k_x}\right)^2+\left(y_D-y_{wD}\right)^2}\right]d\alpha\Bigg\}\end{aligned}\tag{A.4}$$

If the integral limits are assumed to be two dummy variables, *a* and *b*, (A.4) can be written as follows:

$$\overline{F} = \frac{1}{s}\left(\frac{2L}{L_h}\sqrt{\frac{k_z}{k}}\right)\sum_{n=1}^{\infty}\left\{\cos n\pi z_D \cos n\pi z_{wD} \int_a^b K_0\left[\varepsilon_n\sqrt{\left(x_D - x_{wD} - \alpha\sqrt{k/k_x}\right)^2 + \left(y_D - y_{wD}\right)^2}\right]d\alpha\right\} \tag{A.5}$$

To avoid computation problems, $\overline{F}$ in (A.5) needs to be recast into the following terms (Ozkan 1988):

$$\overline{F}\left[x_D \geq \left(x_{wD} + b\sqrt{k/k_x}\right)\right] = \frac{1}{s}\left(\frac{2L}{L_h}\sqrt{\frac{k_z}{k}}\right)\sum_{n=1}^{\infty}\frac{1}{\varepsilon_n}\cos n\pi z_D \cos n\pi z_{wD} \left\{\int_0^{\varepsilon_n\left[x_D - \left(x_{wD} + a\sqrt{k/k_x}\right)\right]} K_0\left[\sqrt{\xi^2 + \varepsilon_n^2\left(y_D - y_{wD}\right)^2}\right]d\xi - \int_0^{\varepsilon_n\left[x_D - \left(x_{wD} + b\sqrt{k/k_x}\right)\right]} K_0\left[\sqrt{\xi^2 + \varepsilon_n^2\left(y_D - y_{wD}\right)^2}\right]d\xi\right\} \tag{A.6}$$

$$\overline{F}\left[x_D \leq \left(x_{wD} + a\sqrt{k/k_x}\right)\right] = \frac{1}{s}\left(\frac{2L}{L_h}\sqrt{\frac{k_z}{k}}\right)\sum_{n=1}^{\infty}\frac{1}{\varepsilon_n}\cos n\pi z_D \cos n\pi z_{wD} \left\{\int_0^{\varepsilon_n\left[\left(x_{wD} + b\sqrt{k/k_x}\right) - x_D\right]} K_0\left[\sqrt{\xi^2 + \varepsilon_n^2\left(y_D - y_{wD}\right)^2}\right]d\xi - \int_0^{\varepsilon_n\left[\left(x_{wD} + a\sqrt{k/k_x}\right) - x_D\right]} K_0\left[\sqrt{\xi^2 + \varepsilon_n^2\left(y_D - y_{wD}\right)^2}\right]d\xi\right\} \tag{A.7}$$

$$\overline{F}\left[\left(x_{wD} + a\sqrt{k/k_x}\right) \leq x_D \leq \left(x_{wD} + b\sqrt{k/k_x}\right)\right] = \frac{1}{s}\left(\frac{2L}{L_h}\sqrt{\frac{k_z}{k}}\right)\sum_{n=1}^{\infty}\frac{1}{\varepsilon_n}\cos n\pi z_D \cos n\pi z_{wD} \left\{\int_0^{\varepsilon_n\left[x_D - \left(x_{wD} + a\sqrt{k/k_x}\right)\right]} K_0\left[\sqrt{\xi^2 + \varepsilon_n^2\left(y_D - y_{wD}\right)^2}\right]d\xi + \int_0^{\varepsilon_n\left[\left(x_{wD} + b\sqrt{k/k_x}\right) - x_D\right]} K_0\left[\sqrt{\xi^2 + \varepsilon_n^2\left(y_D - y_{wD}\right)^2}\right]d\xi\right\} \tag{A.8}$$

(A.8) needs to be modified because it converges slowly due to the large value of *s* (small *t*). To overcome this obstacle, we can use the following definition (Raghavan and Ozkan 1994):

$$\int_0^x K_0\left(\sqrt{\xi^2 + a^2}\right)d\xi = \frac{\pi}{2}\exp\left(-|a|\right) - \int_x^{\infty} K_0\left(\sqrt{\xi^2 + a^2}\right)d\xi \tag{A.9}$$

or

$$\int_0^x K_0\left(\sqrt{\xi^2+a^2}\right)d\xi = \frac{\pi}{2}\exp\left(-|a|\right) - K_{i1}(x) \tag{A.10}$$

Thus, using (A.10), (A.6) to (A.8) can be written as follows, respectively:

$$\begin{aligned}\overline{F}\left[x_D \ge \left(x_{wD}+b\sqrt{k/k_x}\right)\right] &= \frac{1}{s}\left(\frac{2L}{L_h}\sqrt{\frac{k_z}{k}}\right)\sum_{n=1}^{\infty}\frac{1}{\varepsilon_n}\cos n\pi z_D \cos n\pi z_{wD} \\ &\left\{K_{i1}\left(\varepsilon_n\left[x_D-\left(x_{wD}+b\sqrt{k/k_x}\right)\right]\right)-K_{i1}\left(\varepsilon_n\left[x_D-\left(x_{wD}+a\sqrt{k/k_x}\right)\right]\right)\right\}\end{aligned} \tag{A.11}$$

$$\begin{aligned}\overline{F}\left[x_D \le \left(x_{wD}+a\sqrt{k/k_x}\right)\right] &= \frac{1}{s}\left(\frac{2L}{L_h}\sqrt{\frac{k_z}{k}}\right)\sum_{n=1}^{\infty}\frac{1}{\varepsilon_n}\cos n\pi z_D \cos n\pi z_{wD} \\ &\left\{K_{i1}\left(\varepsilon_n\left[\left(x_{wD}+a\sqrt{k/k_x}\right)-x_D\right]\right)-K_{i1}\left(\varepsilon_n\left[\left(x_{wD}+b\sqrt{k/k_x}\right)-x_D\right]\right)\right\}\end{aligned} \tag{A.12}$$

$$\begin{aligned}\overline{F}\left[\left(x_{wD}+a\sqrt{k/k_x}\right)\le x_D \le \left(x_{wD}+b\sqrt{k/k_x}\right)\right] &= \overline{F}_1 - \frac{1}{s}\left(\frac{2L}{L_h}\sqrt{\frac{k_z}{k}}\right)\sum_{n=1}^{\infty}\frac{1}{\varepsilon_n}\cos n\pi z_D \cos n\pi z_{wD} \\ &\left\{K_{i1}\left(\varepsilon_n\left[x_D-\left(x_{wD}+a\sqrt{k/k_x}\right)\right]\right)+K_{i1}\left(\varepsilon_n\left[\left(x_{wD}+b\sqrt{k/k_x}\right)-x_D\right]\right)\right\}\end{aligned} \tag{A.13}$$

where

$$\overline{F}_1 = \frac{\pi}{s}\left(\frac{2L}{L_h}\sqrt{\frac{k_z}{k}}\right)\sum_{n=1}^{\infty}\frac{1}{\varepsilon_n}\cos n\pi z_D \cos n\pi z_{wD}\exp\left[-\varepsilon_n\left|\left(y_D-y_{wD}\right)\right|\right] \tag{A.14}$$

The series in (A.14) still needs to be recast into small and large values of *s* to make it more appropriate for calculation (Raghavan and Ozkan 1994):

- For large *s* (small *t*):

$$\begin{aligned}\overline{F}_1 = \frac{z_{eD}}{2s}\left(\frac{2L}{L_h}\sqrt{\frac{k_z}{k}}\right)\sum_{n=-\infty}^{+\infty}&\left\{K_0\left[\sqrt{\left(z_D+z_{wD}-2n\right)^2 z_{eD}^2+\left(y_D-y_{wD}\right)^2}\sqrt{u}\right]\right. \\ &\left.+K_0\left[\sqrt{\left(z_D-z_{wD}-2n\right)^2 z_{eD}^2+\left(y_D-y_{wD}\right)^2}\sqrt{u}\right]\right\} \\ &-\frac{\pi\exp\left[-\sqrt{u}\left(y_D-y_{wD}\right)\right]}{2s\sqrt{u}}\left(\frac{2L}{L_h}\sqrt{\frac{k_z}{k}}\right)\end{aligned} \tag{A.15}$$

It can also be written as:

$$\begin{aligned}\overline{F}_1 = \frac{z_{eD}}{2s}\left(\frac{2L}{L_h}\sqrt{\frac{k_z}{k}}\right)\Bigg\{&K_0\left[\sqrt{\left(z_D - z_{wD}\right)^2 z_{eD}^2 + \left(y_D - y_{wD}\right)^2}\sqrt{u}\right] + \\ &K_0\left[\sqrt{\left(z_D + z_{wD}\right)^2 z_{eD}^2 + \left(y_D - y_{wD}\right)^2}\sqrt{u}\right]\Bigg\} + \\ \frac{z_{eD}}{2s}\left(\frac{2L}{L_h}\sqrt{\frac{k_z}{k}}\right)\sum_{n=1}^{\infty}\Bigg\{&K_0\left[\sqrt{\left(z_D - z_{wD} - 2n\right)^2 z_{eD}^2 + \left(y_D - y_{wD}\right)^2}\sqrt{u}\right] + \\ &K_0\left[\sqrt{\left(z_D + z_{wD} - 2n\right)^2 z_{eD}^2 + \left(y_D - y_{wD}\right)^2}\sqrt{u}\right] + \\ &K_0\left[\sqrt{\left(z_D - z_{wD} + 2n\right)^2 z_{eD}^2 + \left(y_D - y_{wD}\right)^2}\sqrt{u}\right] + \\ &K_0\left[\sqrt{\left(z_D + z_{wD} + 2n\right)^2 z_{eD}^2 + \left(y_D - y_{wD}\right)^2}\sqrt{u}\right]\Bigg\} \\ &-\frac{\pi\exp\left[-\sqrt{u}\left(y_D - y_{wD}\right)\right]}{2s\sqrt{u}}\left(\frac{2L}{L_h}\sqrt{\frac{k_z}{k}}\right)\end{aligned} \tag{A.16}$$

- For small *s* (large *t*):

$$\begin{aligned}\overline{F}_1 = &\frac{\pi}{s}\left(\frac{2L}{L_h}\sqrt{\frac{k_z}{k}}\right)\sum_{n=1}^{\infty}\cos n\pi z_D \cos n\pi z_{wD} \\ &\left[\frac{\exp\left[-\varepsilon_n\left|\left(y_D - y_{wD}\right)\right|\right]}{\varepsilon_n} - \frac{\exp\left[-n\pi\left|\left(y_D - y_{wD}\right)\right|/z_{eD}\right]}{n\pi/z_{eD}}\right] + \frac{z_{eD}}{4s}\left(\frac{2L}{L_h}\sqrt{\frac{k_z}{k}}\right) \\ &\Bigg[\ln\frac{1}{1-2\exp\left[-\pi\left|\left(y_D - y_{wD}\right)\right|/z_{eD}\right]\cos\left[\pi\left(z_D + z_{wD}\right)/z_{eD}\right] + \exp\left[-2\pi\left|\left(y_D - y_{wD}\right)\right|/z_{eD}\right]} \\ &+\ln\frac{1}{1-2\exp\left[-\pi\left|\left(y_D - y_{wD}\right)\right|/z_{eD}\right]\cos\left[\pi\left(z_D - z_{wD}\right)/z_{eD}\right] + \exp\left[-2\pi\left|\left(y_D - y_{wD}\right)\right|/z_{eD}\right]}\Bigg]\end{aligned} \tag{A.17}$$

APPENDIX B

TABULATED RESULTS

This appendix shows the tabulated results for one of the cases described in Section 4.1, which addresses the sensitivity of the number of hydraulic fractures (n_{FA} and n_{FO}).

Table B.1. Pressure responses for n_{FA} and n_{FO} = 3

n_{FA} = 3 & n_{FO} = 3				
t_D	p_{wDA}	$dp_{wDA}/dlnt_D$	p_{wDO}	$dp_{wDO}/dlnt_D$
1.E-06	8.49E-03	2.28E-03	0.00E+00	0.00E+00
2.E-06	1.04E-02	3.17E-03	0.00E+00	0.00E+00
4.E-06	1.30E-02	4.38E-03	0.00E+00	0.00E+00
1.E-05	1.79E-02	6.64E-03	0.00E+00	0.00E+00
2.E-05	2.33E-02	8.95E-03	0.00E+00	0.00E+00
4.E-05	3.05E-02	1.18E-02	0.00E+00	0.00E+00
1.E-04	4.33E-02	1.64E-02	3.50E-12	1.34E-11
2.E-04	5.60E-02	2.03E-02	2.11E-09	6.74E-09
4.E-04	7.15E-02	2.45E-02	1.81E-08	8.64E-08
1.E-03	9.65E-02	2.99E-02	8.37E-08	4.92E-07
2.E-03	1.19E-01	3.39E-02	2.67E-06	1.16E-05
4.E-03	1.43E-01	3.77E-02	3.09E-05	9.08E-05
1.E-02	1.80E-01	4.30E-02	2.73E-04	5.30E-04
2.E-02	2.12E-01	4.70E-02	8.96E-04	1.36E-03
4.E-02	2.46E-01	5.09E-02	2.31E-03	2.84E-03
1.E-01	2.95E-01	5.61E-02	6.30E-03	6.15E-03
2.E-01	3.35E-01	5.97E-02	1.18E-02	9.92E-03
4.E-01	3.77E-01	6.30E-02	2.02E-02	1.46E-02
1.E+00	4.37E-01	6.70E-02	3.72E-02	2.25E-02
2.E+00	4.85E-01	7.52E-02	5.54E-02	3.10E-02
4.E+00	5.46E-01	1.03E-01	8.24E-02	4.96E-02
1.E+01	6.65E-01	1.57E-01	1.50E-01	1.03E-01
2.E+01	7.87E-01	1.98E-01	2.40E-01	1.61E-01
4.E+01	9.44E-01	2.57E-01	3.77E-01	2.36E-01
1.E+02	1.22E+00	3.47E-01	6.38E-01	3.35E-01
2.E+02	1.48E+00	4.04E-01	8.92E-01	3.97E-01
4.E+02	1.78E+00	4.45E-01	1.18E+00	4.41E-01
1.E+03	2.20E+00	4.76E-01	1.61E+00	4.75E-01
2.E+03	2.54E+00	4.88E-01	1.94E+00	4.87E-01
4.E+03	2.88E+00	4.94E-01	2.28E+00	4.94E-01
1.E+04	3.33E+00	4.98E-01	2.73E+00	4.97E-01
2.E+04	3.68E+00	4.99E-01	3.08E+00	4.99E-01
4.E+04	4.02E+00	4.99E-01	3.43E+00	4.99E-01
1.E+05	4.48E+00	5.00E-01	3.88E+00	5.00E-01
2.E+05	4.83E+00	5.00E-01	4.23E+00	5.00E-01
4.E+05	5.17E+00	5.00E-01	4.58E+00	5.00E-01
1.E+06	5.63E+00	5.00E-01	5.03E+00	5.00E-01

Table B.2. Pressure responses for n_{FA} and n_{FO} = 5

n_{FA} = 5 & n_{FO} = 5				
t_D	p_{wDA}	$dp_{wDA}/dlnt_D$	p_{wDO}	$dp_{wDO}/dlnt_D$
1.E-06	6.66E-03	1.37E-03	0.00E+00	0.00E+00
2.E-06	7.79E-03	1.90E-03	0.00E+00	0.00E+00
4.E-06	9.35E-03	2.63E-03	0.00E+00	0.00E+00
1.E-05	1.23E-02	3.98E-03	0.00E+00	0.00E+00
2.E-05	1.56E-02	5.37E-03	0.00E+00	0.00E+00
4.E-05	1.99E-02	7.09E-03	0.00E+00	0.00E+00
1.E-04	2.76E-02	9.84E-03	2.29E-12	7.17E-12
2.E-04	3.52E-02	1.22E-02	1.16E-09	3.70E-09
4.E-04	4.45E-02	1.47E-02	1.03E-08	4.88E-08
1.E-03	5.95E-02	1.80E-02	4.81E-08	2.83E-07
2.E-03	7.28E-02	2.04E-02	1.55E-06	6.77E-06
4.E-03	8.78E-02	2.27E-02	1.81E-05	5.35E-05
1.E-02	1.10E-01	2.58E-02	1.61E-04	3.15E-04
2.E-02	1.29E-01	2.82E-02	5.33E-04	8.13E-04
4.E-02	1.49E-01	3.06E-02	1.38E-03	1.70E-03
1.E-01	1.79E-01	3.41E-02	3.80E-03	3.78E-03
2.E-01	2.03E-01	3.71E-02	7.25E-03	6.35E-03
4.E-01	2.30E-01	4.09E-02	1.28E-02	1.00E-02
1.E+00	2.71E-01	4.77E-02	2.52E-02	1.74E-02
2.E+00	3.07E-01	5.77E-02	3.99E-02	2.60E-02
4.E+00	3.55E-01	8.46E-02	6.34E-02	4.44E-02
1.E+01	4.60E-01	1.48E-01	1.27E-01	1.02E-01
2.E+01	5.82E-01	2.06E-01	2.20E-01	1.71E-01
4.E+01	7.47E-01	2.72E-01	3.66E-01	2.51E-01
1.E+02	1.04E+00	3.58E-01	6.41E-01	3.47E-01
2.E+02	1.30E+00	4.12E-01	9.03E-01	4.06E-01
4.E+02	1.60E+00	4.50E-01	1.20E+00	4.47E-01
1.E+03	2.03E+00	4.78E-01	1.62E+00	4.77E-01
2.E+03	2.37E+00	4.89E-01	1.96E+00	4.88E-01
4.E+03	2.71E+00	4.95E-01	2.30E+00	4.94E-01
1.E+04	3.16E+00	4.98E-01	2.75E+00	4.98E-01
2.E+04	3.51E+00	4.99E-01	3.10E+00	4.99E-01
4.E+04	3.85E+00	4.99E-01	3.45E+00	4.99E-01
1.E+05	4.31E+00	5.00E-01	3.90E+00	5.00E-01
2.E+05	4.66E+00	5.00E-01	4.25E+00	5.00E-01
4.E+05	5.00E+00	5.00E-01	4.60E+00	5.00E-01
1.E+06	5.46E+00	5.00E-01	5.05E+00	5.00E-01

Table B.3. Pressure responses for n_{FA} and n_{FO} = 10

n_{FA} = 10 & n_{FO} = 10				
t_D	p_{wDA}	$dp_{wDA}/dlnt_D$	p_{wDO}	$dp_{wDO}/dlnt_D$
1.E-06	5.29E-03	6.89E-04	0.00E+00	0.00E+00
2.E-06	5.85E-03	9.54E-04	0.00E+00	0.00E+00
4.E-06	6.63E-03	1.32E-03	0.00E+00	0.00E+00
1.E-05	8.13E-03	1.99E-03	0.00E+00	0.00E+00
2.E-05	9.74E-03	2.69E-03	0.00E+00	0.00E+00
4.E-05	1.19E-02	3.56E-03	5.28E-23	3.66E-23
1.E-04	1.58E-02	4.94E-03	1.39E-12	2.48E-12
2.E-04	1.96E-02	6.14E-03	4.41E-10	1.42E-09
4.E-04	2.43E-02	7.39E-03	4.50E-09	2.05E-08
1.E-03	3.18E-02	9.03E-03	2.12E-08	1.26E-07
2.E-03	3.85E-02	1.02E-02	7.06E-07	3.14E-06
4.E-03	4.60E-02	1.14E-02	8.59E-06	2.57E-05
1.E-02	5.74E-02	1.34E-02	8.13E-05	1.66E-04
2.E-02	6.74E-02	1.57E-02	2.91E-04	4.85E-04
4.E-02	7.93E-02	1.87E-02	8.37E-04	1.18E-03
1.E-01	9.88E-02	2.42E-02	2.69E-03	3.12E-03
2.E-01	1.17E-01	2.94E-02	5.71E-03	5.80E-03
4.E-01	1.40E-01	3.54E-02	1.10E-02	9.87E-03
1.E+00	1.76E-01	4.46E-02	2.35E-02	1.79E-02
2.E+00	2.10E-01	5.53E-02	3.89E-02	2.71E-02
4.E+00	2.57E-01	8.25E-02	6.34E-02	4.65E-02
1.E+01	3.61E-01	1.48E-01	1.30E-01	1.07E-01
2.E+01	4.83E-01	2.07E-01	2.27E-01	1.77E-01
4.E+01	6.49E-01	2.73E-01	3.77E-01	2.56E-01
1.E+02	9.39E-01	3.59E-01	6.57E-01	3.51E-01
2.E+02	1.21E+00	4.13E-01	9.21E-01	4.08E-01
4.E+02	1.51E+00	4.51E-01	1.22E+00	4.48E-01
1.E+03	1.94E+00	4.79E-01	1.64E+00	4.78E-01
2.E+03	2.27E+00	4.89E-01	1.98E+00	4.89E-01
4.E+03	2.61E+00	4.95E-01	2.32E+00	4.94E-01
1.E+04	3.07E+00	4.98E-01	2.78E+00	4.98E-01
2.E+04	3.41E+00	4.99E-01	3.12E+00	4.99E-01
4.E+04	3.76E+00	4.99E-01	3.47E+00	4.99E-01
1.E+05	4.22E+00	5.00E-01	3.93E+00	5.00E-01
2.E+05	4.56E+00	5.00E-01	4.27E+00	5.00E-01
4.E+05	4.91E+00	5.00E-01	4.62E+00	5.00E-01
1.E+06	5.37E+00	5.00E-01	5.08E+00	5.00E-01

Table B.4. Pressure responses for n_{FA} and n_{FO} = 15

n_{FA} = 15 & n_{FO} = 15				
t_D	p_{wDA}	$dp_{wDA}/dlnt_D$	p_{wDO}	$dp_{wDO}/dlnt_D$
1.E-06	4.83E-03	4.62E-04	0.00E+00	0.00E+00
2.E-06	5.21E-03	6.38E-04	0.00E+00	0.00E+00
4.E-06	5.73E-03	8.79E-04	0.00E+00	0.00E+00
1.E-05	6.73E-03	1.33E-03	0.00E+00	0.00E+00
2.E-05	7.80E-03	1.80E-03	1.83E-24	1.27E-24
4.E-05	9.25E-03	2.38E-03	3.16E-19	2.19E-19
1.E-04	1.18E-02	3.31E-03	1.10E-12	9.06E-13
2.E-04	1.44E-02	4.11E-03	2.00E-10	6.61E-10
4.E-04	1.75E-02	4.95E-03	2.58E-09	1.12E-08
1.E-03	2.26E-02	6.06E-03	1.21E-08	7.47E-08
2.E-03	2.71E-02	6.98E-03	4.39E-07	2.00E-06
4.E-03	3.24E-02	8.30E-03	5.97E-06	1.91E-05
1.E-02	4.12E-02	1.11E-02	6.76E-05	1.50E-04
2.E-02	4.98E-02	1.40E-02	2.67E-04	4.74E-04
4.E-02	6.07E-02	1.76E-02	8.16E-04	1.20E-03
1.E-01	7.95E-02	2.36E-02	2.73E-03	3.23E-03
2.E-01	9.77E-02	2.89E-02	5.86E-03	6.01E-03
4.E-01	1.20E-01	3.50E-02	1.14E-02	1.02E-02
1.E+00	1.56E-01	4.41E-02	2.43E-02	1.84E-02
2.E+00	1.90E-01	5.47E-02	4.00E-02	2.78E-02
4.E+00	2.36E-01	8.14E-02	6.51E-02	4.75E-02
1.E+01	3.38E-01	1.46E-01	1.33E-01	1.08E-01
2.E+01	4.59E-01	2.05E-01	2.31E-01	1.79E-01
4.E+01	6.23E-01	2.71E-01	3.83E-01	2.58E-01
1.E+02	9.12E-01	3.58E-01	6.63E-01	3.52E-01
2.E+02	1.18E+00	4.12E-01	9.27E-01	4.09E-01
4.E+02	1.48E+00	4.50E-01	1.23E+00	4.48E-01
1.E+03	1.91E+00	4.79E-01	1.65E+00	4.78E-01
2.E+03	2.24E+00	4.89E-01	1.99E+00	4.89E-01
4.E+03	2.58E+00	4.95E-01	2.33E+00	4.94E-01
1.E+04	3.04E+00	4.98E-01	2.78E+00	4.98E-01
2.E+04	3.38E+00	4.99E-01	3.13E+00	4.99E-01
4.E+04	3.73E+00	4.99E-01	3.47E+00	4.99E-01
1.E+05	4.19E+00	5.00E-01	3.93E+00	5.00E-01
2.E+05	4.53E+00	5.00E-01	4.28E+00	5.00E-01
4.E+05	4.88E+00	5.00E-01	4.62E+00	5.00E-01
1.E+06	5.34E+00	5.00E-01	5.08E+00	5.00E-01

Table B.5. Pressure responses for n_{FA} and n_{FO} = 20

n_{FA} = 20 & n_{FO} = 20				
t_D	p_{wDA}	$dp_{wDA}/dlnt_D$	p_{wDO}	$dp_{wDO}/dlnt_D$
1.E-06	4.60E-03	3.48E-04	0.00E+00	0.00E+00
2.E-06	4.88E-03	4.80E-04	0.00E+00	0.00E+00
4.E-06	5.28E-03	6.60E-04	0.00E+00	0.00E+00
1.E-05	6.03E-03	9.99E-04	3.94E-28	2.73E-28
2.E-05	6.84E-03	1.35E-03	3.36E-23	2.32E-23
4.E-05	7.92E-03	1.79E-03	5.71E-18	3.96E-18
1.E-04	9.87E-03	2.49E-03	1.04E-12	7.60E-14
2.E-04	1.18E-02	3.10E-03	7.61E-11	2.83E-10
4.E-04	1.42E-02	3.73E-03	1.69E-09	6.47E-09
1.E-03	1.80E-02	4.68E-03	8.59E-09	4.94E-08
2.E-03	2.16E-02	5.81E-03	3.34E-07	1.61E-06
4.E-03	2.62E-02	7.51E-03	5.26E-06	1.77E-05
1.E-02	3.44E-02	1.07E-02	6.57E-05	1.50E-04
2.E-02	4.29E-02	1.37E-02	2.68E-04	4.85E-04
4.E-02	5.36E-02	1.75E-02	8.34E-04	1.24E-03
1.E-01	7.23E-02	2.34E-02	2.81E-03	3.33E-03
2.E-01	9.03E-02	2.87E-02	6.03E-03	6.17E-03
4.E-01	1.12E-01	3.47E-02	1.17E-02	1.04E-02
1.E+00	1.48E-01	4.36E-02	2.48E-02	1.88E-02
2.E+00	1.81E-01	5.41E-02	4.08E-02	2.82E-02
4.E+00	2.27E-01	8.05E-02	6.63E-02	4.81E-02
1.E+01	3.28E-01	1.44E-01	1.35E-01	1.09E-01
2.E+01	4.48E-01	2.03E-01	2.34E-01	1.80E-01
4.E+01	6.11E-01	2.70E-01	3.85E-01	2.58E-01
1.E+02	8.99E-01	3.57E-01	6.66E-01	3.52E-01
2.E+02	1.17E+00	4.12E-01	9.30E-01	4.09E-01
4.E+02	1.47E+00	4.50E-01	1.23E+00	4.48E-01
1.E+03	1.89E+00	4.79E-01	1.65E+00	4.78E-01
2.E+03	2.23E+00	4.89E-01	1.99E+00	4.89E-01
4.E+03	2.57E+00	4.95E-01	2.33E+00	4.94E-01
1.E+04	3.03E+00	4.98E-01	2.79E+00	4.98E-01
2.E+04	3.37E+00	4.99E-01	3.13E+00	4.99E-01
4.E+04	3.72E+00	4.99E-01	3.48E+00	4.99E-01
1.E+05	4.17E+00	5.00E-01	3.94E+00	5.00E-01
2.E+05	4.52E+00	5.00E-01	4.28E+00	5.00E-01
4.E+05	4.87E+00	5.00E-01	4.63E+00	5.00E-01
1.E+06	5.33E+00	5.00E-01	5.09E+00	5.00E-01

APPENDIX C

MATLAB® CODE

The computer code in this thesis is written in Matlab®. All the codes are stored in the CD in this thesis. The files are described in the table below.

Table C.1. List of codes used in this study

File Name	Description
two_fractured_hz_wells	main program of the code (including Stehfest algorithm)
integral_I0	integral of modified Bessel functions of the first kind of order zero
integral_K0	integral of modified Bessel functions of the second kind of order zero
repeated_integral_K0	integral representation of modified Bessel functions of the second kind of order zero
f_s_dual_por	transfer function between matrix and fracture for dual-porosity reservoir
comp_simp	composite Simpson's rule for integral
p_fracture_inf	pressure solution for a fracture in an infinite reservoir
p_fracture_closed_rec	pressure solution for a fracture in a closed rectangular reservoir
p_hz_well_inf	pressure solution for a horizontal well in an infinite reservoir
calc_int_Vi	Vi function in Stehfest algorithm
frac_discretization	discretization function for a fracture
frac_discretization_cross_frac	discretization function for a crossing fracture
hz_well_discretization	discretization function for a horizontal well
fracture_flow	function to calculate fracture flow within a fracture
crossing_fracture_flow	function to calculate fracture flow within a stand-alone fracture
matrix_variable	matrix variable function for additional flow in Matrix A
matrix_variable_with_crossing_frac	matrix variable function for additional flow (including a stand-alone fracture) in Matrix A